This is to certify that the

dissertation entitled

CENTRAL DELAMINATION IN GLASS/EPOXY LAMINATES

presented by

Seongho Hong

has been accepted towards fulfillment
of the requirements for

Ph.D. degree in Engineering Mechanics

Dahsin Liu
Major professor

Date March 8, 1990

CENTRAL DELAMINATION IN GLASS/EPOXY LAMINATES

By

Seongho Hong

A DISSERTATION

Submitted to
Michigan State University
in partial fulfillment of the requirements
for the degree of

DOCTOR OF PHILOSOPHY

Department of Metallurgy, Mechanics, and Materials Science

1990

ABSTRACT

CENTRAL DELAMINATION IN GLASS/EPOXY LAMINATES

BY

Seongho Hong

Central delamination has been found to be the major damage mode in composite laminates subjected to low-velocity impact. Although it is invisible, it can cause severe structural degradation such as reduction in compressive strength. Therefore, the investigation of central delamination has become an important study in the characterization of composite strength. This study examined the impacted-induced delamination with the use of edge replication. It was concluded that fiber orientation, laminate thickness, and stacking sequence had significant effects on delamination resistance. Since the behavior of a composite laminate under low-velocity impact is very similar to that under global bending, a technique for quasi-static central loading was explored. A great deal of similarity between the delaminations from low-velocity impact and quasi-static loading was obtained. It was concluded that it was feasible to use quasi-static loading in the central delamination analysis. A high-order shear deformation theory was then used to calculate the interlaminar stresses of the composite laminates subjected to static central loading. Analytical solutions were found to be consistent with the experimental observations. The peanut-shaped delamination was the fundamental unit of delamintion in the composite laminates under central loading. The major axis of a delamination was aligned with the fiber direction of the composite lamina beneath the interface. The delamination area, however, was affected by the fiber orientation, laminate thickness, and stacking sequence. In order to reduce the delamination area, a through-the-thickness stitching was presented. Its effects on the interlaminar shear strength and the strain energy release rate of mode II were also concluded to be effective.

ACKNOWLEDGMENTS

I would like to take this opportunity to thank Dr. Dahsin Liu for his constant support and guidance during this research. Without his encouragement and help this work would have been far from reality.

The guidance and comments of the members of my thesis advisory and examining committees, Dr. N.J. Altiero, Dr. Yvonne Jasuik, and Dr. David Yen are greatly appreciated.

I would like to thank the Centre for Composite Materials and Structures for financial support for this research.

I would also like to thank my mother and family; without their patience, nothing would have become reality; and to my lovely wife Jeonghee, to my lovely daughter Melody for their patience, understanding, and encouragement. Finally, I would like to thank my friends and my colleagues, especially Mr. C.Y. Lee and Mr. X. Lu for their friendship, and Mr. Chienhom Lee who helped me for the finite element method.

TABLE OF CONTENTS

LIST OF TABLES

LIST OF FIGURES

Page

Chapter 1

Introduction

Because of their high stiffness-to-weight and high strength-to-weight ratios, fiber-reinforced polymer matrix composite materials are excellent for high-performance structures. However, being different from the conventional structure metals, the composite materials can be tailored and laminated together [1]. Consequently, by using the composite materials, it is possible to achieve an optimum structure design which requires different strengths at different locations and different directions of the structure. Both the characteristics of the design flexibility and light weight make the composite materials very promising for the aerospace and military industries. However, because of their lamination in nature, the composite laminates are very vulnerable to through-the-thickness stresses [2]. For example, if a composite laminate is subjected to out-of-plane loading such as bending, due to the high interlaminar stresses, delamination can easily occur on the composite interface [2]. The damage to the integrity of the composite laminate can cause serious structural degradation [2-5]. Accordingly, in studying the strength of a composite material, it is necessary to investigate both in-plane strength and through-the-thickness strength.

1.1 Delamination

The damage modes of laminated composite materials can be classified into fiber breakage, matrix cracking, fiber-matrix debonding, and delamination [6]. Fiber breakage and matrix cracking are related to the failures of the constituents while debonding and delamination are due to the damage on the composite interfaces. Debonding is damage between fiber and matrix while delamination is damage on the interface between adjacent laminae [7]. In order to have a high-strength composite laminate, both high-strength constituents and high bonding strength between fiber and matrix are necessary. The fibers are the primary reinforcement in composite material and therefore carry the majority of the load. The stronger the fiber, the stronger the composite materials. On the contrary, matrix is the load transfer in the composite materials. Without good bonding between fiber and matrix, the stresses in some fibers cannot be propagated to and shared by the fibers in other parts of the composite material. In addition to the bonding strength, the strength of the matrix itself is also of importance because the composite laminates are simply bonded by the matrix in the thickness direction. Both low matrix strength and poor bonding between fiber and matrix can cause damage on the composite interface.

Delamination is damage on the composite interface. It is a unique damage mode in the laminated composite materials. In opaque composite materials such as graphite/epoxy and Kevlar/epoxy, delamination is invisible. Often times, a damaged composite material only shows minor surface damage even though severe delamination may exist. This type of internal damage requires extra effort for inspection. Many nondestructive techniques have been developed for delamination investigation. Among them, ultrasonic C-scan [2-5] and X-ray radiography [8-11] are the most popular ones. Ultrasonic C-scan can give the overall outline of many delamination areas. However, it cannot resolve the overlapped delaminations into individual ones. X-ray radiography, if used with a penetrant, is able to distinguish the delaminations on the different interfaces. However, it is limited to the composite laminates with less than four interfaces [5]. If a composite laminate has many delamination interfaces, X-ray radiography also fails to distinguish the individual delamination. Recently, a so-called ultrasonic imaging system was introduced by Ho [12]. It is based on ultrasonic scanning to detect the delamination. An image processing technique is then used to reconstruct the delamination. It has the capability to detect composite laminates with a thickness of lamina more than 0.5 mm. However, it also experiences difficulty when there are many delamination interfaces. In addition to nondestructive techniques, destructive techniques, such as the deply technique [4] and edge replication [13-14], have also been used for delamination investigation. The former uses gold chloride to cover the delamination area before the resin is pyrolyzed while the latter simply slices the damaged composite laminates into strips and examines the internal damage from the edges. Both techniques have been verified to be useful for delamination investigation.

In addition to identifying the location and the size of delamination, it is also important to characterize the structural properties of composite laminates with delamination, e.g., residual stiffness and strength [15]. It has been found that delamination causes little reduction in tensile properties [7]. However, the compressive strength of composite laminates can be significantly decreased by delamination [16-17]. Many investigations regarding the compressive testing technique [18-20] have been presented. Some special testing fixtures have been designed to avoid global buckling of the delaminated composite materials during compressive testing. The technique has now become a standard procedure for the characterization of delaminated composite materials. In addition, a great deal of papers [21-22] have been devoted to the analysis of post-delamination buckling. The behavior of composite materials with delamination is further examined with use of fracture mechanics [23-25]. Studies have concluded that delamination plays a very important role in the structure degradation of composite materials [2-5].

In terms of location, two types of delamination have been widely investigated. One is edge delamination [26-31] and the other is central delamination [32-36]. Many studies have contributed to the investigation of edge delamination. Due to free-edge effect, the interlaminar stresses on the composite interface can become very high and can cause delamination. Both experimental techniques and analytical methods have been used to investigate the composite laminates subjected to uniaxial tension. The effects due to the stacking sequence and laminate thickness on the edge delamination have been examined. It is noted that due to the mismatch of Poisson's ratio between adjacent laminae [31], high interlaminar shear stress can take place on the composite interface along the free edge of cross-ply laminates. In addition, due to the nature of three-dimensional effects around the laminate edges, namely free-edge effects, the interlaminar normal stress on the composite interface of angle-ply laminates can become very significant [37-38]. All studies have shown the importance of edge delamination in laminate design.

Instead of having delamination along the free edge of composite laminates, central delamination is referred to as the delamination located far from the free edge. Usually, this type of delamination is due to low-velocity impact or other kinds of central loading. Around the area of central loading, the interlaminar stresses are highly concentrated and can cause delamination initiation on the composite interface. Most studies in central delamination can be found in the papers of low-velocity impact [39-49] because impact-induced damage has been recognized as one of the major concerns in composite strength characterization [41-49]. In fact, the compressive strength after impact has been used as an indicator of the impact resistance of composite materials. Because delamination is the major damage mode in impacted composite laminates and because of its important effect on structure degradation, further studies on the mechanisms of central delamination is necessary.

1.2 Low-velocity Impact

Low-velocity impact has become one of the major technique for composite material characterization, not only because it can cause invisible delamination but also because it occurs frequently in structures. There are many studies on low-velocity impact [2-6, 8-11, 13-17, 39-49]. Techniques, such as drop-weight impact [50] and instrumented hammer [51-55], have been widely used for the investigation. The majority of the studies have been on the examination of impact dynamics, e.g., the measurements of contact force history between impactor and material, the strain wave propagation in the composite materials, and the laminate deformations during impact. Force transducers, displacement transducers, and strain gages are frequently used in the measurements. In addition, high-speed movie cameras have also been used to record the behavior of composite laminates under impact [2, 44]. The post-impact inspection and the residual property characterization are also as important as the measurements during impact. Both impact momentum and impact energy have been used to correlate with the residual properties and impact damage. To establish a relation between an input quantity, such as the impact momentum of energy, and residual property is very useful for laminate design.

In addition to experimental investigation, some analytical methods have also been used to examine the behavior of composite laminate under low-velocity impact. An indentation law has been presented by Tan and Sun [56]. It can fairly predict the dynamic behavior of a composite laminate under low-velocity impact. Numerical studies such as finite element methods [57-58] have also been used to calculate the stress states of composite laminates under dynamic loading. However, only overall stress distributions have been presented. There is a lack of further discussion regarding the effect of interlaminar stresses on impact damage. Based on experimental observation and fracture mechanics, some efforts have been contributed toward the prediction of the initiations of delamination and matrix cracking [45-47]. A few modelings [36, 49] have been presented for the study of impact resistance. However, the studies on delamination itself, such as the fundamentals of delamination shape and area, are still deficient. Impact-induced delamination is a very sophisticated problem. In order to better understand the delamination mechanisms, it is necessary to consider as many aspects of impact dynamics as possible.

The damage of a composite laminate subjected to impact loading is strongly dependent on the impact velocity. Generally speaking, if the impact velocity is very high, a thin composite laminate will be perforated and the major damage area will be relatively localized in the impacted area [59]. However, if the impact velocity is low, the damage of the thin composite laminate will be spread over a relatively large region [60]. This is because the behavior of a thin composite laminate subjected to low-velocity impact is very similar to that under global bending and the damage is mainly attributed to bending [33].

Similar arguments have also been used to interpret the thickness effect on impact damage. In low-velocity impact, a thick composite laminate has a relatively smaller damage area than a thin one. In fact, the major damage in the thick composite laminates is of local indentation and fiber breakage [60]. However, the damage in the thin composite laminates covers a larger area; and delamination has been found to be the major damage mode. The difference due to the thickness effect again can be viewed from the concepts of global bending and local indentation.

In addition to impact velocity and laminate thickness, the material properties of a composite laminate can also affect the damage mode and the degree of damage. For example, a composite material which is made of fibers with high failure strain can have high perforation resistance. It has also been accepted as a rule of thumb that a low bonding strength between fiber and matrix usually results in a high fracture toughness in the composite material [7]. In low-velocity impact, the impact energy has to be either dissipated away in the form of heat, or absorbed by the composite material in the form of permanent deformation and damage [60]. Therefore, with high fiber strain and low bonding strength, Kevlar/epoxy can absorb a lot of energy without being perforated [61]. In fact, it has been widely used as a bullet-proof material. On the contrary, glass/epoxy has high bonding strength [62]. Although glass fibers have high failure strain, they are very sensitive to defects. The third kind of fiber-reinforced polymer matrix composite material, widely used as a structural material [1], is graphite/epoxy. It has intermediate bonding strength but low failure strain of fiber. Therefore, both glass/epoxy and graphite/epoxy do not have perforation resistance as high as Kevlar/epoxy [59]. In addition, it should be noted that although the epoxies of the three types of composite material are different, they are all brittle materials. In studying the impact resistance of composite materials, it is necessary to take the properties of the constituents and the bonding strength into consideration.

Beside the properties of the constituents and the bonding strength, the configuration of a composite laminate can also affect the stress distribution during impact. The study of the configuration should include the geometry, dimensions, boundary conditions, fiber orientation, laminate thickness, and stacking sequence of a composite laminate. The study on geometry effect have been mentioned in some papers [48-49]. The effect of laminate curvature has also been pointed out to be an important parameter in low-velocity impact [60]. The effect due to dimension can be found in the study of scale effect [63]. Moreover, the boundary conditions also play an important role in low-velocity impact. Since the major concern of this study is to investigate the mechanisms of delamination of composite laminates, the non-material related parameters such as geometry, dimensions, and boundary condition will not be included.

1.3 Summary

Delamination is a very important damage mode in composite laminates. In order to improve the strength of a composite laminate, it is necessary to increase the delamination resistance. Since low-velocity impact can cause serious central delamination and result in severe structure degradation, it has been one of the major investigations in the study of composite materials. Accordingly, low-velocity impact has been used to study central delamination. In addition, compared to edge delamination, there are relatively fewer studies on central delamination. It then is the objective of this study is to look into the mechanisms of central delamination from low-velocity impact and to further understand the parameters to increase the delamination resistance of composite laminates. Because of its low-price and simplicity in fabrication, glass/epoxy laminates were selected for this study.

This study can be divided into three parts. The first part is for experimental observation. The second part is numerical analysis while the third part presents a technique to increase delamination resistance. Since central delamination was first observed in the composite laminates subjected to low-velocity impact, Chapter 2 is about the testing results from low-velocity impact. The effects of fiber orientation, laminate thickness, and stacking sequence on the delamination resistance are of interest. Chapter 3 presents a technique for quasi-static central loading and examines the similarity and difference between the damage due to low-velocity impact and quasi-static loading. The analytical study presented in Chapter 4 is based on static analysis. A high-order shear deformation theory is used to calculate the interlaminar stresses, while examining the behavior of a composite laminate under quasi-static central loading. Chapter 5 investigates the effect of through-the-thickness stitching on the interlaminar strengths. Chapter 6 presents the conclusions of the study.

Chapter 2

Low-velocity Impact

2.1 Impact Testing

The objective of this study was to investigate the effects of fiber orientation, laminate thickness, and stacking sequence on delamination resistance of composite structures under low-velocity impact. In order to simulate the behavior of a structure in the laboratory, square specimens with dimensions of 152 mm by 152 mm were chosen. The size of specimen was equivalent to one quarter of the largest composite panel that could be fabricated from the autoclave housed on campus. The thickness of the composite laminates varied from 9 plies to 21 plies. As a result, they ranged from 2.3 mm to 5.3 mm, depending upon the stacking sequence. Comparing the thickness with dimensions, a minimum aspect ratio of 28 was achieved. The impact testing could then be treated as two-dimensional plate problem.

In the impact testing, each specimen was clamped around four edges by an aluminum holder. The specimen-and-holder was then fixed on a steel frame in front of a gas gun. The specimen was subjected to central impact by a free impactor. Figure 1 shows the experimental set-up for the ballistic impact testing. The cylindrical impactor, which had a spherical nose of 12.5 mm in diameter, 25 mm in length, was made of steel. Depending upon the gas (nitrogen) pressure, the impact velocity ranged from 20 m/s to 100 m/s. The measurement of velocity was made by using two infrared sensors mounted on the gun barrel at 50 mm apart. The distance between the testing specimen and the nearer sensor was set at 31.3 mm. The rebound velocity could also be measured by the same sensors. The difference between the kinetic energy introduced to and

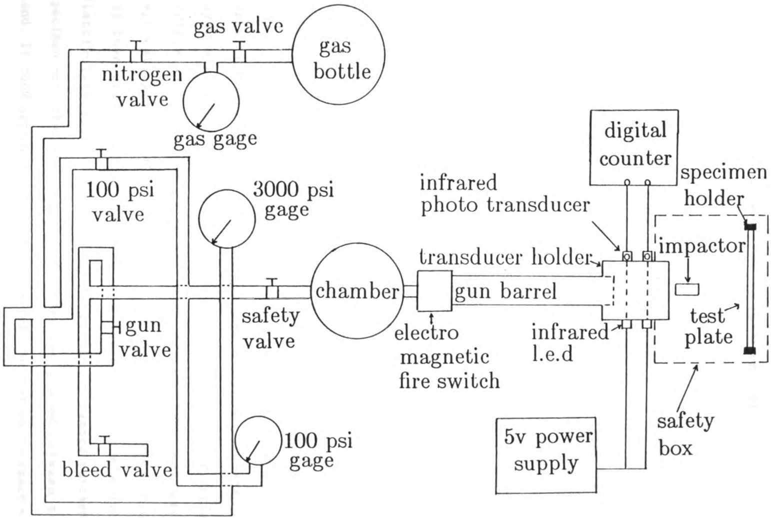

Fig 1 Experimental set-up for Ballistic Impact Testing

rebounded from the specimen was called impact energy and could be as high as 50 J (joules) in this study. With such an energy level, neither visible fiber breakage was found on specimen surfaces nor delamination was extended to the specimen boundaries.

2.2 Edge Replication

After impact, the composite laminates were subject to damage investigation. It was found that delamination was the major damage mode. Both the nondestructive technique of high-intensity light and the destructive technique of edge replication were used for delamination investigation. High-intensity light was useful for translucent glass/epoxy laminates. It could distinguish individual delamination in composite laminates with less than four interfaces. Accordingly, a destructive technique such as edge replication was required for composite laminates with many interfaces. Because it did not require any special equipment, edge replication was selected in this study.

In edge replication, damaged composite laminates were sliced into strips of 5 mm in width. One side of each strip was polished consecutively with emery paper and aluminum oxides of grain sizes of five, three, and one micron. Diamond paste was used as the final polishing material. Once the polishing procedure was completed, a thin layer of acetone was uniformly applied on the polished surface by a syringe. A section of clean cellulose acetate tape was used as a replicating material. It was placed on top of the acetone. Hand force was then used to press the tape onto the strip. Since a uniformly distributive force was necessary to print the damage pattern of the specimen onto the tape, a piece of rubber was placed between tape and hand. It took approximately one minute for the acetone to react with the tape and dry. The details of the damage pattern were then recorded on the tape and were ready for investigation. By using a microfilm viewer, the delamination lengths on every interface of the strips could be determined. The delamination on the composite interfaces could then be obtained by assembling the individual crack lengths. This procedure was done by connecting the crack tips with straight lines. Figure 2 shows the delamination areas on the 20 interfaces of a $[0/90/0/...]_{21}$ laminate. It was verified in a study by Liu et al [13-14] that the delamination areas obtained from edge replication agreed quite well with those from high-intensity light.

2.3 Experimental Results

Of each stacking sequence shown in Table 1, four specimens were fabricated and tested. Delamination was found to be the major damage mode in the composite laminates subjected to low-velocity impact. The peanut-shaped delaminations, as shown in Figure 3, were recognized to be the fundamental unit of delamination on the composite interface. Moreover, the major axis of a delamination was always aligned with the fiber direction of the composite lamina beneath the interface. The relationships between delamination area and impact energy are presented in the following sections. The presentations aim at the investigations of the effects of fiber orientation, laminate thickness, and stacking sequence on delamination resistance.

A. Effect of Fiber Orientation - In order to determine the effect of fiber orientation on delamination resistance, two types of laminates were investigated. One was $[0_5/\theta_5/0_5]$ and the other was $[\theta_3/0_3/\theta_3]$. In both cases, θ was equal to 0, 15, 30, 45, 60, and 90.

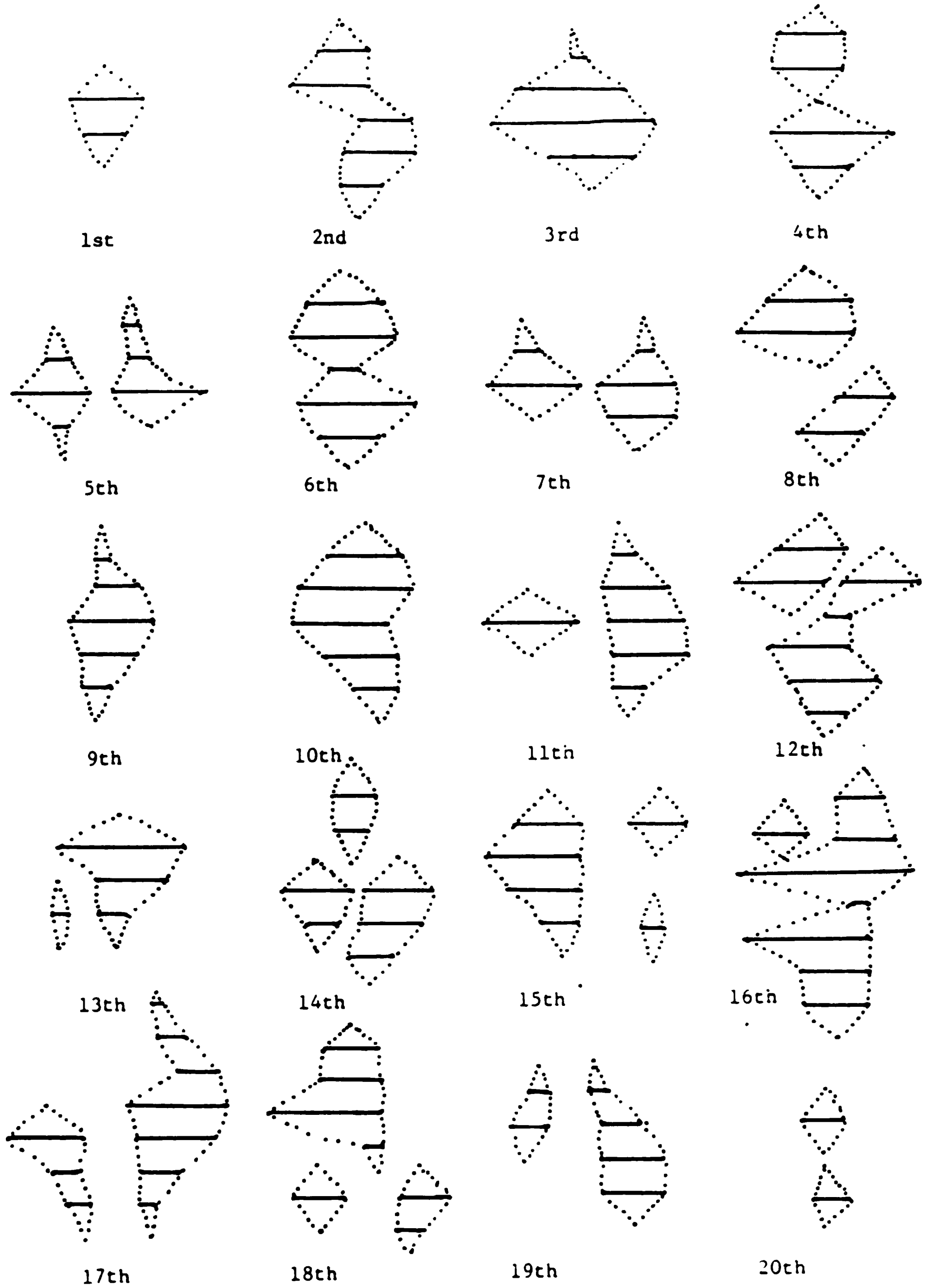

Fig 2 Delaminations in an impacted $[0/90/0/...]_{21}$ glass/epoxy laminate

Table 1 : Stacking Sequence of Composite Laminates and Initiation Energy for Delamination in Low-Velocity Impact

1. Fiber Orientation

Group 1-	$[0_5/15_5/0_5]$	$[0_5/30_5/0_5]$	$[0_5/45_5/0_5]$	$[0_5/60_5/0_5]$	$[0_5/90_5/0_5]$
	12.44J	9.37J	7.73J	5.36J	3.98J
Group 2-	$[15_3/0_3/15_3]$	$[30_3/0_3/30_3]$	$[45_3/0_3/45_3]$	$[60_3/0_3/60_3]$	$[90_3/0_3/90_3]$
	9.97J	5.68J	9.84J	9.87J	3.57J

2. Laminate Thickness

Group 1-	$[0_3/90_3/0_3]$	$[0_5/90_5/0_5]$	$[0_7/90_7/0_7]$
	3.59J	3.98J	*
Group 2-	$[0_3/90_3/0_3]$	$[0_3/90_3/0_3/\ldots]_{15}$	$[0_3/90_3/0_3/\ldots]_{21}$
	3.59J	13.05J	5.78J
Group 3-	$[0/90/0/\ldots]_9$	$[0/90/0/\ldots]_{15}$	$[0/90/0/\ldots]_{21}$
	16.94J	21.79J	12.41J

3. Stacking Sequence

Group 1-	$[0/90/0/\ldots]_9$	$[0_3/90_3/0_3]$	
	16.94J	3.59J	
Group 2-	$[0/90/0/\ldots]_{15}$	$[0_3/90_3/0_3/\ldots]_{15}$	$[0_5/90_5/0_5]$
	21.79J	13.05J	3.98J
Group 3-	$[0/90/0/\ldots]_{21}$	$[0_3/90_3/0_3/\ldots]_{21}$	$[0_7/90_7/0_7]$
	12.41J	5.78J	*

* negative number from least-squares

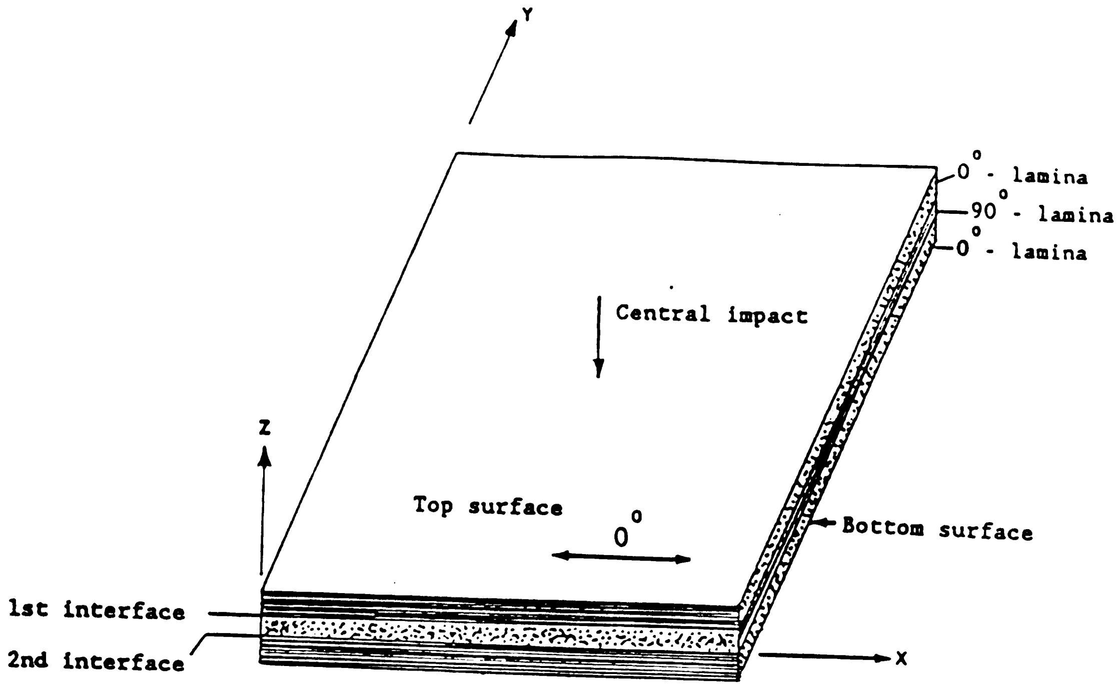

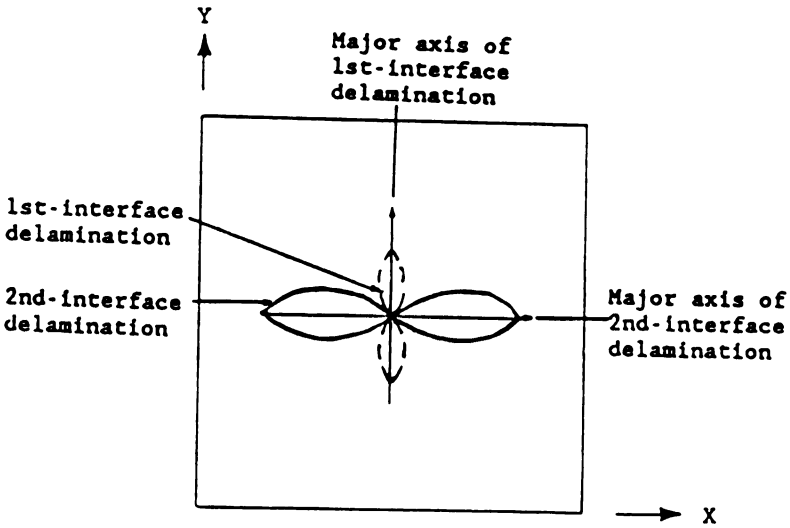

Fig 3 Peanut-shaped delaminations in [0/90/0] composite laminate

Experimental results showed that there was no delamination in the interfaces of $[0_5/0_5/0_5]$ laminates. As shown in Figure 4, under the same impact energy, the delamination area in the laminates of $[0_5/\theta_5/0_5]$ increases as θ increases. It is important to point out that a linear relationship can be used to correlate the delamination area with impact energy in every set of specimen tested. The straight lines in Figure 4 were obtained from least-squares calculations. The intercepts indicate that the minimum energy for the delamination initiation is dependent on θ. The higher the angle θ, the smaller the minimum energy. In addition, it is noted that the slopes of the least-squares, which represent the incremental delamination area per unit impact energy, are about the same. Similar results can also be found in the laminates of $[\theta_3/0_3/\theta_3]$, shown in Figure 5, except that the 30^o lamina has a larger delamination area than those of 45^o and 60^o ones. The results for 45^o and 60^o appear to be indistinguishable from one another.

B. Effect of Laminate Thickness - As shown in Table 1, three different groups of thickness effect were studied. Group 1 includes the laminates of $[0_n/90_n/0_n]$, in which n is equal to 3, 5, and 7. Every specimen in group 1 has three laminae while the thickness of each lamina changes from three to five, and to seven plies. In group 2 and group 3, the thickness of each lamina remains constant, but the number of the lamina in each laminate changes. Group 2 is of $[0_3/90_3/0_3/\ldots]_n$ while group 3 is of $[0/90/0/\ldots]_n$. In both cases, n can be 9, 15, or 21.

Figures 6, 7, and 8 show the relationships between delamination area and impact energy for groups 1, 2, and 3, respectively. Again, linear relationships can be established in every set of specimen. From these

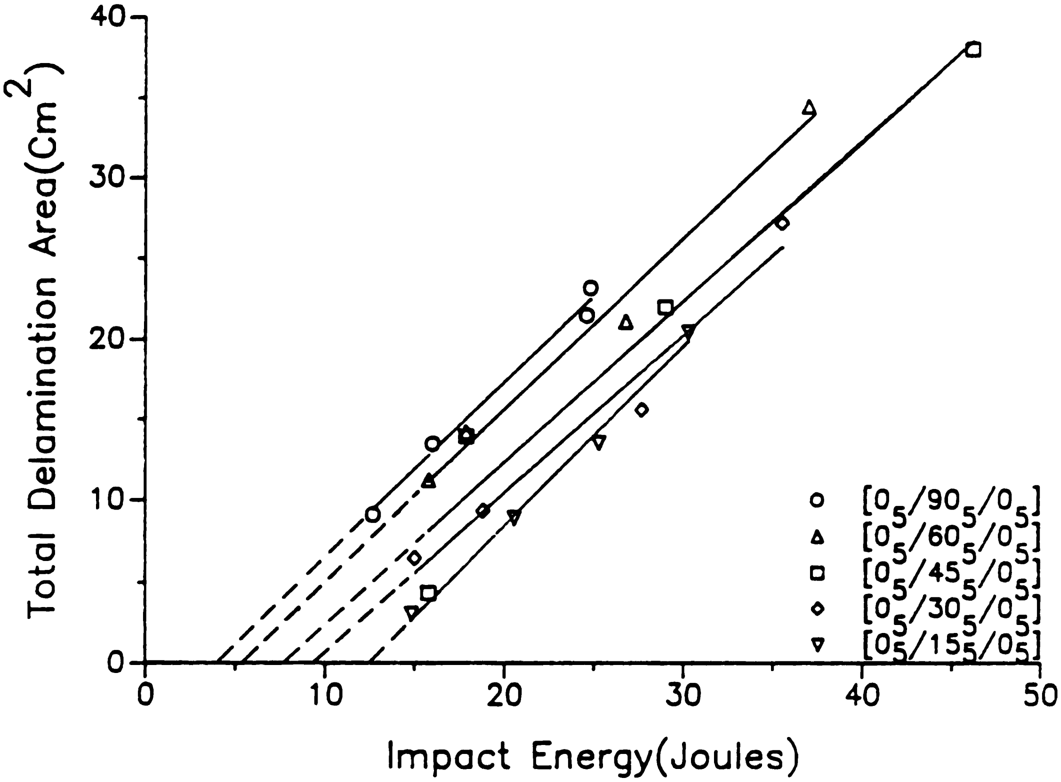

Fig 4 The Effect of fiber orientation on the relationship between delamination area and impact-group 1

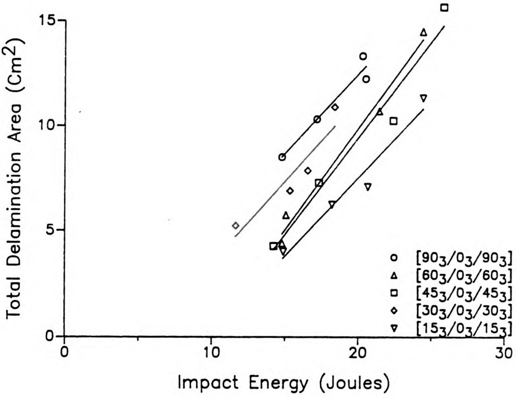

Fig 5 The Effect of fiber orientation on the relationship between delamination area and impact energy-group 2

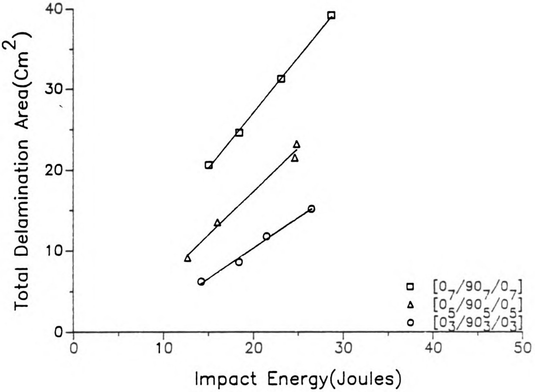

Fig 6 The Effect of laminate thickness on the relationship between delamination area and impact energy-group 1

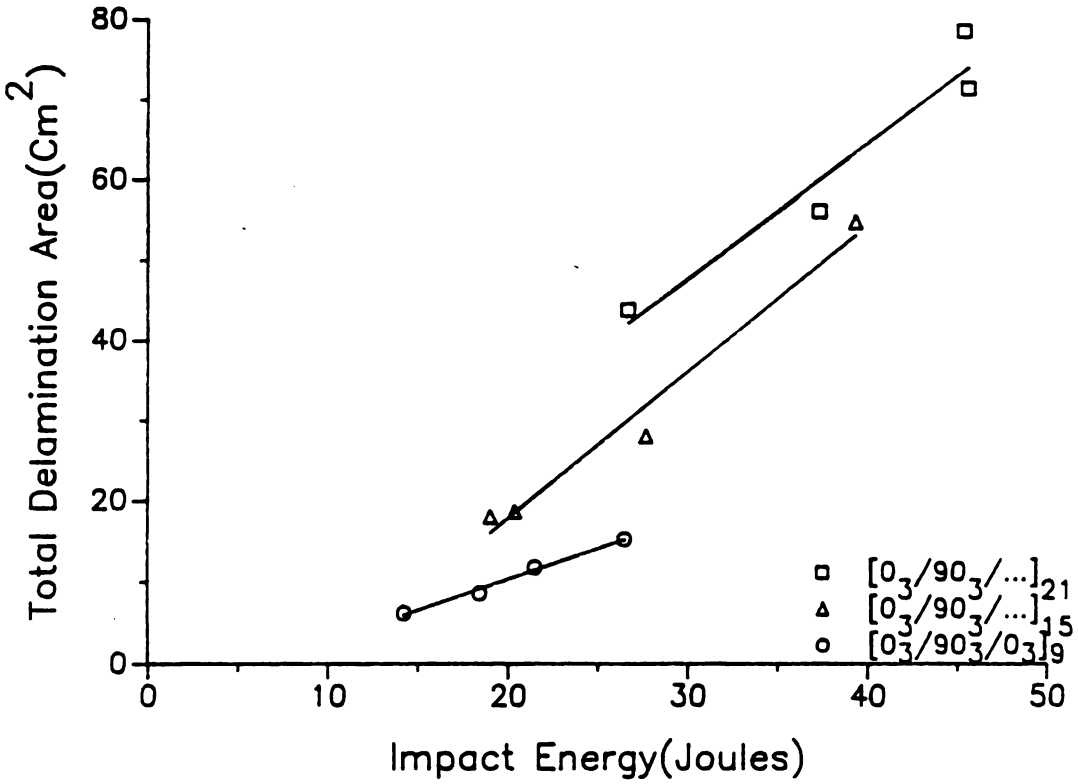

Fig 7 The Effect of laminate thickness on the relationship between delamination area and impact energy-group 2

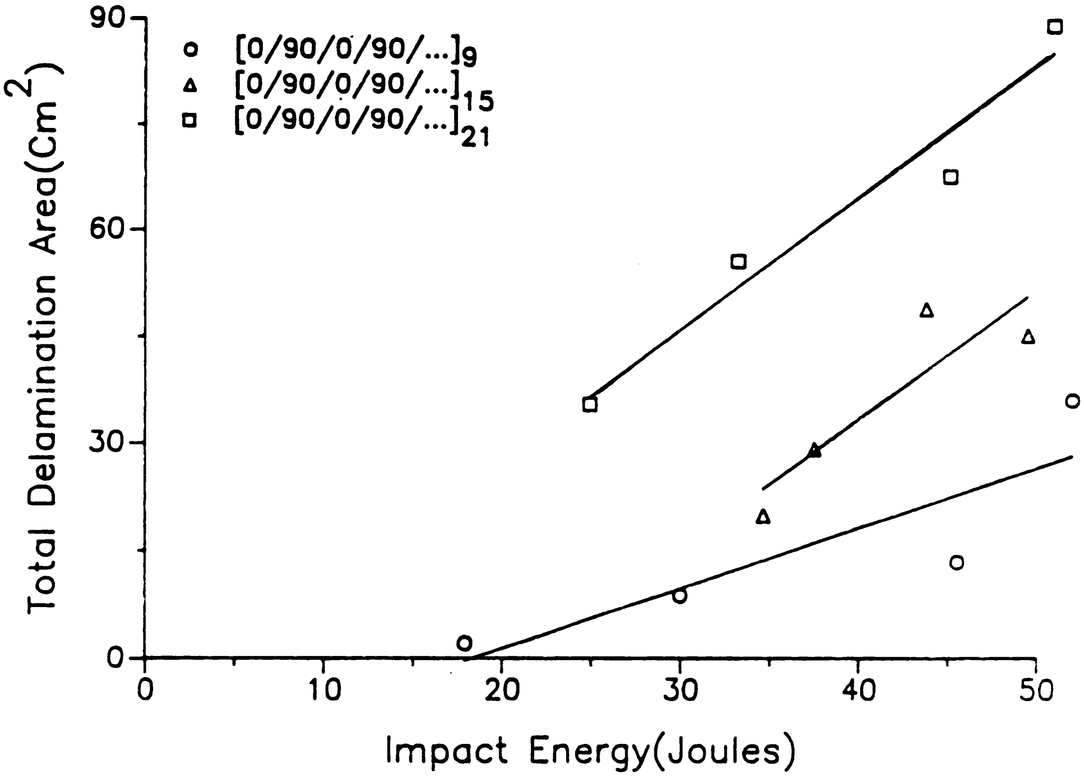

Fig 8 The Effect of laminate thickness on the relationship between delamination area and impact energy-group 3

three figures, it is also concluded that under the same impact energy the total delamination area increases as the thickness increases.

C. Effect of Stacking Sequence - This study investigated the delamination areas in the composite laminates which had the same thickness but different stacking sequences. The same specimens presented in the previous section are regrouped on the basis of the total number of ply, i.e. 9-ply, 15-ply, and 21-ply groups. The 9-ply group has two different stacking sequences, $[0_3/90_3/0_3]$ and $[0/90/0/...]_9$. The 15-ply group has stacking sequences of $[0_5/90_5/0_5]$, $[0_3/90_3/0_3/...]_{15}$, and $[0/90/0/...]_{15}$ while the 21-ply group includes $[0_7/90_7/0_7]$, $[0_3/90_3/0_3/...]_{21}$, and $[0/90/0/...]_{21}$ laminates.

The relationships between the delamination area and impact energy of these three groups are shown in Figures 9, 10, and 11. In the 21-ply group, all the data points are located within a narrow band and the slopes of the three types of specimen are very similar. This indicates that if the thickness remains the same, the increase in delamination area per unit impact energy remains constant even if there is a change in the stacking sequence. However, this result does not exist in 9-ply and 15-ply plates since the bands are much wider in these two groups.

2.4 Discussions

One of the important experimental results is the linear relationship between delamination area and impact energy. By further analyzing the energy per unit delamination area, some conclusions regarding the delamination mechanisms in low-velocity impact can be made.

A. The stresses that cause delamination in the impacted composite laminates are mainly due to bending. It has been presented in a study by Liu [36] that a hypothesis based on bending stiffness mismatch can be

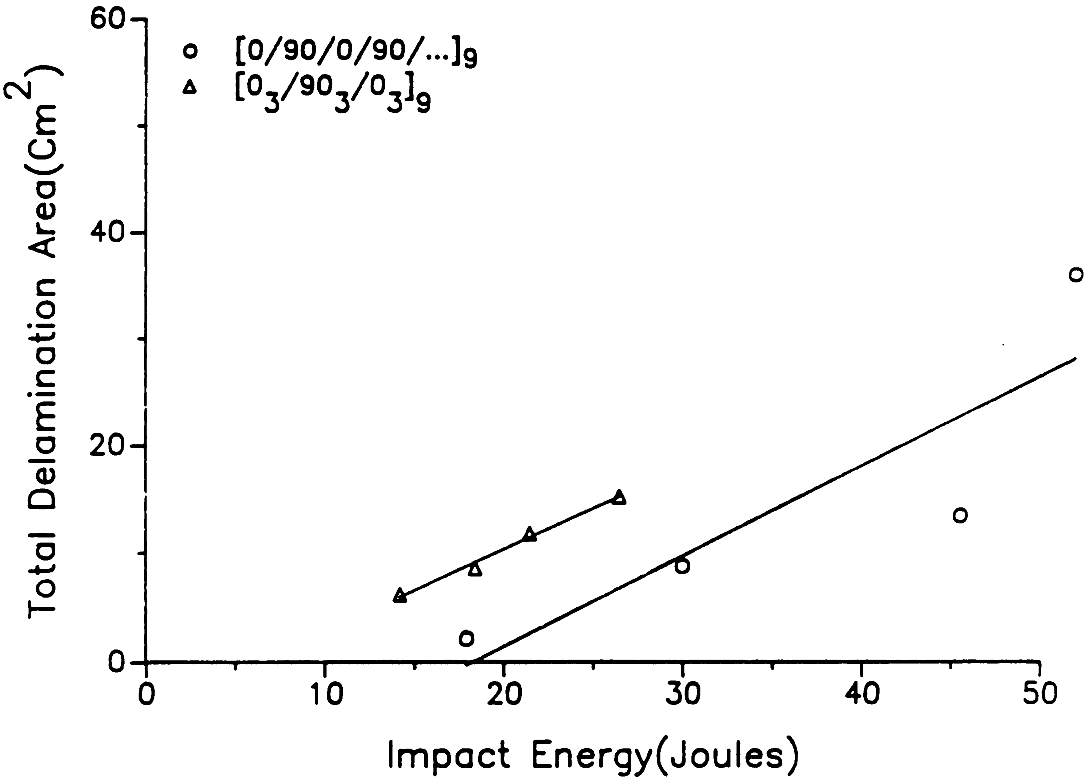

Fig 9 The Effect of stacking sequence on the relationship between delamination area and impact energy-group 1

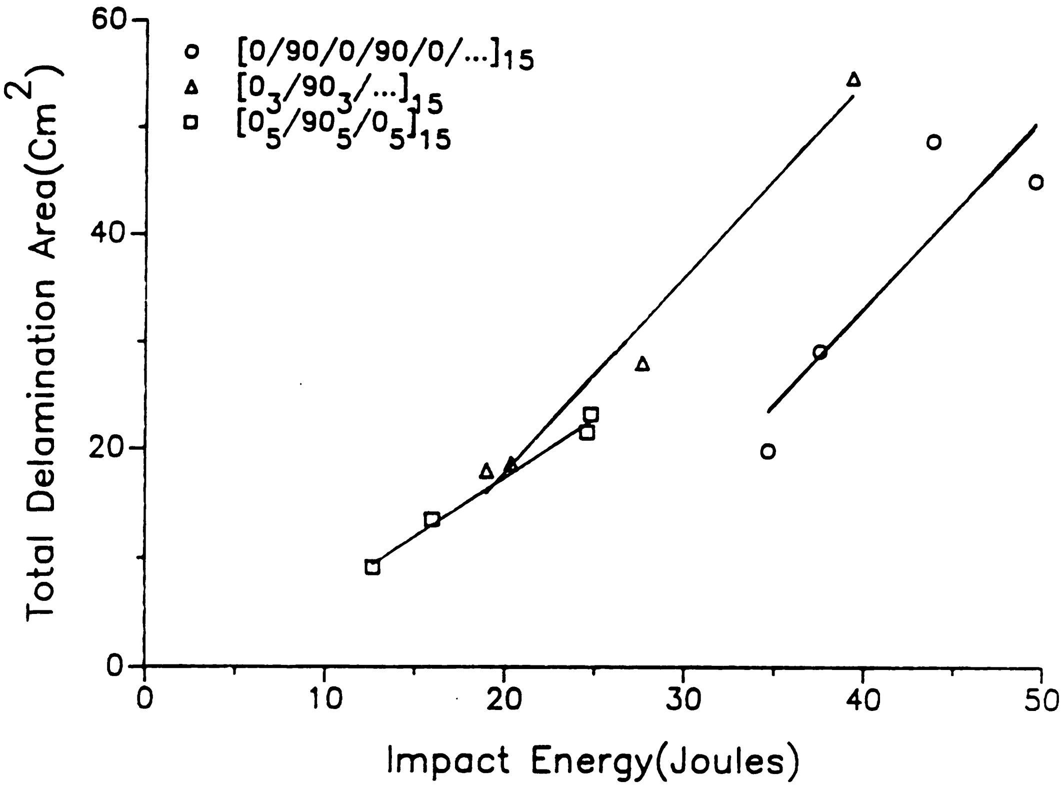

Fig 10 The Effect of stacking sequence on the relationship between delamination area and impact energy-group 2

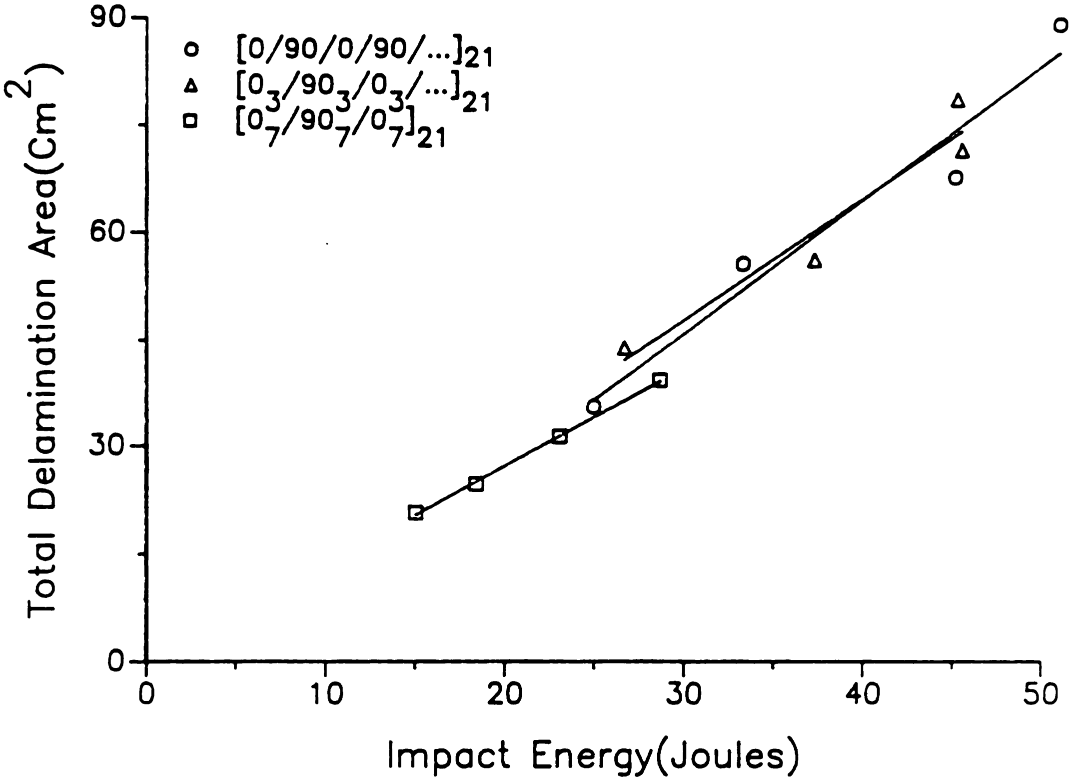

Fig 11 The Effect of stacking sequence on the relationship between delamination area and impact energy-group 3

used to qualitatively interpret the delamination on the composite interface. The hypothesis suggests that the delamination area on an interface of a composite laminate subjected to low-velocity impact is proportional to the mismatch of bending stiffness between the laminae on each side of the interface. In other words, the delamination area in the interface of an impacted $[\theta_a/\theta_b]$ laminate increases as the mismatch of the bending stiffness D_{ij} between the laminae increases. For simplicity, if only the largest term D_{11} is considered, the mismatch of bending stiffness is then defined as $M = D_{11}(\theta_b) - D_{11}(\theta_a)$, where θ_a and θ_b are the fiber orientations of the lamina above and below the interface, respectively. The definition of D_{11} can be found in Jones [1].

Figure 12 shows the relationship between the normalized delamination area and the difference of the fiber angle between adjacent laminae. Both the calculations from the hypothesis and the least-squares of the experimental results are presented in the figure. The line calculated from the hypothesis is for $[\theta/0]$ laminates and has been normalized by a 90^o mismatch, i.e. a [90/0] laminate. Similarly, the least-squares of the experimental results of $[0_5/\theta_5/0_5]$ laminates have been normalized by the delamination area of $[0_5/90_5/0_5]$. It is important to indicate that the lower the impact energy the better the agreement between the hypothesis and the experiments. This verifies that the behavior of a thin composite laminate at low-velocity impact is close to that under quasi-static bending. Accordingly, the delamination area in a thin composite laminate subjected to low-velocity impact can be correlated to the mismatch of bending stiffness. Similar results can also be found in other groups of specimens. Figure 13 shows the comparison between the

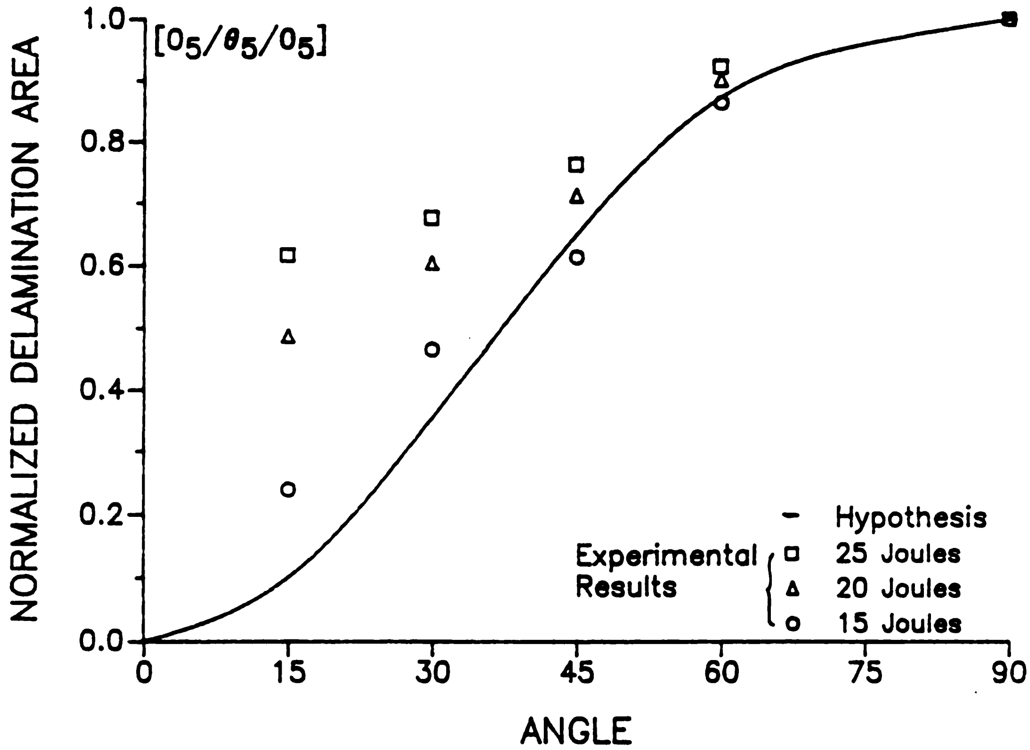

Fig 12 The relationship between the normalized delamination area and the difference of the fiber angle between adjacent laminae

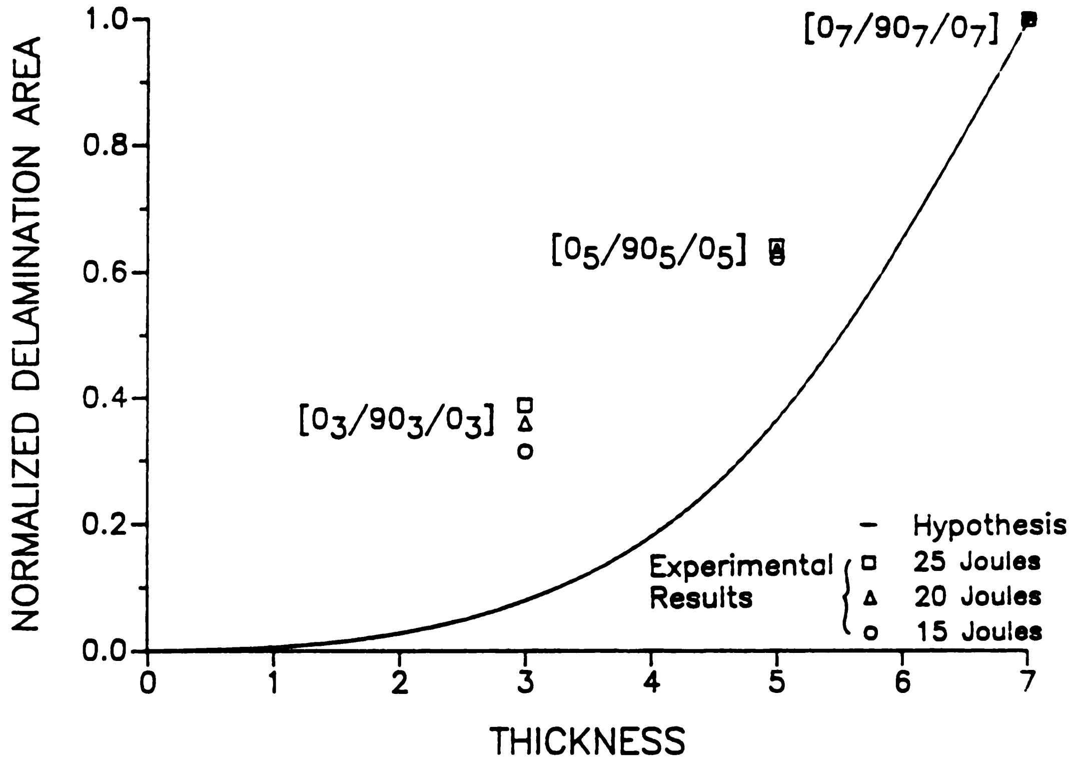

Fig 13 The relationship between the normalized delamination area and thickness of lamina

hypothesis and experimental results for $[0_n/90_n/0_n]$ laminates, in which n is equal to 3, 5, and 7. The overall agreement in Figure 13 doesn't seem to be as good as Figure 12.

B. Table 1 also shows the minimum energy required for delamination initiation. For the composite laminates with stacking sequence of $[0_5/\theta_5/0_5]$, the higher the difference of fiber angle between adjacent laminae, the smaller the initiation energy for delamination. However, this trend is not found in $[\theta_3/0_3/\theta_3]$ laminates. Another trend can be concluded from the study of the effect due to stacking sequence. According to Table 1, if the thickness remains constant, the one with the higher number of interfaces requires higher energy for delamination initiation. For example, the initiation energy of $[0/90/0/\ldots]_{15}$ is higher than that of $[0_3/90_3/0_3/\ldots]_{15}$, which is higher than that of $[0_5/90_5/0_5]$. However, there is no clear trend in the study of thickness effect. The trends of the relationship between initiation energy and stacking sequence provide important information for the design of delamination resistance in composite laminates subjected to low-velocity impact.

C. In an impact event, part of the impact energy is converted into elastic deformation and vibration, which is then dissipated in the form of heat. However, the remaining part of the impact energy is absorbed by the specimen and results in permanent deformation and damage in the specimen. In this study, no energy of dissipation was measured, as well as, damage other than delamination. In ignoring these factors, the relationship between the impact energy per unit delamination area and the impact energy which causes delamination can be established. Figure

14 shows a typical relationship. Apparently, the impact energy per unit delamination area decreases as the impact energy increases in 9-ply and 15-ply laminates. Also shown in Figure 14, the slope (negative) of the 9-ply one is higher than that of the 15-ply one. However, the energy per unit delamination area is independent of the level of impact energy in 21-ply laminates. These results may imply that the energy of dissipation in a 9-ply laminate is higher than that of a 15-ply laminate. And the energy of dissipation in the 21-ply laminate is, either independent of the level of impact energy, or very small.

D. In the study of composite failure, the strain energy release rates such as G_{Ic} [25] and G_{IIc} [23] have been used widely as indicators of energy absorption for a composite material. Neglecting the damage other than delamination and assuming the energy of dissipation to be small, it requires about 0.75 J (from Figure 14) to create a delamination area of one cm^2 in 21-ply glass/epoxy laminates. It is believed that this amount of dynamic fracture energy has a close relation with the critical strain energy release rates of the glass/epoxy laminate. If the energy of dissipation and energy of absorption other than delamination can be known, the energy per unit delamination area obtained from low-velocity impact can be used as an indicator for delamination resistance of the composite material.

E. Typical distributions of the delamination through the thickness for some impacted composite laminates are shown in Figure 15. For $[0_3/90_3/0_3/...]_n$ laminates, the delamination areas in the bottom half, which is the half close to the non-impacted surface, are larger than those in the top half. However, as the number of interfaces increase, the difference in area between the two halves decrease. For the

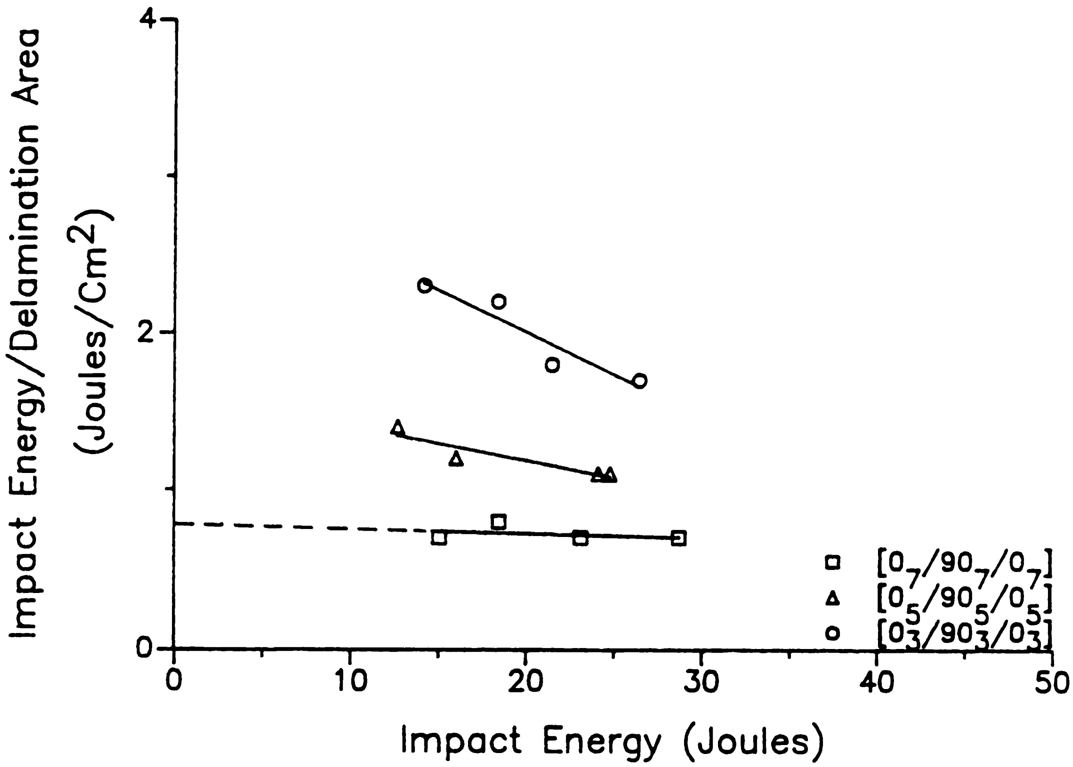

Fig 14 The relationship between the impact energy per unit delamination area and the impact energy which causes delamination

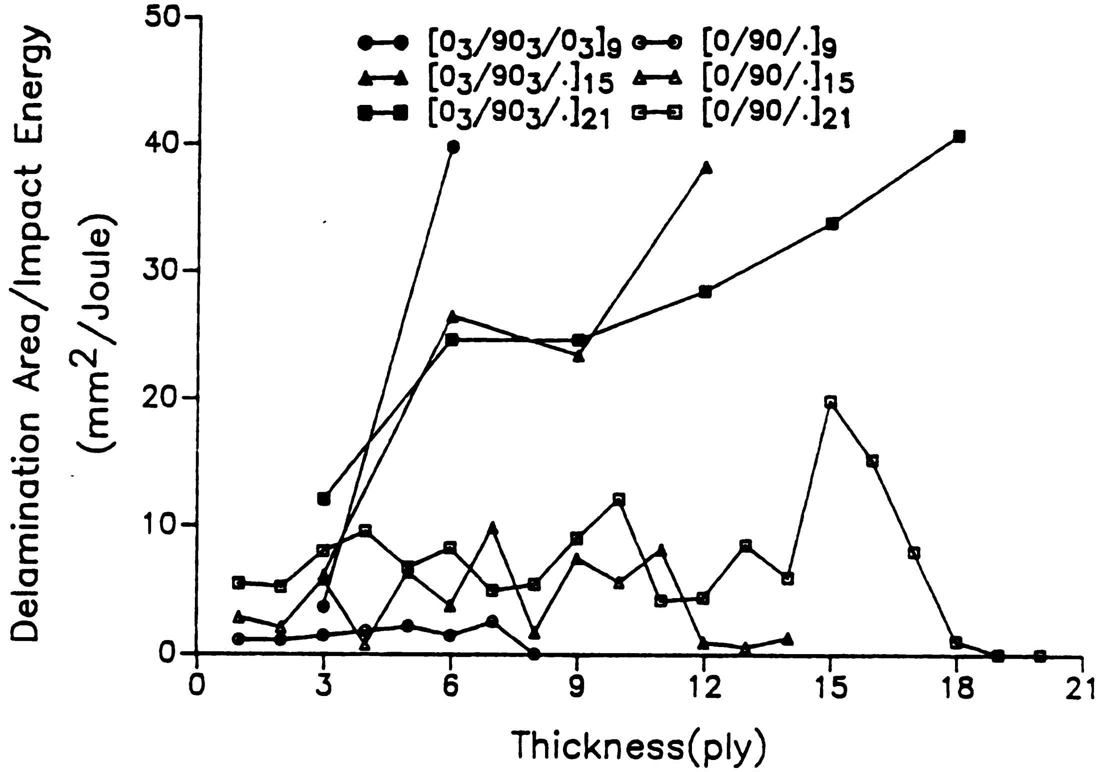

Fig 15 The distributions of the delamination through the thickness of impacted composite laminates

laminates of $[0/90/0/\ldots]_n$, the difference of delamination areas in different interfaces is not as distinct as that of $[0_3/90_3/0_3/\ldots]_n$.

2.5 Summary

This study verified some important delamination mechanisms of composite laminates subjected to low-velocity impact:

A. Peanut-shaped delamination is the fundamental unit of delamination on the composite interface. Its major axis coincides with the fiber direction of the composite lamina beneath the interface.

B. The energy required for delamination initiation increases when the difference of the fiber orientation between adjacent laminae decreases.

C. Experimental results show that a thicker laminate requires less energy for the delamination to grow than a thinner one in low-velocity impact. However, it also implies that a thinner laminate may dissipate more energy than a thicker laminate.

D. The study from stacking sequence points out that it requires more energy for delamination initiation in composite laminates with a higher number of interfaces, even if they have the same thickness.

E. The behavior of a thin composite laminate under low-velocity impact is very similar to that caused by global bending.

Chapter 3

Quasi-static Central Loading

3.1 Quasi-static Loading

From the study of low-velocity impact, it was concluded that when the impact velocity was very low, the behavior of a composite laminate could be very similar to that under static loading. It was the objective of this study to investigate the difference and similarity between low-velocity impact and quasi-static central loading.

In this study, a technique for quasi-static central loading was presented. The specimen dimensions were identical to those used in low-velocity impact while the fixed boundary conditions were changed to simply supported. This change was verified to have no significant effect on damage mode [47]. However, only some cross-ply laminates, as listed in Table 2, were examined.

Figure 16 depicts the experimental set-up for the quasi-static central loading. A steel rod, 12.5 mm in diameter with a spherical nose, was made. An Instron testing machine was used to conduct the quasi-static loading. The speed of the loading head was set to be 0.033 mm/s. In addition, the maximum central force was kept under a level so that delamination did not spread to the specimen boundaries.

3.2 Experimental Results

A. A typical curve for central force and central deflection is shown in Figure 17. There exists a nonlinear relationship between these two parameters. A few discontinuities can also be seen in the curve. They were verified to result from matrix cracking. No other sudden change on the force-deflection curve can be identified as the point of

Table 2: Stacking Sequence of Composite Laminates and Loading Levels for Delamination Initiation in Quasi-static Central Loading

	$[0_3/90_3/0_3]$	$[0_5/90_5/0_5]$	$[0_7/90_7/0_7]$	$[0_3/90_3/0_3/90_3/0_3]$
	0.94 kN	1.16 kN	2.00 kN	0.88 kN
	0.97 kN	1.16 kN	2.06 kN	0.93 kN
	0.97 kN	1.18 kN	2.14 kN	0.92 kN
		1.19 kN		
	1.20 kN	1.40 kN	2.41 kN	
	1.21 kN	1.41 kN	2.42 kN	
		1.42 kN	2.45 kN	
		1.43 kN		
Average:	1.06 kN	1.29 kN	2.24 kN	0.91 kN

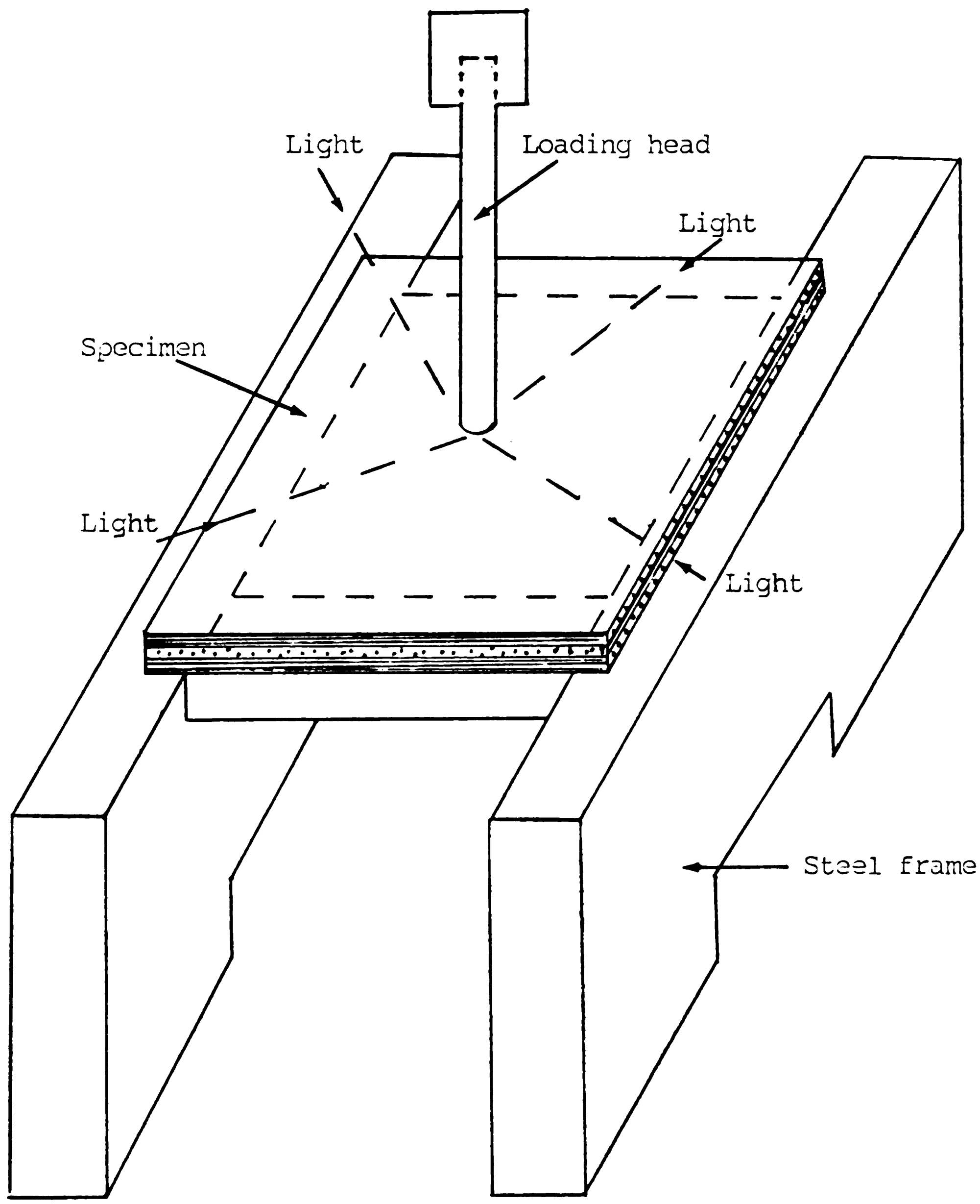

Fig 16 Experimental set-up for quasi-static central loading

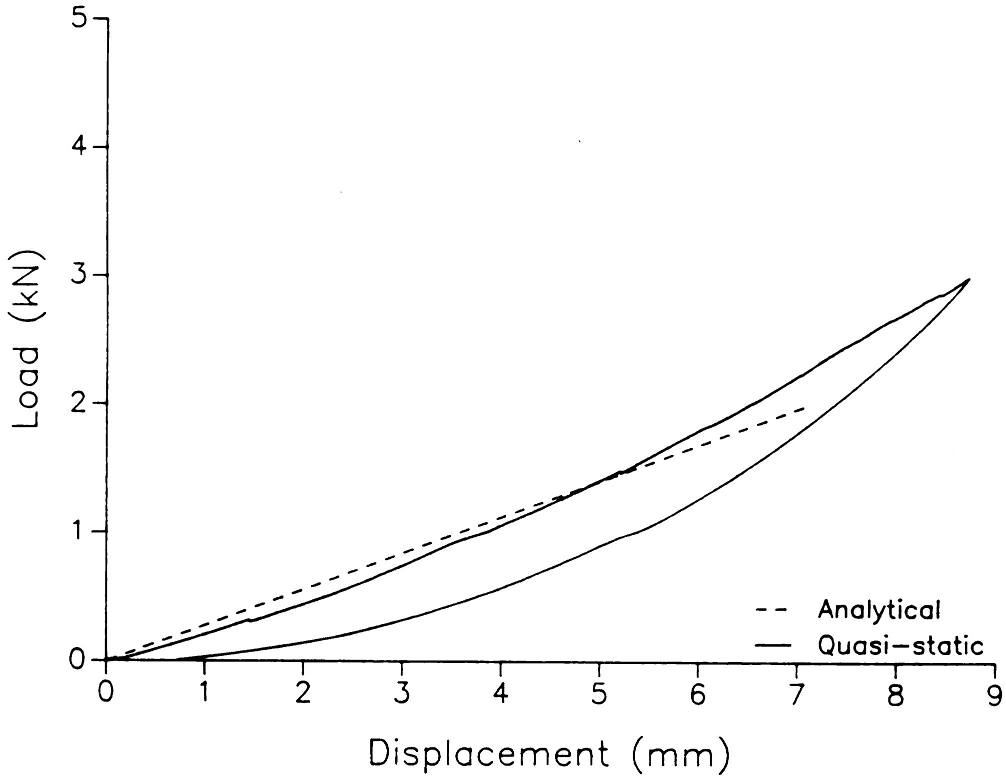

Fig 17 A typical force-deflection curve for central loading

delamination initiation. In other words, delamination due to the quasi-static central loading was of stable fracture. Accordingly, extra effort was required for delamination observation. Figure 16 shows four high-intensity lights beams from the four corners of the steel frame. They proved to be very helpful in identifying the delamination initiation during testing.

B. Delamination was again verified to be the major damage mode. It had the same peanut shape as those from low-velocity impact, shown in Figure 3. In a three-lamina composite laminate, the delamination took place from each side of the central loading on the second interface. It propagated in the x-direction along the centerline of the laminate. The delamination on the first interface occurred later and propagated along the centerline of the laminate in the y-direction. Consequently, the delamination area on the second interface is larger than that on the first interface. This result is similar to that from low-velocity impact. However, the indentation, due to the quasi-static loading, was more severe than those of low-velocity impact. On the contrary, the surface matrix cracking, due to quasi-static loading, was not as dense as that from low-velocity impact. In fact, the matrix cracking spreads entirely on both surfaces of an impacted laminate, while very few cracks appear around the central area in the laminate subjected to quasi-static loading. Figure 18 shows the comparison.

C. The loading levels to cause delamination initiation for different thicknesses and stacking sequences are listed in Table 2. It can be concluded that the thicker the specimen, the higher the force for delamination initiation. In addition to the force to cause delamination initiation, the energy introduced to the specimens is also of interest. It is calculated from the enclosed area of the force-deflection curve.

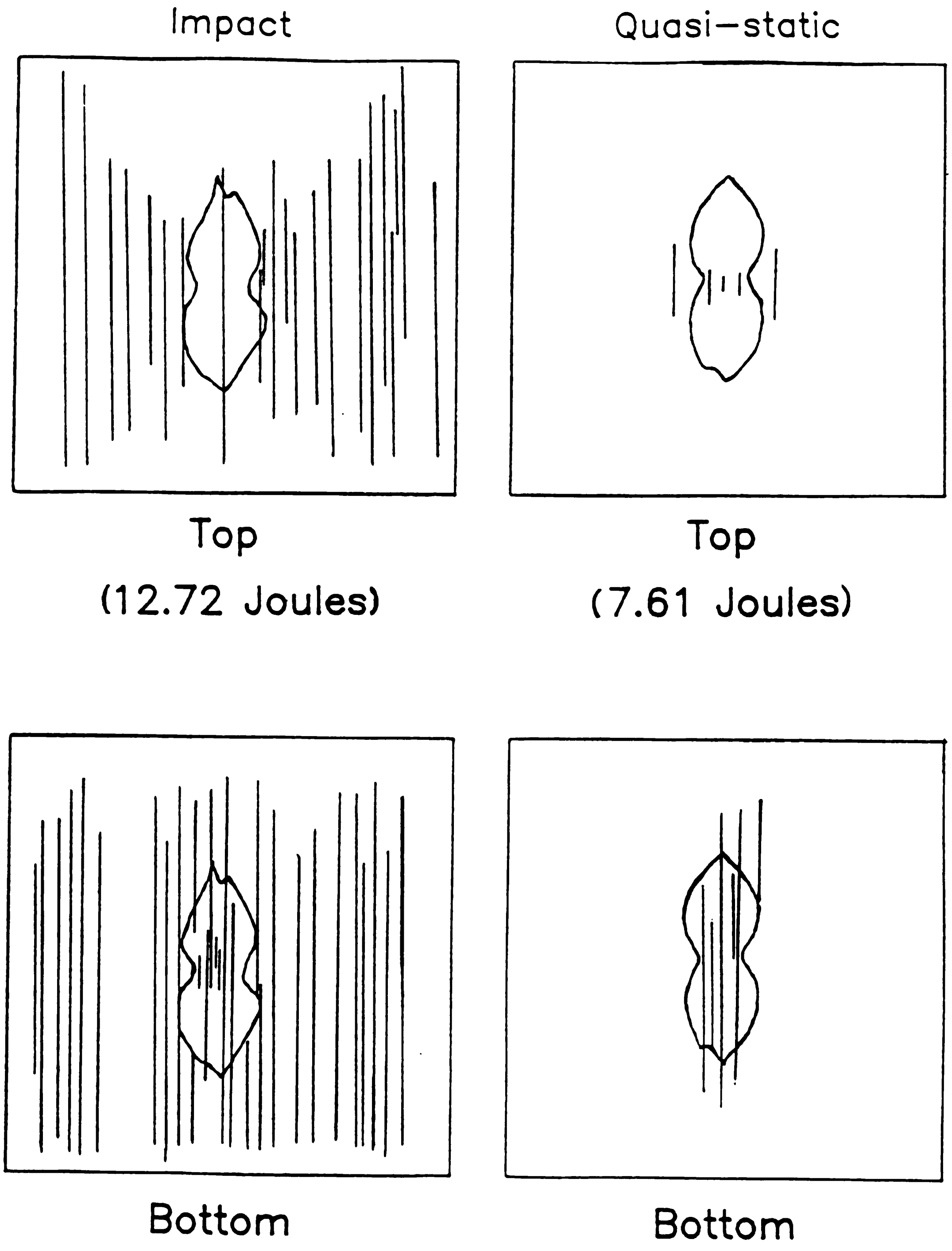

Fig 18 Comparisons of second interface delamination and matrix cracking on top and bottom surfaces of composite laminates subjected to low-velocity impact and quasi-static central loading

Experimental results reveal that, of the same energy, the thicker laminates have larger delamination area than the thinner ones, as shown in Figures 19 and 20. This result is similar to that in low-velocity impact, also shown in the figures.

D. From the study of stacking sequence, it is concluded that it takes a smaller force for a composite laminate with more interfaces to have delamination than one with less interfaces. However, the energy to cause delamination initiation is quite low in both cases.

3.3 Discussions

A. As shown in Figures 19 and 20, the slopes of delamination area versus energy from impact testing are not the same as those from quasi-static loading. It should be noted that there is a difference in the composition of energy between low-velocity impact and quasi-static central loading. In low-velocity impact, vibration energy plays an important role while in quasi-static loading indentation energy.

B. Figure 21 shows the comparison of the critical strain energy release rate between low-velocity impact and quasi-static loading. The result from 21-ply composite laminates subjected to low-velocity impact is around 0.75 J/cm^2. The majority of the results from quasi-static loading is between 0.5 J/cm^2 and 0.75 J/cm^2. The critical strain energy release rate of mode II, G_{IIc}, from End Notch Flexure (ENF), is also presented for reference. It should be noted that the result from ENF is for the second mode, while those from low-velocity impact and quasi-static central loading are of mixed-mode delamination.

3.4 Summary

Although the damage in quasi-static loading is not exactly the same as that in low-velocity impact, delamination is the major damage mode.

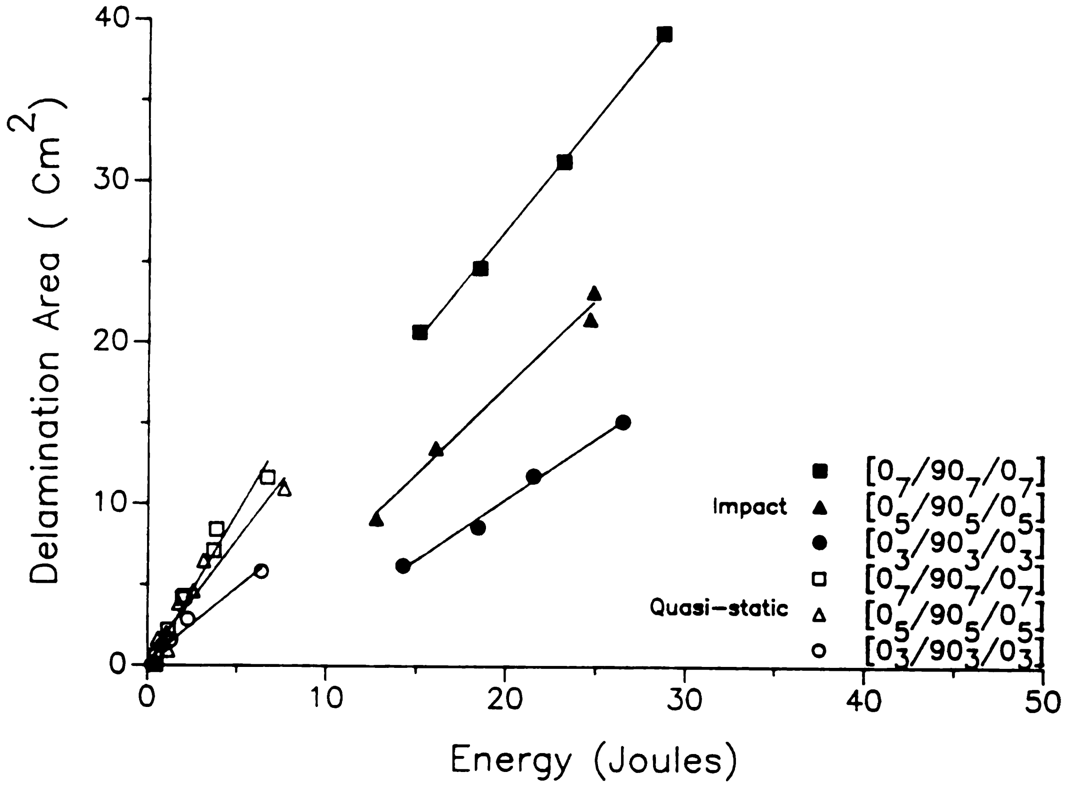

Fig 19 The relationship between delamination area and energy for both low-velocity impact and quasi-static central loading

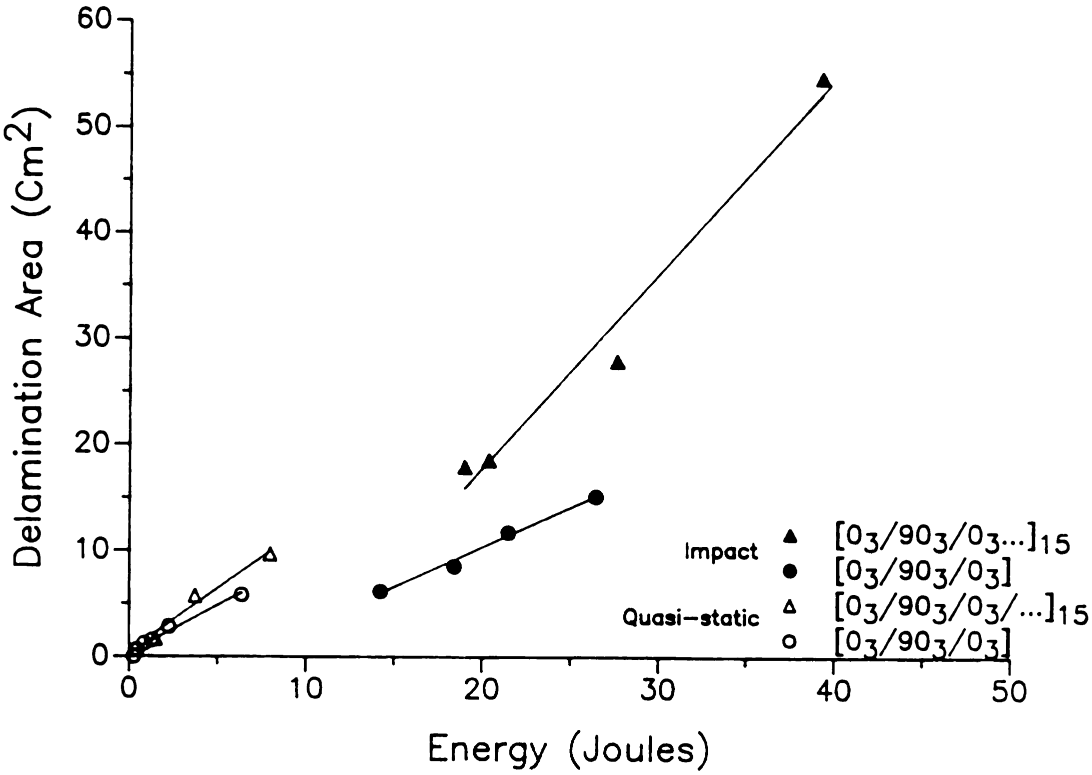

Fig 20 The relationship between delamination area and energy for both low-velocity impact and quasi-static central loading

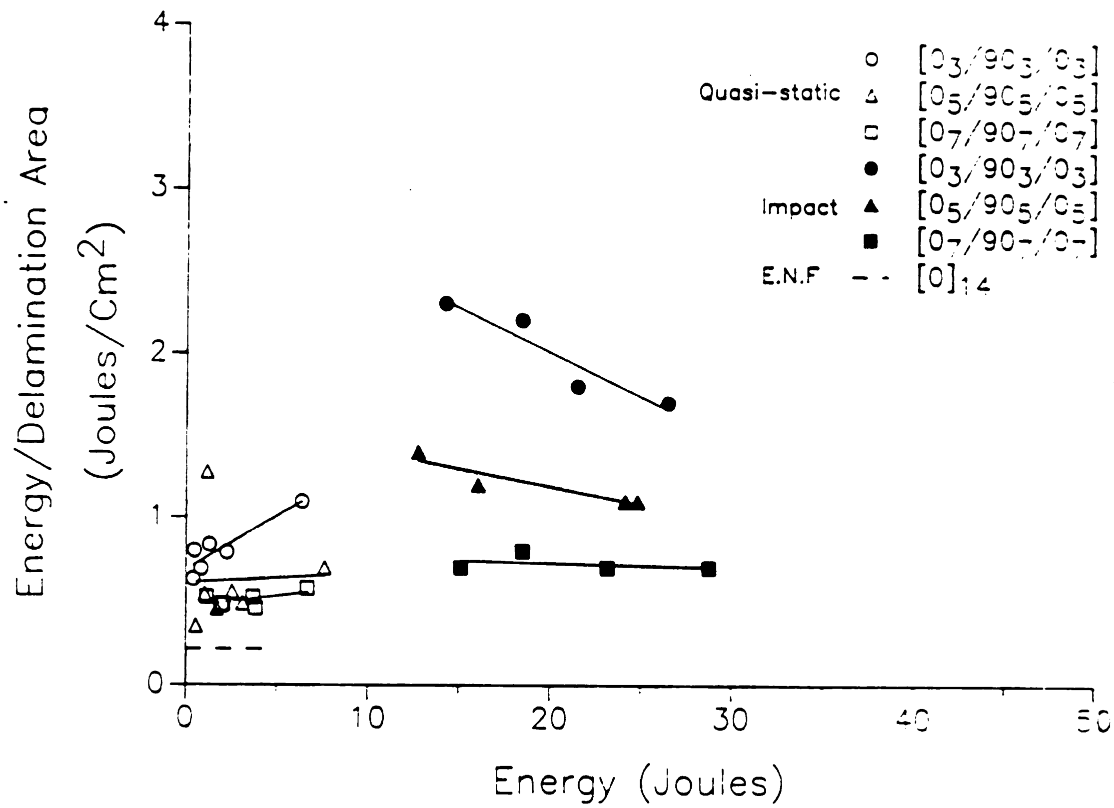

Fig 21 Comparison of the critical strain energy release rates

In addition, several similar results between low-velocity impact and quasi-static loading can be concluded in this study. Accordingly, it is feasible to use quasi-static central loading to study the mechanisms for central delamination. However, due to its nature of stable fracture, extra effort is required to identify the loading level for delamination initiation in the quasi-static loading. In addition, since peanut-shaped delamination is also found in quasi-static central loading, this indicates that the shape is not dependent on the type of loading. Since boundary conditions, different combinations of fiber and matrix, and different types of impacting head have been verified to have no effect on the peanut-shape delamination, dependence on the composite lamination needs to be checked. Consequently, the study regarding the stress state on the composite interface is required.

Chapter 4

Interlaminar Stress Analysis

4.1 A High-order Shear Deformation Theory

Delamination is damage on the composite interface. It has been noted that high interlaminar stresses are responsible for the cause of delamination. Accordingly, in order to understand the delamination initiation, it is important to calculate the stress distribution on the composite interface. Both an elasticity and plate theory [64-65] approach have been successfully used in the stress analysis for composite laminates. Pagano [66] has used three-dimensional elasticity to calculate the interlaminar stresses in a [0/90/0] laminate under sinusoidal loading. Lo, Christensen, and Wu [67-68] and Reddy [69] have also presented closed-form solutions for the same cross-ply laminate. Their approaches are based on high-order plate theories which account for large shear deformation. The high-order theories have been verified to be effective for thick composite laminates or composite laminates with low interlaminar shear moduli. It was found that the in-plane stresses from their high-order theories agree quite well with Pagano's elasticity solutions. However, since through-the-thickness continuity equations are not included in the high-order theories, interlaminar stresses are not continuous between laminae. Lo, Christensen, and Wu have indicated that by using equilibrium equations, instead of constitutive equations, excellent results of interlaminar stresses can be obtained.

In order to examine the effects of interlaminar stresses on delamination initiation, it is important to obtain accurate stresses on the interfaces. A closed-form solution is then desired. However, the technique for a closed-form solution is only valid for cross-ply laminates, i.e., laminates made of 0°, 90°, and isotropic layers. In selecting the solution technique, the advantage and disadvantage of an elasticity approach and plate theory should be compared. Although the elasticity approach can give more accurate results, the plate theory is more flexible for laminates with different kinds of stacking sequence. Therefore, high-order shear deformation theory was chosen for this study. In addition, since the interlaminar normal stress also plays an important role in delamination [14], it is necessary to include high-order terms for displacement in the thickness direction. Among the different theories [67-81] accounted for shear deformation, the following displacement field was used because it satisfied free shear traction on both top and bottom surfaces, and also accounted for through-the-thickness strain.

$$
\begin{aligned}
u_1(x,y,z) &= u^o(x,y)+z\psi_x(x,y)+z^3\phi_x \,, \\
u_2(x,y,z) &= v^o(x,y)+z\psi_y(x,y)+z^3\phi_y \,, \qquad (1) \\
u_3(x,y,z) &= w(x,y)+z^2\zeta_z \,.
\end{aligned}
$$

In this study, linear strain-displacement relations were assumed. Each composite lamina was also assumed to follow the orthotropic constitutive equations, i.e.,

$$
\begin{Bmatrix} \sigma_1 \\ \sigma_2 \\ \sigma_3 \\ \sigma_4 \\ \sigma_5 \\ \sigma_6 \end{Bmatrix}
=
\begin{bmatrix}
C_{11} & C_{12} & C_{13} & 0 & 0 & 0 \\
C_{21} & C_{22} & C_{23} & 0 & 0 & 0 \\
C_{31} & C_{32} & C_{33} & 0 & 0 & 0 \\
0 & 0 & 0 & C_{44} & 0 & 0 \\
0 & 0 & 0 & 0 & C_{55} & 0 \\
0 & 0 & 0 & 0 & 0 & C_{66}
\end{bmatrix}
\begin{Bmatrix} \epsilon_1 \\ \epsilon_2 \\ \epsilon_3 \\ \epsilon_4 \\ \epsilon_5 \\ \epsilon_6 \end{Bmatrix} . \qquad (2)
$$

Using the linear strain-displacement relations and setting the shear tractions to be free for both top and bottom surfaces, i.e.,

$$\sigma_4(x,y,\pm\frac{h}{2})=0 \quad \text{and} \quad \sigma_5(x,y,\pm\frac{h}{2})=0 \ , \tag{3}$$

equation (1) could be further simplified. In fact, if the surface layers of a composite laminate were made of either 0° or 90° ply, equations (3) were equivalent to the requirement that the shear strains be zero on both surfaces. Since

$$\epsilon_4 = \frac{\partial u_2}{\partial z} + \frac{\partial u_3}{\partial y} = \psi_y + 3z^2\phi_y + \frac{\partial w}{\partial y} + z^2\frac{\partial \zeta_z}{\partial y} \ ,$$

$$\epsilon_5 = \frac{\partial u_1}{\partial z} + \frac{\partial u_3}{\partial x} = \psi_x + 3z^2\phi_x + \frac{\partial w}{\partial x} + z^2\frac{\partial \zeta_z}{\partial x} \ , \tag{4}$$

by setting $\epsilon_5(x,y,\pm\frac{h}{2})$ and $\epsilon_4(x,y,\pm\frac{h}{2})$ to zero, it was concluded that

$$\phi_x = -\frac{4}{3h^2}\left(\psi_x + \frac{\partial w}{\partial x} + \frac{h^2}{4}\frac{\partial \zeta_z}{\partial x}\right) \ ,$$

$$\phi_y = -\frac{4}{3h^2}\left(\psi_y + \frac{\partial w}{\partial y} + \frac{h^2}{4}\frac{\partial \zeta_z}{\partial y}\right) \ . \tag{5}$$

The displacement field could then be rewritten as follows:

$$u_1 = u^{o}+z\{\psi_x - \frac{4}{3}(\frac{z}{h})^2[\psi_x + \frac{\partial w}{\partial x} + \frac{h^2}{4}\frac{\partial \zeta_z}{\partial x}]\} \ ,$$

$$u_2 = v^{o}+z\{\psi_y - \frac{4}{3}(\frac{z}{h})^2[\psi_y + \frac{\partial w}{\partial y} + \frac{h^2}{4}\frac{\partial \zeta_z}{\partial y}]\} \ , \tag{6}$$

$$u_3 = w + z^2\zeta_z \ ,$$

where h represents the thickness of the composite laminate. The strain-displacement relations become

$$\epsilon_1 = \epsilon_1^{o} + z(k_1^{o} + z^2k_1^{2}) \ ,$$

$$\epsilon_2 = \epsilon_2^{o} + z(k_2^{o} + z^2k_2^{2}) \ ,$$

$$\epsilon_3 = zk_3^o ,$$

$$\epsilon_4 = k_4^o + z^2 k_4^2 , \tag{7}$$

$$\epsilon_5 = k_5^o + z^2 k_5^2 ,$$

$$\epsilon_6 = \epsilon_6^o + zk_6^o + z^3 k_6^2 , \text{ where}$$

$$\epsilon_1^o = \frac{\partial u^o}{\partial x} , \; k_1^o = \frac{\partial \psi_x}{\partial x} , \; k_1^2 = -\frac{4}{3h^2} \left(\frac{\partial \psi_x}{\partial x} + \frac{\partial^2 w}{\partial x^2} + \frac{h^2}{4} \frac{\partial^2 \varsigma_z}{\partial x^2}\right) ,$$

$$\epsilon_2^o = \frac{\partial v^o}{\partial y} , \; k_2^o = \frac{\partial \psi_y}{\partial y} , \; k_2^2 = -\frac{4}{3h^2} \left(\frac{\partial \psi_y}{\partial y} + \frac{\partial^2 w}{\partial y^2} + \frac{h^2}{4} \frac{\partial^2 \varsigma_z}{\partial y^2}\right), \; k_3^o = 2\varsigma_z ,$$

$$k_4^o = \psi_y + \frac{\partial w}{\partial y} , \; k_4^2 = -\frac{4}{h^2}\left(\psi_y + \frac{\partial w}{\partial y}\right) ,$$

$$k_5^o = \psi_x + \frac{\partial w}{\partial x} , \; k_5^2 = -\frac{4}{h^2}\left(\psi_x + \frac{\partial w}{\partial x}\right) ,$$

$$\epsilon_6^o = \frac{\partial u^o}{\partial y} + \frac{\partial v^o}{\partial x} , \; k_6^o = \frac{\partial \psi_x}{\partial y} + \frac{\partial \psi_y}{\partial x} ,$$

$$k_6^2 = -\frac{4}{3h^2}\left(2\frac{\partial^2 w}{\partial x \partial y} + \frac{\partial \psi_x}{\partial y} + \frac{\partial \psi_y}{\partial x} + \frac{h^2}{2} \frac{\partial^2 \varsigma_z}{\partial x \partial y}\right) .$$

4.2 Governing Equations

In order to formulate the governing equations and boundary conditions, the principle of virtual displacement [82] was used, i.e.,

$$0 = \int_{-\frac{h}{2}}^{\frac{h}{2}} \int_{\Omega} (\sigma_1 \delta\epsilon_1 + \sigma_2 \delta\epsilon_2 + \sigma_3 \delta\epsilon_3 + \sigma_4 \delta\epsilon_4 + \sigma_5 \delta\epsilon_5 + \sigma_6 \delta\epsilon_6)\, dA dz$$

$$- \int_{\Omega} (q\delta w + \tilde{q}\delta\varsigma_z) dA \tag{8}$$

where $\tilde{q} = qh^2/4$. Substituting equations (2) and (7) into equation (8) and using the definition of stress resultants, equation (8) becomes

$$0 = \int_\Omega [\ N_1 \frac{\partial \delta u^o}{\partial x} + M_1 \frac{\partial \delta \psi_x}{\partial x} - \frac{4P_1}{3h^2} (\frac{\partial \delta \psi_x}{\partial x} + \frac{\partial^2 \delta w}{\partial x^2} + \frac{h^2}{4} \frac{\partial^2 \delta \zeta_z}{\partial x^2})$$

$$+ N_2 \frac{\partial \delta v^o}{\partial y} + M_2 \frac{\partial \delta \psi_y}{\partial y} - \frac{4P_2}{3h^2} (\frac{\partial \delta \psi_y}{\partial y} + \frac{\partial^2 \delta w}{\partial y^2} + \frac{h^2}{4} \frac{\partial^2 \delta \zeta_z}{\partial y^2})$$

$$+ 2M_3 \delta \zeta_z + Q_2 (\delta \psi_y + \frac{\partial \delta w}{\partial y}) - \frac{4R_2}{h^2} (\delta \psi_y + \frac{\partial \delta w}{\partial y}) + Q_1 (\delta \psi_x + \frac{\partial \delta w}{\partial x})$$

$$- \frac{4R_1}{h^2} (\delta \psi_x + \frac{\partial \delta w}{\partial x}) + N_6 (\frac{\partial \delta u^o}{\partial x} + \frac{\partial \delta v^o}{\partial y}) + M_6 (\frac{\partial \delta \psi_x}{\partial y} + \frac{\partial \delta \psi_y}{\partial x})$$

$$- \frac{4P_6}{3h^2} (2 \frac{\partial^2 \delta w}{\partial x \partial y} + \frac{\partial \delta \psi_x}{\partial y} + \frac{\partial \delta \psi_y}{\partial x} + \frac{h^2}{2} \frac{\partial^2 \delta \zeta_z}{\partial x \partial y} - q \delta w - \bar{q} \delta \zeta_z] dA \ , \tag{9}$$

where

$$(N_i,\ P_i) = \int_{-\frac{h}{2}}^{\frac{h}{2}} \sigma_i (1, z^3) dz \quad (i = 1,2,6) \ ,$$

$$M_i = \int_{-\frac{h}{2}}^{\frac{h}{2}} \sigma_i (z) dz \quad (i=1,2,3,6) \ , \tag{10}$$

$$(Q_1,\ R_1) = \int_{-\frac{h}{2}}^{\frac{h}{2}} \sigma_5 (1, z^2) dz \ ,$$

$$(Q_2,\ R_2) = \int_{-\frac{h}{2}}^{\frac{h}{2}} \sigma_4 (1, z^2) dz \ .$$

Integrating equation (9) by parts and collecting similar terms, the equilibrium equations in the domain Ω are obtained as follows:

$$\delta u^o: \quad \frac{\partial N_1}{\partial x} + \frac{\partial N_6}{\partial y} = 0 \ ,$$

$$\delta v^o: \quad \frac{\partial N_6}{\partial x} + \frac{\partial N_2}{\partial y} = 0 \ ,$$

$$\delta w: \quad \frac{4}{3h^2}\left(\frac{\partial^2 P_1}{\partial x^2} + \frac{\partial^2 P_2}{\partial y^2} + \frac{2\partial^2 P_6}{\partial x \partial y}\right) + \frac{\partial Q_1}{\partial x} + \frac{\partial Q_2}{\partial y} - \frac{4}{h^2}\left(\frac{\partial R_1}{\partial x} + \frac{\partial R_2}{\partial y}\right) + q = 0 ,$$

$$\delta\psi_x: \quad -\frac{4}{3h^2}\left(\frac{\partial P_1}{\partial x} + \frac{\partial P_6}{\partial y} - 3R_1\right) + \frac{\partial M_1}{\partial x} + \frac{\partial M_6}{\partial y} - Q_1 = 0 , \qquad (11)$$

$$\delta\psi_y: \quad -\frac{4}{3h^2}\left(\frac{\partial P_2}{\partial y} + \frac{\partial P_6}{\partial x} - 3R_2\right) + \frac{\partial M_2}{\partial y} + \frac{\partial M_6}{\partial x} - Q_2 = 0 ,$$

$$\delta\zeta_z: \quad \frac{1}{3}\left(\frac{\partial^2 P_1}{\partial x^2} + \frac{\partial^2 P_2}{\partial y^2} + \frac{2\partial^2 P_6}{\partial x \partial y} - 6M_3\right) + \tilde{q} = 0 .$$

The boundary conditions to be specified are

$$u_n \text{ or } N_n ,$$

$$u_{ns} \text{ or } N_{ns} ,$$

$$w \text{ or } Q_n ,$$

$$\frac{\partial w}{\partial n} \text{ or } P_n ,$$

$$\psi_n \text{ or } M_n , \qquad (12)$$

$$\psi_{ns} \text{ or } M_{ns} ,$$

$$\zeta_z \text{ or } \frac{\partial P_{ns}}{\partial ns} ,$$

$$\frac{\partial \zeta_z}{\partial n} \text{ or } P_n , \text{ and}$$

$$u_n = \overset{o}{u} n_x + \overset{o}{v} n_y , \quad u_{ns} = -\overset{o}{u} n_y + \overset{o}{v} n_x ,$$

$$\overset{o}{u} = u_n n_x - u_{ns} n_y , \quad \overset{o}{v} = u_n n_y + u_{ns} n_x ,$$

$$\frac{\partial}{\partial n} = n_x \frac{\partial}{\partial x} + n_y \frac{\partial}{\partial y} , \quad \frac{\partial}{\partial ns} = n_x \frac{\partial}{\partial y} - n_y \frac{\partial}{\partial x} ,$$

$$\frac{\partial}{\partial x} = n_x \frac{\partial}{\partial n} - n_y \frac{\partial}{\partial ns} , \quad \frac{\partial}{\partial y} = n_y \frac{\partial}{\partial n} + n_x \frac{\partial}{\partial ns} ,$$

$$N_n = N_1 n_x^2 + N_2 n_y^2 + 2N_6 n_x n_y , \quad N_{ns} = (N_2 - N_1) n_x n_y + N_6 (n_x^2 - n_y^2) ,$$

$$P_n = P_1 n_x^2 + P_2 n_y^2 + 2P_6 n_x n_y,\quad P_{ns} = (P_2 - P_1) n_x n_y + P_6 (n_x^2 - n_y^2)\ , \tag{13}$$

$$M_n = \hat{M}_1 n_x^2 + \hat{M}_2 n_y^2 + 2\hat{M}_6 n_x n_y\ ,\quad M_{ns} = (\hat{M}_2 - \hat{M}_1) n_x n_y + \hat{M}_6 (n_x^2 - n_y^2)\ ,$$

$$Q_n = \hat{Q}_1 n_x + \hat{Q}_2 n_y - \frac{4}{3h^2} \frac{\partial P_{ns}}{\partial ns},$$

$$\hat{M}_i = M_i - \frac{4}{3h^2} P_i \quad (i=1,2,6)\ ,\quad \hat{Q}_i = Q_i - \frac{4}{3h^2} R_i \quad (i=1,2)\ .$$

The relations between the stress resultants, strains, and curvatures could then be expressed in terms of laminate stiffnesses:

$$\left\{\begin{array}{c} \begin{bmatrix} N_1 \\ N_2 \\ N_6 \end{bmatrix} \\ \begin{bmatrix} M_1 \\ M_2 \\ M_3 \\ M_6 \end{bmatrix} \\ \begin{bmatrix} P_1 \\ P_2 \\ P_6 \end{bmatrix} \end{array}\right\} = \left(\begin{array}{ccc} \begin{bmatrix} A_{11} & A_{12} & A_{16} \\ A_{12} & A_{22} & A_{26} \\ A_{16} & A_{26} & A_{66} \end{bmatrix} & \begin{bmatrix} B_{11} & B_{12} & B_{13} & B_{16} \\ B_{12} & B_{22} & B_{23} & B_{26} \\ B_{16} & B_{26} & B_{36} & B_{66} \end{bmatrix} & \begin{bmatrix} E_{11} & E_{12} & E_{16} \\ E_{12} & E_{22} & E_{26} \\ E_{16} & E_{26} & E_{66} \end{bmatrix} \\ \begin{bmatrix} B_{11} & B_{12} & B_{16} \\ B_{12} & B_{22} & B_{26} \\ B_{13} & B_{23} & B_{36} \\ B_{16} & B_{26} & B_{66} \end{bmatrix} & \begin{bmatrix} D_{11} & D_{12} & D_{13} & D_{16} \\ D_{12} & D_{22} & D_{23} & D_{26} \\ D_{13} & D_{23} & D_{33} & D_{36} \\ D_{16} & D_{26} & D_{36} & D_{66} \end{bmatrix} & \begin{bmatrix} F_{11} & F_{12} & F_{16} \\ F_{12} & F_{22} & F_{26} \\ F_{13} & F_{23} & F_{36} \\ F_{16} & F_{26} & F_{66} \end{bmatrix} \\ \begin{bmatrix} E_{11} & E_{12} & E_{16} \\ E_{12} & E_{22} & E_{26} \\ E_{16} & E_{26} & E_{66} \end{bmatrix} & \begin{bmatrix} F_{11} & F_{12} & F_{13} & F_{16} \\ F_{12} & F_{22} & F_{23} & F_{26} \\ F_{16} & F_{26} & F_{36} & F_{66} \end{bmatrix} & \begin{bmatrix} H_{11} & H_{12} & H_{16} \\ H_{12} & H_{22} & H_{26} \\ H_{16} & H_{26} & H_{66} \end{bmatrix} \end{array}\right) \left\{\begin{array}{c} \begin{bmatrix} \epsilon_1^o \\ \epsilon_2^o \\ \epsilon_6^o \end{bmatrix} \\ \begin{bmatrix} k_1^o \\ k_2^o \\ k_3^o \\ k_6^o \end{bmatrix} \\ \begin{bmatrix} k_1^2 \\ k_2^2 \\ k_6^o \end{bmatrix} \end{array}\right\}$$

$$\begin{Bmatrix} Q_2 \\ Q_1 \\ R_2 \\ R_1 \end{Bmatrix} = \begin{bmatrix} A_{44} & A_{45} & D_{44} & D_{45} \\ A_{45} & A_{55} & D_{45} & D_{55} \\ D_{44} & D_{45} & F_{44} & F_{45} \\ D_{45} & D_{55} & F_{45} & F_{55} \end{bmatrix} \begin{Bmatrix} k_4^o \\ k_5^o \\ k_4^2 \\ k_5^2 \end{Bmatrix}\ , \tag{14}$$

where A_{ij}, B_{ij}, D_{ij}, E_{ij}, F_{ij}, and H_{ij} are defined as:

$$(A_{ij},\ E_{ij},\ H_{ij}) = \int_{-\frac{h}{2}}^{\frac{h}{2}} \bar{C}_{ij} (1, z^3, z^6) dz \quad (i,j=1,2,6)\ , \tag{15}$$

$$(B_{ij},\ D_{ij},\ F_{ij}) = \int_{-\frac{h}{2}}^{\frac{h}{2}} \bar{C}_{ij}(z,z^2,z^4)dz \quad (i,j=1,2,3,6) ,$$

$$(A_{ij},\ D_{ij},\ F_{ij}) = \int_{-\frac{h}{2}}^{\frac{h}{2}} \bar{C}_{ij}(1,z^2,z^4)dz \quad (i,j=4,5) ,$$

and $\bar{C}_{ij}$ is the transformed (from C_{ij}) stiffness matrix.

4.3 Closed-form Solution

In this study, the objective was to find the stress states in symmetric cross-ply laminates with dimensions of a by a, shown in Figure 22. Accordingly,

$B_{ij}=E_{ij}=0$ for $i,j=1,2,3,4,5,6$ and

$$A_{16}=A_{26}=D_{16}=D_{26}=F_{16}=F_{26}=F_{36}=H_{16}=H_{26}=A_{45}=D_{45}=F_{45}=0 . \qquad (16)$$

In addition, for the simply supported case, the boundary conditions are:

$$w(x,0)=w(x,a)=w(0,y)=w(a,y)=0 ,$$

$$P_2(x,0)=P_2(x,a)=P_1(0,y)=P_1(a,y)=0 ,$$

$$M_2(x,0)=M_2(x,a)=M_1(0,y)=M_1(a,y)=0 , \qquad (17)$$

$$\psi_x(x,0)=\psi_x(x,a)=\psi_y(0,y)=\psi_y(a,y)=0 ,$$

$$\zeta_z(x,0)=\zeta_z(x,a)=\zeta_z(0,y)=\zeta_z(a,y)=0 .$$

The resultant forces of equation (14) were expressed, for symmetric cross-ply laminates, in terms of displacements as follows:

$$N_1 = A_{11}\frac{\partial u^o}{\partial x} + A_{12}\frac{\partial v^o}{\partial y} ,$$

$$N_2 = A_{12}\frac{\partial u^o}{\partial x} + A_{22}\frac{\partial v^o}{\partial y} ,$$

$$N_6 = A_{66}\left(\frac{\partial u^o}{\partial y} + \frac{\partial v^o}{\partial x}\right) ,$$

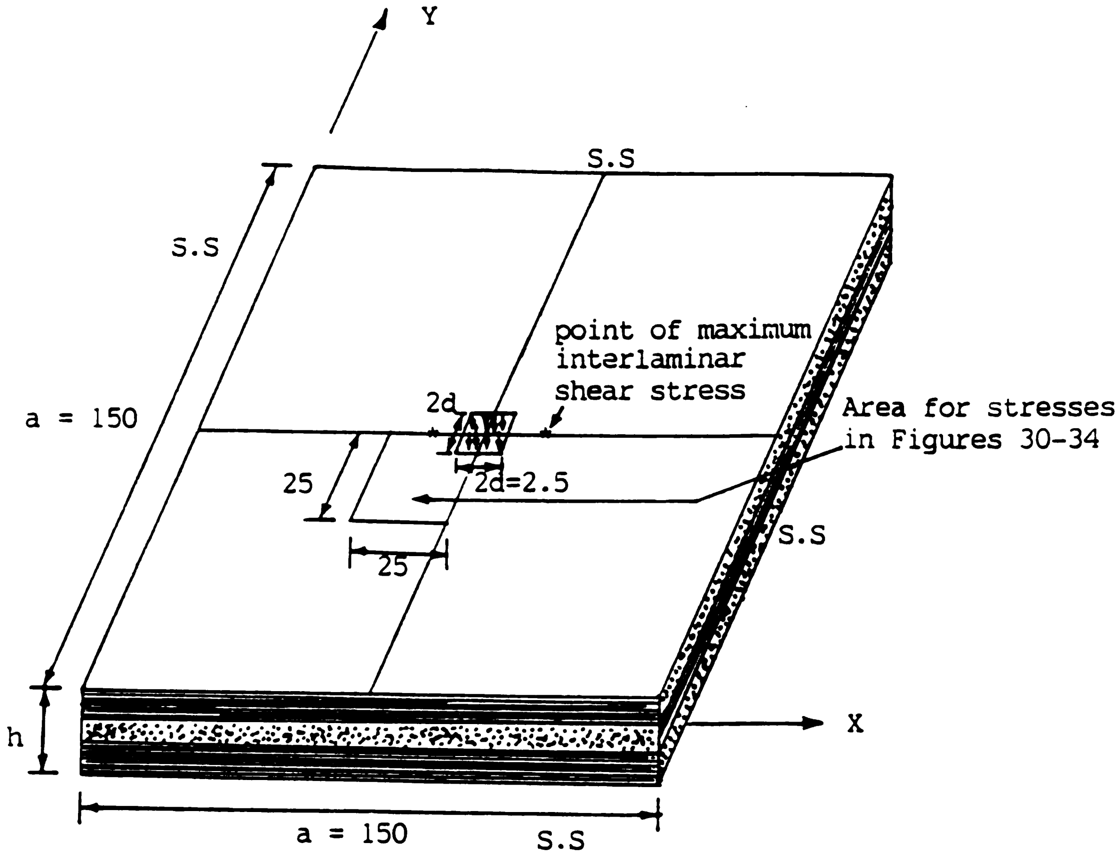

Fig 22 Dimensions of a composite laminate under central loading
All dimensions are in mm

$$M_1 = D_{11}\frac{\partial \psi_x}{\partial x} + D_{12}\frac{\partial \psi_y}{\partial y} + 2D_{13}\zeta_z + F_{11}\left[-\frac{4}{3h^2}\left(\frac{\partial \psi_x}{\partial x} + \frac{\partial^2 w}{\partial x^2} + \frac{h^2}{4}\frac{\partial^2 \zeta_z}{\partial x^2}\right)\right]$$

$$+ F_{12}\left[-\frac{4}{3h^2}\left(\frac{\partial \psi_y}{\partial y} + \frac{\partial^2 w}{\partial y^2} + \frac{h^2}{4}\frac{\partial^2 \zeta_z}{\partial y^2}\right)\right] ,$$

$$M_2 = D_{12}\frac{\partial \psi_x}{\partial x} + D_{22}\frac{\partial \psi_y}{\partial y} + 2D_{23}\zeta_z + F_{12}\left[-\frac{4}{3h^2}\left(\frac{\partial \psi_x}{\partial x} + \frac{\partial^2 w}{\partial x^2} + \frac{h^2}{4}\frac{\partial^2 \zeta_z}{\partial x^2}\right)\right]$$

$$+ F_{22}\left[-\frac{4}{3h^2}\left(\frac{\partial \psi_y}{\partial y} + \frac{\partial^2 w}{\partial y^2} + \frac{h^2}{4}\frac{\partial^2 \zeta_z}{\partial y^2}\right)\right] ,$$

$$M_3 = D_{13}\frac{\partial \psi_x}{\partial x} + D_{23}\frac{\partial \psi_y}{\partial y} + 2D_{33}\zeta_z + F_{13}\left[-\frac{4}{3h^2}\left(\frac{\partial \psi_x}{\partial x} + \frac{\partial^2 w}{\partial x^2} + \frac{h^2}{4}\frac{\partial^2 \zeta_z}{\partial x^2}\right)\right]$$

$$+ F_{23}\left[-\frac{4}{3h^2}\left(\frac{\partial \psi_y}{\partial y} + \frac{\partial^2 w}{\partial y^2} + \frac{h^2}{4}\frac{\partial^2 \zeta_z}{\partial y^2}\right)\right] ,$$

$$M_6 = D_{66}\left(\frac{\partial \psi_x}{\partial y} + \frac{\partial \psi_y}{\partial x}\right) + F_{66}\left[-\frac{4}{3h^2}\left(2\frac{\partial^2 w}{\partial x \partial y} + \frac{\partial \psi_x}{\partial y} + \frac{\partial \psi_y}{\partial x} + \frac{h^2}{2}\frac{\partial^2 \zeta_z}{\partial x \partial y}\right)\right] ,$$

$$Q_1 = A_{55}\left(\psi_x + \frac{\partial w}{\partial x}\right) + D_{55}\left[-\frac{4}{h^2}\left(\psi_x + \frac{\partial w}{\partial x}\right)\right] ,$$

$$Q_2 = A_{44}\left(\psi_y + \frac{\partial w}{\partial y}\right) + D_{44}\left[-\frac{4}{h^2}\left(\psi_y + \frac{\partial w}{\partial y}\right)\right] ,$$

$$R_1 = D_{55}\left(\psi_x + \frac{\partial w}{\partial x}\right) + F_{55}\left[-\frac{4}{h^2}\left(\psi_x + \frac{\partial w}{\partial x}\right)\right] ,$$

$$R_2 = D_{44}\left(\psi_y + \frac{\partial w}{\partial y}\right) + F_{44}\left[-\frac{4}{h^2}\left(\psi_y + \frac{\partial w}{\partial y}\right)\right] ,$$

$$P_1 = F_{11}\frac{\partial \psi_x}{\partial x} + F_{12}\frac{\partial \psi_y}{\partial y} + 2F_{13}\zeta_z + H_{11}\left[-\frac{4}{3h^2}\left(\frac{\partial \psi_x}{\partial x} + \frac{\partial^2 w}{\partial x^2} + \frac{h^2}{4}\frac{\partial^2 \zeta_z}{\partial x^2}\right)\right]$$

$$+ H_{12}\left[-\frac{4}{3h^2}\left(\frac{\partial \psi_y}{\partial y} + \frac{\partial^2 w}{\partial y^2} + \frac{h^2}{4}\frac{\partial^2 \zeta_z}{\partial y^2}\right)\right] ,$$

$$P_2 = F_{12}\frac{\partial\psi_x}{\partial x} + F_{22}\frac{\partial\psi_y}{\partial y} + 2F_{23}\zeta_z + H_{12}\left[-\frac{4}{3h^2}\left(\frac{\partial\psi_x}{\partial x} + \frac{\partial^2 w}{\partial x^2} + \frac{h^2}{4}\frac{\partial^2\zeta_z}{\partial x^2}\right)\right]$$

$$+ H_{22}\left[-\frac{4}{3h^2}\left(\frac{\partial\psi_y}{\partial y} + \frac{\partial^2 w}{\partial y^2} + \frac{h^2}{4}\frac{\partial^2\zeta_z}{\partial y^2}\right)\right] ,$$

$$P_6 = F_{66}\left(\frac{\partial\psi_x}{\partial y} + \frac{\partial\psi_y}{\partial x}\right) + H_{66}\left[-\frac{4}{3h^2}\left(2\frac{\partial^2 w}{\partial x\partial y} + \frac{\partial\psi_x}{\partial y} + \frac{\partial\psi_y}{\partial x} + \frac{h^2}{2}\frac{\partial^2\zeta_z}{\partial x\partial y}\right)\right] . \quad (18)$$

In order to simulate a central loading, the composite laminates were loaded by a static force at a small area 2d by 2d around the center of the plate. The force is expressed by a double Fourier series:

$$q = \sum_{m,n=1}^{\infty} Q_{mn}\sin\alpha x \sin\beta y \quad (19)$$

where $Q_{mn} = \frac{16P_o}{mn\pi^2}\sin\frac{\alpha a}{2}\sin\alpha d\sin\frac{\beta a}{2}\sin\beta d$, P_o the intensity of the force in the loading area, $\alpha = \frac{m\pi}{a}$, and $\beta = \frac{n\pi}{a}$. The technique of Navier's solution was used in this study. For small deformation, there was no interaction between in-plane deformations and out-of-plane loading; therefore, the first two governing equations in equation (11) were automatically satisfied. Accordingly, only four governing equations needed to be considered. By using double Fourier series, the displacement parameters w, ψ_x, ψ_y, and ζ_z are be expressed as follows:

$$w = \sum_{m,n=1}^{\infty} W_{mn}\sin\alpha x \sin\beta y$$

$$\psi_x = \sum_{m,n=1}^{\infty} X_{mn}\cos\alpha x \sin\beta y$$

$$\psi_y = \sum_{m,n=1}^{\infty} Y_{mn}\sin\alpha x \cos\beta y \quad (20)$$

$$\zeta_z = \sum_{m,n=1}^{\infty} Z_{mn}\sin\alpha x \sin\beta y .$$

By using equation (18), the remaining four equations of equation (10) become

$$D_{11}\frac{\partial^2\psi_x}{\partial x^2} + D_{12}\frac{\partial^2\psi_y}{\partial x\partial y} + 2D_{13}\frac{\partial\zeta_z}{\partial x} - \frac{4F_{11}}{3h^2}\left(\frac{\partial^2\psi_x}{\partial x^2} + \frac{\partial^3 w}{\partial x^3} + \frac{h^2}{4}\frac{\partial^3\zeta_z}{\partial x^3}\right)$$

$$+ D_{66}\left(\frac{\partial^2\psi_x}{\partial y^2} + \frac{\partial^2\psi_y}{\partial x\partial y}\right) - A_{55}\left(\psi_x + \frac{\partial w}{\partial x}\right) + D_{55}\left(\frac{8}{h^2}\right)\left(\psi_x + \frac{\partial w}{\partial x}\right)$$

$$- \frac{4F_{12}}{3h^2}\left(\frac{\partial^2\psi_y}{\partial x\partial y} + \frac{\partial^3 w}{\partial x\partial y^2} + \frac{h^2}{4}\frac{\partial^3\zeta_z}{\partial x\partial y^2}\right) - \frac{4F_{66}}{3h^2}\left(\frac{\partial^2\psi_x}{\partial y^2} + \frac{\partial^2\psi_y}{\partial x\partial y} + 2\frac{\partial^3 w}{\partial x\partial y^2} + \frac{h^2}{2}\frac{\partial^3\zeta_z}{\partial x\partial y^2}\right)$$

$$-F_{55}\left(\frac{16}{h^4}\right)\left(\psi_x + \frac{\partial w}{\partial x}\right) - \frac{4}{3h^2}\Big[F_{11}\frac{\partial^2\psi_x}{\partial x^2} + F_{12}\frac{\partial^2\psi_y}{\partial x\partial y} + 2F_{13}\frac{\partial\zeta_z}{\partial x}$$

$$- \frac{4H_{11}}{3h^2}\left(\frac{\partial^2\psi_x}{\partial x^2} + \frac{\partial^3 w}{\partial x^3} + \frac{h^2}{4}\frac{\partial^3\zeta_z}{\partial x^3}\right) - \frac{4H_{12}}{3h^2}\left(\frac{\partial^2\psi_y}{\partial x\partial y} + \frac{\partial^3 w}{\partial x\partial y^2} + \frac{h^2}{4}\frac{\partial^3\zeta_z}{\partial x\partial y^2}\right)$$

$$+F_{66}\left(\frac{\partial^2\psi_x}{\partial y^2} + \frac{\partial^2\psi_y}{\partial x\partial y}\right) - \frac{4H_{66}}{3h^2}\left(\frac{\partial^2\psi_y}{\partial x\partial y} + 2\frac{\partial^3 w}{\partial x\partial y^2} + \frac{h^2}{2}\frac{\partial^3\zeta_z}{\partial x\partial y^2} + \frac{\partial^2\psi_x}{\partial y^2}\right)\Big] = 0 \qquad (21a)$$

$$D_{22}\frac{\partial^2\psi_y}{\partial y^2} + D_{12}\frac{\partial^2\psi_x}{\partial x\partial y} + 2D_{23}\frac{\partial\zeta_z}{\partial y} - \frac{4F_{22}}{3h^2}\left(\frac{\partial^2\psi_y}{\partial y^2} + \frac{\partial^3 w}{\partial y^3} + \frac{h^2}{4}\frac{\partial^3\zeta_z}{\partial y^3}\right)$$

$$+ D_{66}\left(\frac{\partial^2\psi_y}{\partial x^2} + \frac{\partial^2\psi_x}{\partial x\partial y}\right) - A_{44}\left(\psi_y + \frac{\partial w}{\partial y}\right) + D_{44}\left(\frac{8}{h^2}\right)\left(\psi_y + \frac{\partial w}{\partial y}\right)$$

$$- \frac{4F_{12}}{3h^2}\left(\frac{\partial^2\psi_y}{\partial x\partial y} + \frac{\partial^3 w}{\partial y\partial x^2} + \frac{h^2}{4}\frac{\partial^3\zeta_z}{\partial y\partial x^2}\right) - \frac{4F_{66}}{3h^2}\left(\frac{\partial^2\psi_y}{\partial x^2} + \frac{\partial^2\psi_x}{\partial x\partial y} + 2\frac{\partial^3 w}{\partial y\partial x^2} + \frac{h^2}{2}\frac{\partial^3\zeta_z}{\partial y\partial x^2}\right)$$

$$-F_{44}\left(\frac{16}{h^4}\right)\left(\psi_y + \frac{\partial w}{\partial y}\right) - \frac{4}{3h^2}\Big[F_{22}\frac{\partial^2\psi_y}{\partial y^2} + F_{12}\frac{\partial^2\psi_x}{\partial x\partial y} + 2F_{23}\frac{\partial\zeta_z}{\partial y}$$

$$- \frac{4H_{22}}{3h^2}\left(\frac{\partial^2\psi_y}{\partial y^2} + \frac{\partial^3 w}{\partial y^3} + \frac{h^2}{4}\frac{\partial^3\zeta_z}{\partial y^3}\right) - \frac{4H_{12}}{3h^2}\left(\frac{\partial^2\psi_x}{\partial x\partial y} + \frac{\partial^3 w}{\partial y\partial x^2} + \frac{h^2}{4}\frac{\partial^3\zeta_z}{\partial y\partial x^2}\right)$$

$$+F_{66}\left(\frac{\partial^2\psi_y}{\partial x^2} + \frac{\partial^2\psi_x}{\partial x\partial y}\right) - \frac{4H_{66}}{3h^2}\left(\frac{\partial^2\psi_x}{\partial x\partial y} + 2\,\frac{\partial^3 w}{\partial y\partial x^2} + \frac{h^2}{2}\,\frac{\partial^3\zeta_z}{\partial y\partial x^2} + \frac{\partial^2\psi_y}{\partial x^2}\right)] = 0$$

(21b)

$$A_{55}\left(\frac{\partial\psi_x}{\partial x} + \frac{\partial^2 w}{\partial x^2}\right) + A_{44}\left(\frac{\partial\psi_y}{\partial y} + \frac{\partial^2 w}{\partial y^2}\right) - \frac{4}{h^2}[\ 2D_{55}\left(\frac{\partial\psi_x}{\partial x} + \frac{\partial^2 w}{\partial x^2}\right)$$

$$- F_{55}\left(\frac{4}{h^2}\right)\left(\frac{\partial\psi_x}{\partial x} + \frac{\partial^2 w}{\partial x^2}\right) + 2D_{44}\left(\frac{\partial\psi_y}{\partial y} + \frac{\partial^2 w}{\partial y^2}\right) - F_{44}\left(\frac{4}{h^2}\right)\left(\frac{\partial\psi_y}{\partial y} + \frac{\partial^2 w}{\partial y^2}\right)]$$

$$+ \frac{4}{3h^2}[F_{11}\frac{\partial^3\psi_x}{\partial x^3} + F_{12}\frac{\partial^3\psi_y}{\partial y\partial x^2} + 2F_{13}\,\frac{\partial^2\zeta_z}{\partial x^2}$$

$$- \frac{4H_{11}}{3h^2}\left(\frac{\partial^3\psi_x}{\partial x^3} + \frac{\partial^4 w}{\partial x^4} + \frac{h^2}{4}\,\frac{\partial^4\zeta_z}{\partial x^4}\right) - \frac{4H_{12}}{3h^2}\left(\frac{\partial^3\psi_y}{\partial y\partial x^2} + \frac{\partial^4 w}{\partial y^2\partial x^2} + \frac{h^2}{4}\,\frac{\partial^4\zeta_z}{\partial y^2\partial x^2}\right)$$

$$+2F_{66}\left(\frac{\partial^3\psi_y}{\partial y\partial x^2} + \frac{\partial^3\psi_x}{\partial x\mu y^2}\right) - \frac{8H_{66}}{3h^2}\left(\frac{\partial^3\psi_x}{\partial x\partial y^2} + 2\,\frac{\partial^4 w}{\partial y^2\partial x^2} + \frac{h^2}{2}\,\frac{\partial^4\zeta_z}{\partial y^2\partial x^2} + \frac{\partial^3\psi_y}{\partial y\partial x^2}\right)$$

$$+F_{22}\frac{\partial^3\psi_y}{\partial y^3} + F_{12}\frac{\partial^3\psi_x}{\partial x\partial y^2} + 2F_{23}\,\frac{\partial^2\zeta_z}{\partial y^2} - \frac{4H_{22}}{3h^2}\left(\frac{\partial^3\psi_y}{\partial y^3} + \frac{\partial^4 w}{\partial y^4} + \frac{h^2}{4}\,\frac{\partial^4\zeta_z}{\partial y^4}\right)$$

$$- \frac{4H_{12}}{3h^2}\left(\frac{\partial^3\psi_x}{\partial x\partial y^2} + \frac{\partial^4 w}{\partial y^2\partial x^2} + \frac{h^2}{4}\,\frac{\partial^4\zeta_z}{\partial y^2\partial x^2}\right)] + q = 0 \qquad (21c)$$

$$2\left(D_{13}\,\frac{\partial\psi_x}{\partial x} + D_{23}\,\frac{\partial\psi_y}{\partial y} + 2D_{33}\zeta_z\right) - \frac{8F_{13}}{3h^2}\left(\frac{\partial\psi_x}{\partial x} + \frac{\partial^2 w}{\partial x^2} + \frac{h^2}{4}\,\frac{\partial^2\zeta_z}{\partial x^2}\right)$$

$$- \frac{8F_{23}}{3h^2}\left(\frac{\partial\psi_y}{\partial y} + \frac{\partial^2 w}{\partial y^2} + \frac{h^2}{4}\,\frac{\partial^2\zeta_z}{\partial y^2}\right) - \frac{4}{9h^2}[F_{11}\frac{\partial^3\psi_x}{\partial x^3} + F_{12}\frac{\partial^3\psi_y}{\partial y\partial x^2} + 2F_{13}\,\frac{\partial^2\zeta_z}{\partial x^2}$$

$$- \frac{4H_{11}}{3h^2}\left(\frac{\partial^3\psi_x}{\partial x^3} + \frac{\partial^4 w}{\partial x^4} + \frac{h^2}{4}\,\frac{\partial^4\zeta_z}{\partial x^4}\right) - \frac{4H_{12}}{3h^2}\left(\frac{\partial^3\psi_y}{\partial y\partial x^2} + \frac{\partial^4 w}{\partial y^2\partial x^2} + \frac{h^2}{4}\,\frac{\partial^4\zeta_z}{\partial y^2\partial x^2}\right)$$

$$+2F_{66}\left(\frac{\partial^3\psi_y}{\partial y\partial x^2} + \frac{\partial^3\psi_x}{\partial x\partial y^2}\right) - \frac{8H_{66}}{3h^2}\left(\frac{\partial^3\psi_x}{\partial x\partial y^2} + 2\,\frac{\partial^4 w}{\partial y^2\partial x^2} + \frac{h^2}{2}\,\frac{\partial^4\zeta_z}{\partial y^2\partial x^2} + \frac{\partial^3\psi_y}{\partial y\partial x^2}\right)$$

$$+F_{22}\frac{\partial^3\psi_y}{\partial y^3} + F_{12}\frac{\partial^3\psi_x}{\partial x\partial y^2} + 2F_{23}\frac{\partial^2\zeta_z}{\partial y^2} - \frac{4H_{22}}{3h^2}\left(\frac{\partial^3\psi_y}{\partial y^3} + \frac{\partial^4 w}{\partial y^4} + \frac{h^2}{4}\frac{\partial^4\zeta_z}{\partial y^4}\right)$$

$$- \frac{4H_{12}}{3h^2}\left(\frac{\partial^3\psi_x}{\partial x\partial y^2} + \frac{\partial^4 w}{\partial y^2\partial x^2} + \frac{h^2}{4}\frac{\partial^4\zeta_z}{\partial y^2\partial x^2}\right)] + 0.25qh^2 = 0 \tag{21d}$$

Substituting equations (19) and (20) into equation (21) and collecting similar terms, the following equations for finding the coefficients W_{mn}, X_{mn}, Y_{mn}, and Z_{mn} are obtained as follows:

$$\begin{bmatrix} \tilde{c}_{11} & \tilde{c}_{12} & \tilde{c}_{13} & \tilde{c}_{14} \\ \tilde{c}_{21} & \tilde{c}_{22} & \tilde{c}_{23} & \tilde{c}_{24} \\ \tilde{c}_{31} & \tilde{c}_{32} & \tilde{c}_{33} & \tilde{c}_{34} \\ \tilde{c}_{41} & \tilde{c}_{42} & \tilde{c}_{43} & \tilde{c}_{44} \end{bmatrix} \begin{Bmatrix} W_{mn} \\ X_{mn} \\ Y_{mn} \\ Z_{mn} \end{Bmatrix} = \begin{Bmatrix} -Q_{mn} \\ 0 \\ 0 \\ -Q_{mn}h^2/4 \end{Bmatrix} \tag{22}$$

The coefficients of matrix $[\tilde{c}]$ are given by

$$\tilde{c}_{11} = \frac{4}{3h^2}(\alpha^3F_{11} + 2\alpha\beta^2F_{66} + \alpha\beta^2F_{12}) + \alpha[-A_{55} + (\frac{8}{h^2})D_{55} - (\frac{16}{h^4})F_{55}]$$

$$- \frac{16}{9h^4}(\alpha^3H_{11} + 2\alpha\beta^2H_{66} + \alpha\beta^2H_{12}) ,$$

$$\tilde{c}_{12} = \frac{8}{3h^2}(\alpha^2F_{11} + \beta^2F_{66}) - (\alpha^2D_{11} + \beta^2D_{66}) - \frac{16}{9h^4}(\alpha^2H_{11} + \beta^2H_{66}) - A_{55}$$

$$+ \frac{8}{h^2}[D_{55} - (\frac{2}{h^2})F_{55}] ,$$

$$\tilde{c}_{13} = \alpha\beta(\frac{8}{3h^2})(F_{12} + F_{66}) - \alpha\beta(D_{12} + D_{66}) - \alpha\beta(\frac{16}{9h^4})(H_{12} + H_{66}) ,$$

$$\tilde{c}_{14} = \frac{1}{3}(\alpha^3F_{11} + \alpha\beta^2F_{12} + 2\alpha\beta^2F_{66}) + 2\alpha D_{13} - \frac{8\alpha}{3h^2}F_{13}$$

$$- \frac{4}{9h^2}(\alpha^3H_{11} + \alpha\beta^2H_{12} + 2\alpha\beta^2H_{66}) ,$$

$$\tilde{c}_{21} = \frac{4}{3h^2}(\beta^3F_{22} + 2\alpha^2\beta F_{66} + \alpha^2\beta F_{12}) + \beta[-A_{44} + (\frac{8}{h^2})D_{44} - (\frac{16}{h^4})F_{44}] ,$$

$$- \frac{16}{9h^4}(\beta^3 H_{22} + 2\alpha^2\beta H_{66} + \alpha^2\beta H_{12}) ,$$

$$\tilde{c}_{22} = \alpha\beta(\frac{8}{3h^2})(F_{12} + F_{66}) - \alpha\beta(D_{12} + D_{66}) - \alpha\beta(\frac{16}{9h^4})(H_{12} + H_{66}) ,$$

$$\tilde{c}_{23} = \frac{8}{3h^2}(\alpha^2 F_{66} + \beta^2 F_{22}) - (\alpha^2 D_{66} + \beta^2 D_{22}) - \frac{16}{9h^4}(\alpha^2 H_{66} + \beta^2 H_{22}) - A_{44}$$

$$+ \frac{8}{h^2}[D_{44} - (\frac{2}{h^2})F_{44}] ,$$

$$\tilde{c}_{24} = \frac{1}{3}(\beta^3 F_{11} + \alpha^2\beta F_{12} + 2\alpha^2\beta\, F_{66}) + 2\alpha D_{23} - \frac{8\alpha}{3h^2}F_{23}$$

$$- \frac{4}{9h^2}(\beta^3 H_{22} + \alpha^2\beta H_{12} + 2\alpha^2\beta H_{66}) ,$$

$$\tilde{c}_{31} = \frac{8}{h^2}(\alpha^2 D_{55} + \beta^2 D_{44}) - (\alpha^2 A_{55} + \beta^2 A_{44}) - \frac{16}{h^4}(\alpha^2 F_{55} + \beta^2 F_{44})$$

$$- \frac{16}{9h^4}(\alpha^4 H_{11} + \beta^4 H_{22} + 2\alpha^2\beta^2 H_{12} + 4\alpha^2\beta^2 H_{66}) ,$$

$$\tilde{c}_{32} = \alpha(\frac{8}{h^2}D_{55} - A_{55} - \frac{16}{h^4}F_{55}) - \frac{16}{9h^4}(\alpha^3 H_{11} + \alpha\beta^2 H_{12} + 2\alpha\beta^2 H_{66})$$

$$+ \frac{4}{3h^2}(\alpha^3 F_{11} + \alpha\beta^2 F_{12} + 2\alpha\beta^2 F_{66}) ,$$

$$\tilde{c}_{33} = \beta(\frac{8}{h^2}D_{44} - A_{44} - \frac{16}{h^4}F_{44}) - \frac{16}{9h^4}(\beta^3 H_{22} + \alpha^2\beta H_{12} + 2\alpha^2\beta H_{66})$$

$$+ \frac{4}{3h^2}(\beta^3 F_{22} + \alpha^2\beta F_{12} + 2\alpha^2\beta F_{66}) ,$$

$$\tilde{c}_{34} = - \frac{8}{3h^2}(\alpha^2 F_{13} + \beta^2 F_{23}) - \frac{4}{9h^2}(\alpha^4 H_{11} + \beta^4 H_{22} + 2\alpha^2\beta^2 H_{12} + 4\alpha^2\beta^2 H_{66}) ,$$

$$\tilde{c}_{41} = - \frac{8}{3h^2}(\alpha^2 F_{13} + \beta^2 F_{23}) + \frac{4}{9h^2}(\alpha^4 H_{11} + \beta^4 H_{22} + 2\alpha^2\beta^2 H_{12} + 4\alpha^2\beta^2 H_{66}) ,$$

$$\tilde{c}_{42} = 2\alpha(\frac{4}{3h^2}F_{13} - D_{13}) - \frac{1}{3}(\alpha^3 F_{11} + \alpha\beta^2 F_{12} + 2\alpha\beta^2 F_{66})$$

$$+ \frac{4}{9h^2}(\alpha^3 H_{11} + \alpha\beta^2 H_{12} + 2\alpha\beta^2 H_{66}) ,$$

$$\tilde{c}_{43} = 2\beta(\frac{4}{3h^2}F_{23} - D_{23}) - \frac{4}{9h^2}(\beta^3 H_{22} + \alpha^2\beta H_{12} + 2\alpha^2\beta H_{66})$$

$$- \frac{1}{3}(\beta^3 F_{22} + \alpha^2\beta F_{12} + 2\alpha^2\beta F_{66}) , \tag{23}$$

$$\tilde{c}_{44} = \frac{4}{3}(\alpha^2 F_{13} + \beta^2 F_{23}) + \frac{1}{9}(\alpha^4 H_{11} + \beta^4 H_{22} + 2\alpha^2\beta^2 H_{12} + 4\alpha^2\beta^2 H_{66}) + 4D_{33} .$$

Apparently, $\tilde{c}_{ij}$ are functions of material properties and laminate dimensions. In this study, the following dimensions and parameters are used: a= 150 mm, d= 1.25 mm, and h= 2.25 mm for 9-ply, 3.75 mm for 15-ply, and 5.25 mm for 21-ply laminates. And m and n are equal to 10.

4.4 Numerical Results

A. Interlaminar Stresses from Constitutive Equations

In order to justify the technique used in this study, it was necessary to compare the high-order plate theory with Pagano's elasticity solution. A square graphite/epoxy laminate with stacking sequence of $[0_5/90_5/0_5]$ under sinusoidal loading was examined. Figures 23, 24, and 25 show the normalized σ_{xz}, σ_{yz}, and σ_z at some points of interest. Both the elasticity solution and the results from the plate theory are shown in the figures. They are significantly different. Equilibrium equations as suggested by Lo, Christensen, and Wu, instead of constitutive equations, should be used to calculate the interlaminar stresses.

B. Interlaminar Stresses from Equilibrium Equations

The equilibrium approach was used in conjunction with the following continuity equations along with the boundary conditions:

$$\sigma_{xz}^{(1)}(x,y,h/2) = 0,\ \sigma_{xz}^{(1)}(x,y,h/6) = \sigma_{xz}^{(2)}(x,y,h/6)\ ,\sigma_{xz}^{(3)}(x,y,-h/2) = 0,$$

$$\sigma_{yz}^{(1)}(x,y,h/2) = 0,\ \sigma_{yz}^{(1)}(x,y,h/6) = \sigma_{yz}^{(2)}(x,y,h/6)\ ,\sigma_{yz}^{(3)}(x,y,-h/2) = 0,$$

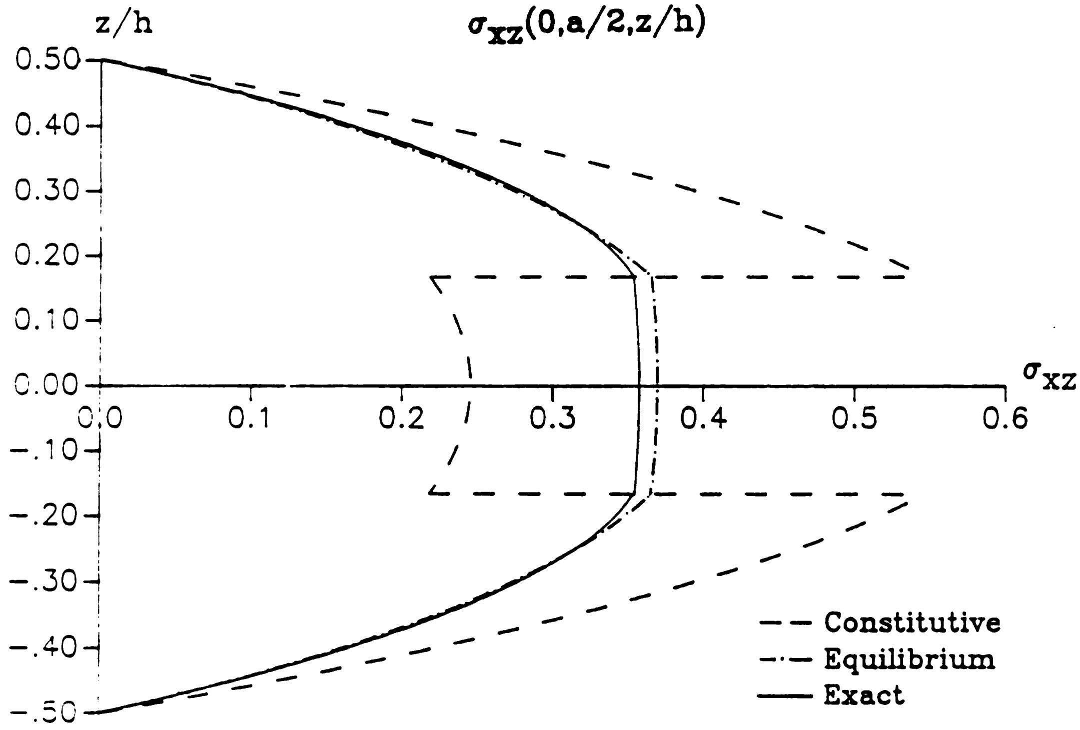

Fig 23 Interlaminar shear stress at (0,a/2,z/h) in $[0_5/90_5/0_5]$ laminate under sinusoidal loading

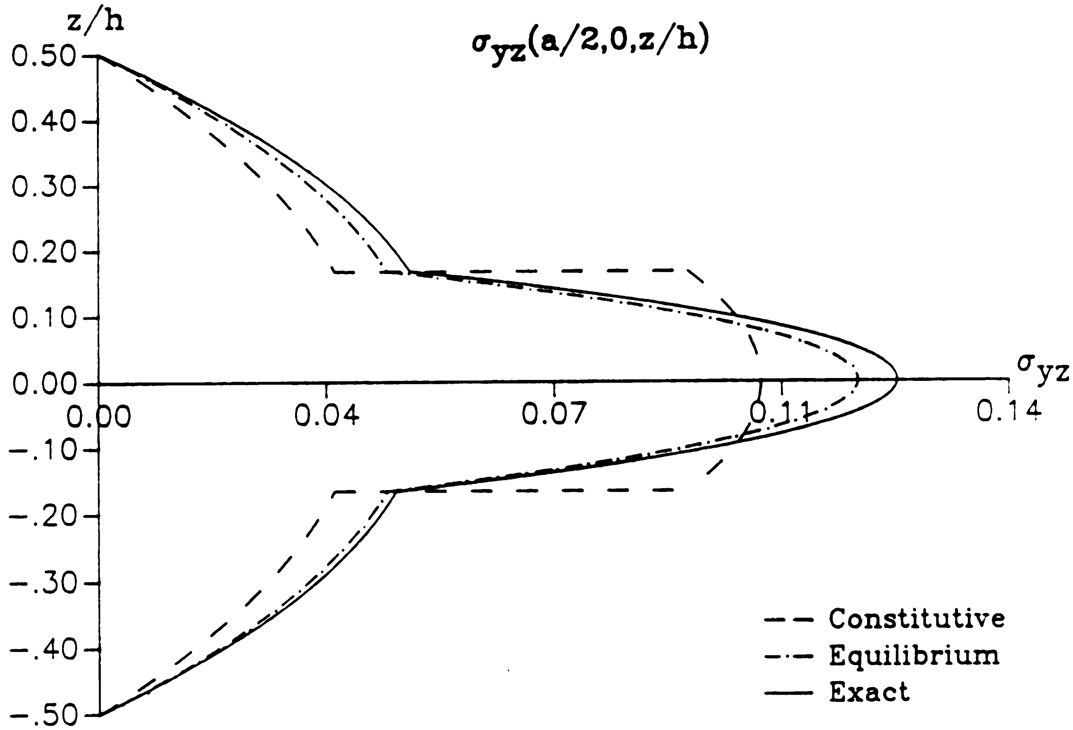

Fig 24 Interlaminar shear stress at (a/2,0,z/h) in $[0_5/90_5/0_5]$ laminate under sinusoidal loading

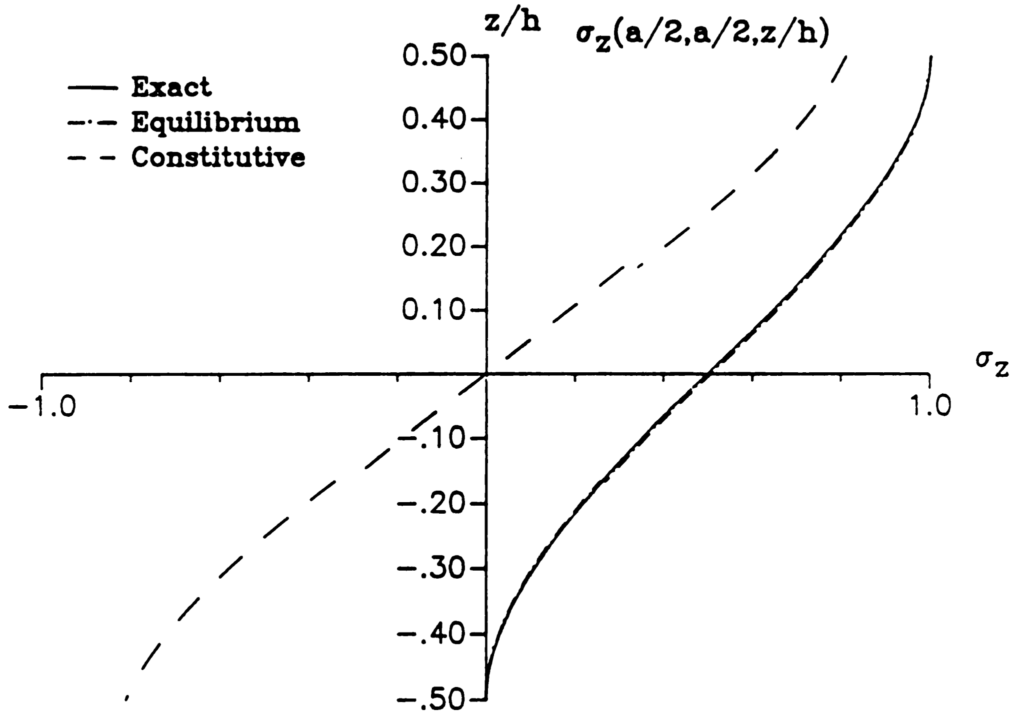

Fig 25 Interlaminar normal stress at (a/2,a/2,z/h) in $[0_5/90_5/0_5]$ laminate under sinusoidal loading

$\sigma_z^{(1)}(x,y,h/2) = q$, $\sigma_z^{(1)}(x,y,h/6) = \sigma_z^{(2)}(x,y,h/6)$,$\sigma_z^{(3)}(x,y,-h/2) = 0$.

Details of derivations can be found in Appendix A. The normalized results are also shown in Figures 23, 24, and 25. Excellent agreements between the elasticity approach and plate theory were then achieved. Accordingly, all the interlaminar stresses in this study were calculated by equilibrium approach thereafter.

C. Interlaminar Stresses due to Central Loading

The same graphite/epoxy laminate, as studied in the previous section, was subjected to central loading. The normalized interlaminar stresses of the whole laminate are depicted in Figures 26-29 for σ_{xz}, σ_{yz}, σ_z of the first interface, and σ_z of the second interface, respectively. Due to the symmetry of the laminate with respect to mid-plane and the small-deformation assumption, the interlaminar shear stresses in the two interfaces are identical to each other. However, the interlaminar normal stress changes with the interface. The interlaminar normal stress σ_z on the first interface reflects higher compression than that on the second interface. There is also a major difference between the two components of interlaminar shear stress on each interface. In comparison with σ_{yz}, σ_{xz} is much higher. Besides, σ_{xz} is symmetric with respect to the y-axis while σ_{yz} the x-axis. Another way to express the interlaminar shear stress is to use a polar coordinate system. Since $\sigma_{\theta z}$ is relatively small, σ_{rz} becomes the dominant component for the interlaminar shear stress. Figure 30 shows the normalized σ_{rz} with an area of 625 mm^2 in a quadrant of the $[0_5/90_5/0_5]$ laminate shown in Figure 22.

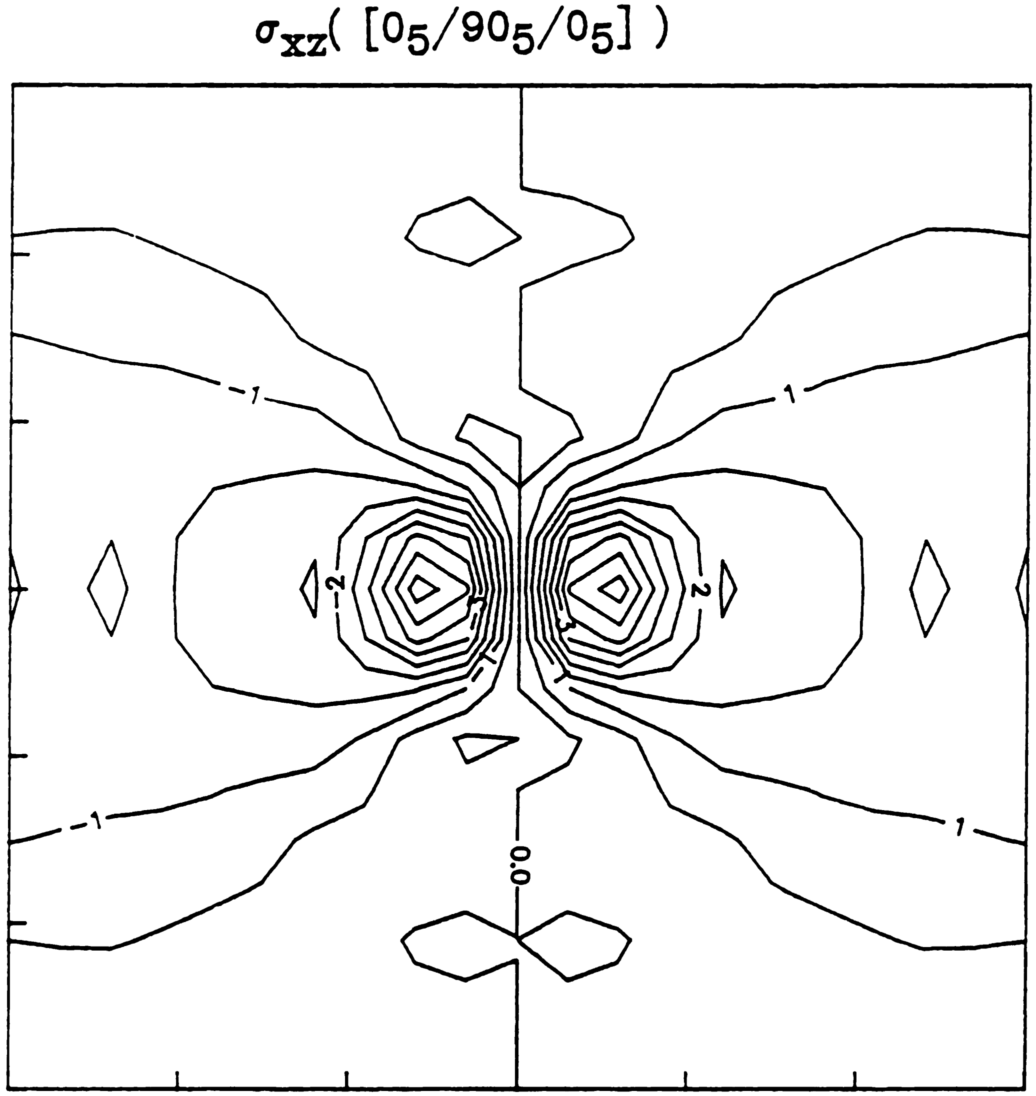

Fig 26 Interlaminar shear stress in the interface of a $[0_5/90_5/0_5]$ laminate under central loading

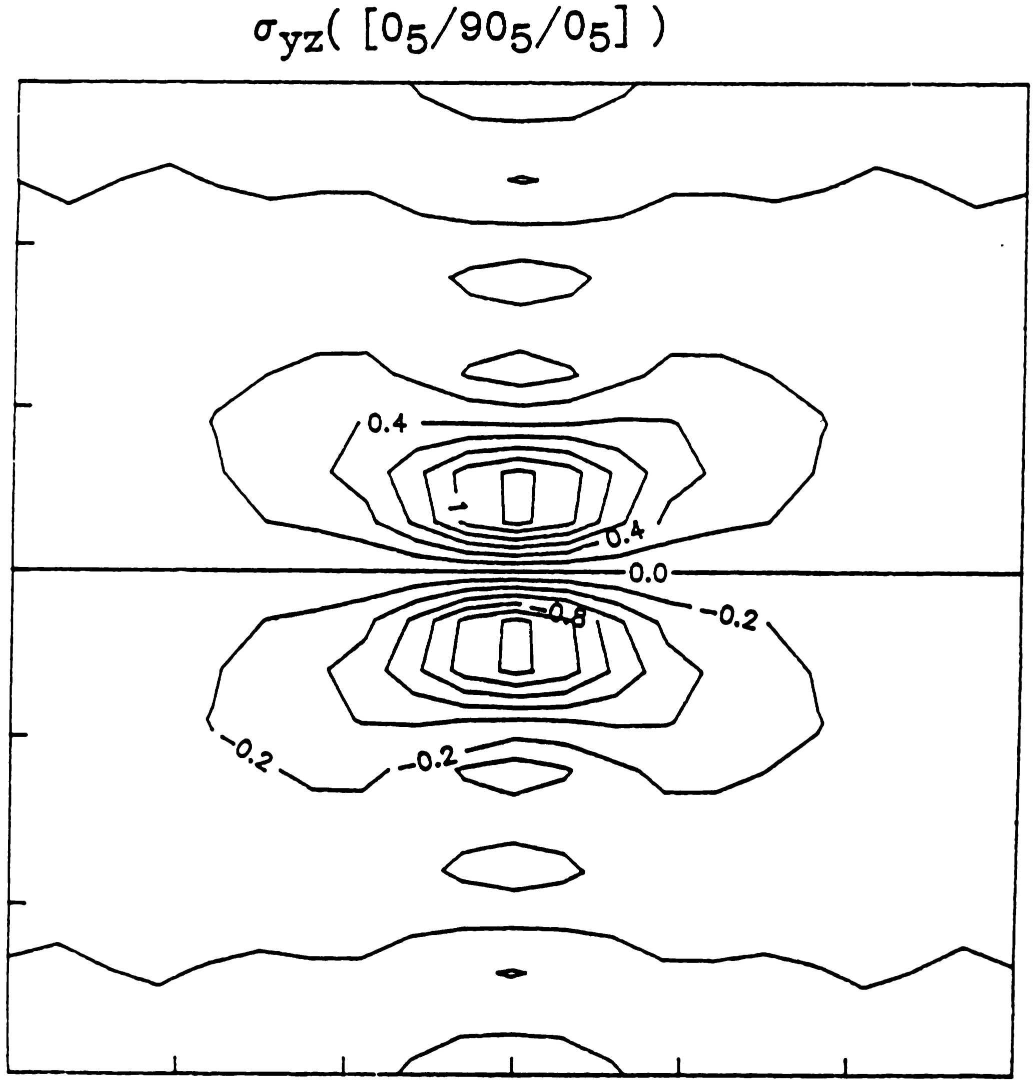

Fig 27 Interlaminar shear stress in the interface of a $[0_5/90_5/0_5]$ laminate under central loading

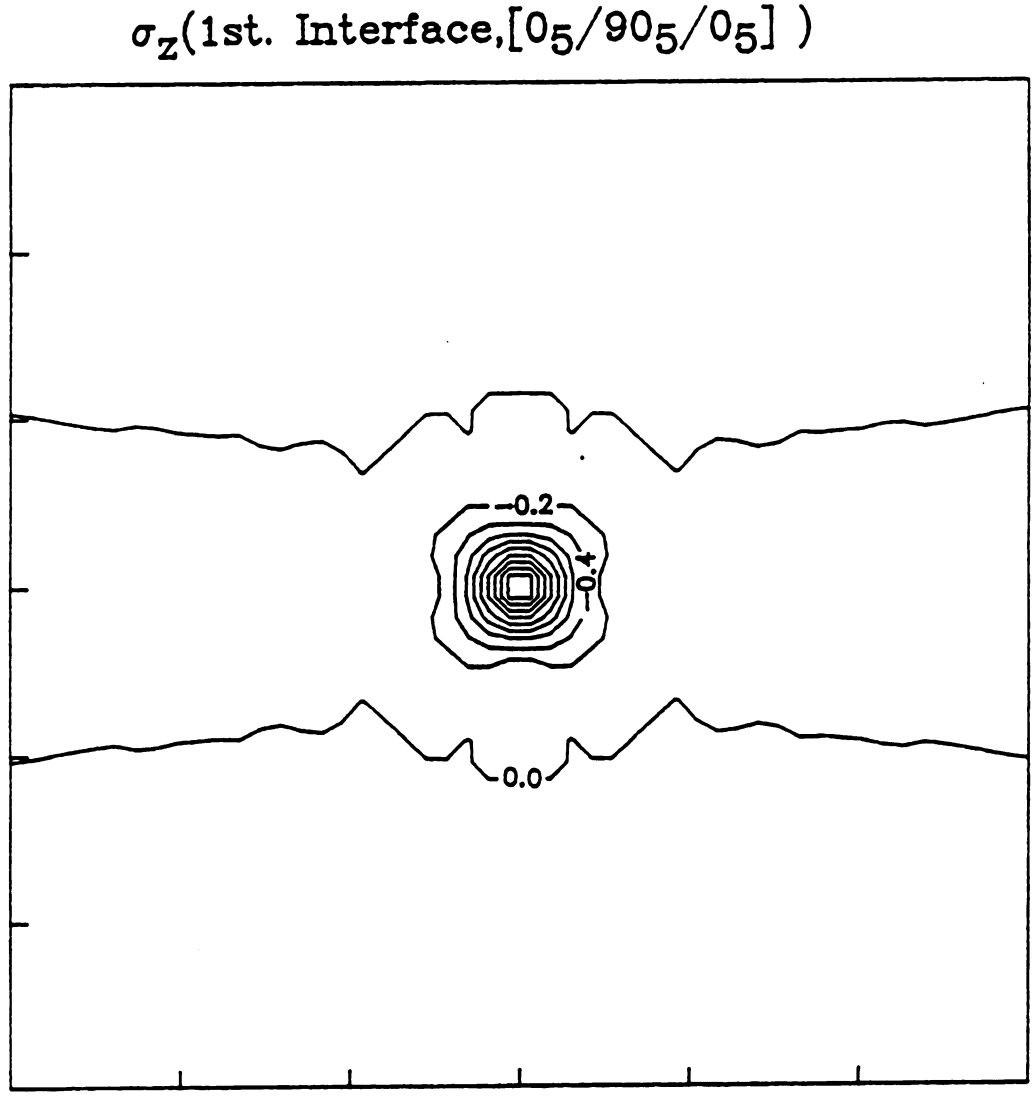

Fig 28 Interlaminar normal stress in the first interface of a $[0_5/90_5/0_5]$ laminate under central loading

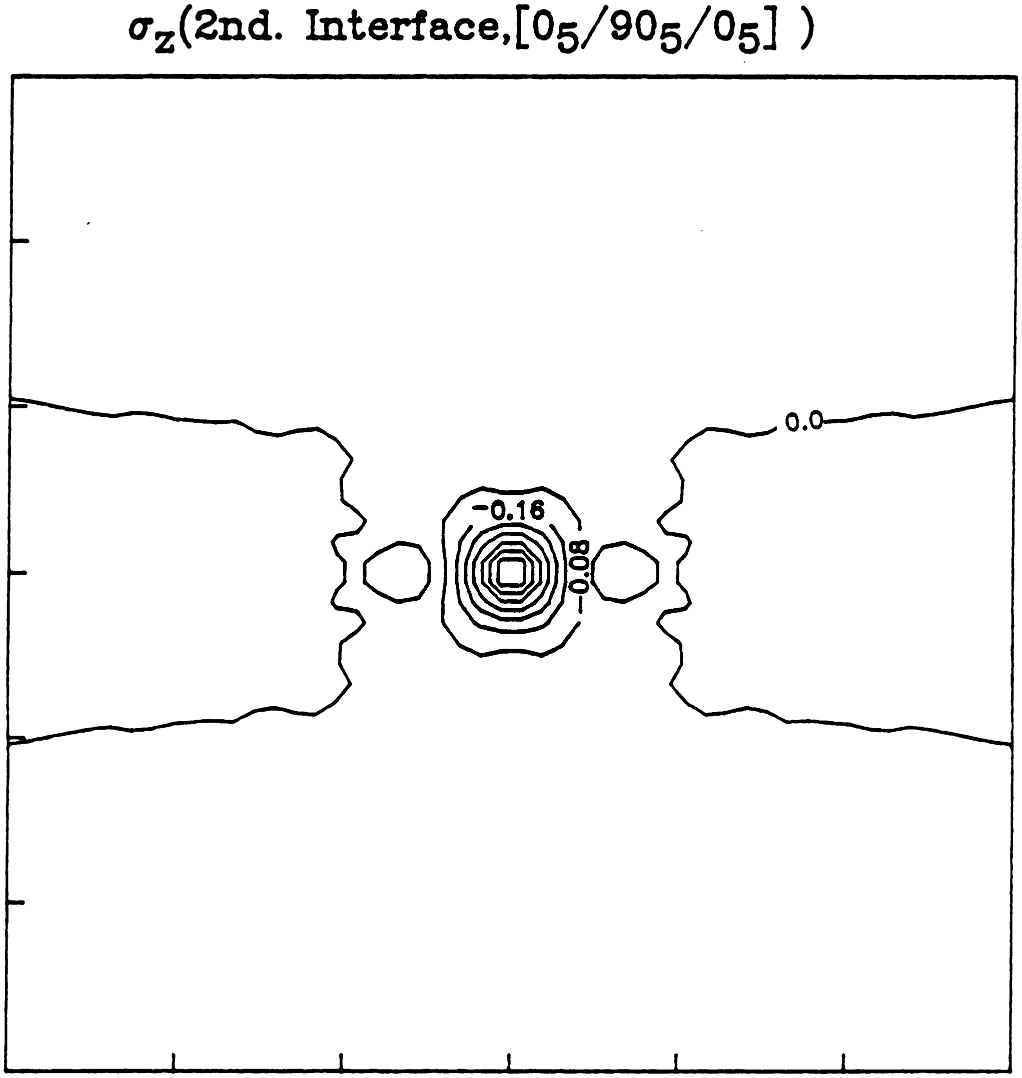

Fig 29 Interlaminar normal stress in the second interface of a [$0_5/90_5/0_5$] laminate under central loading

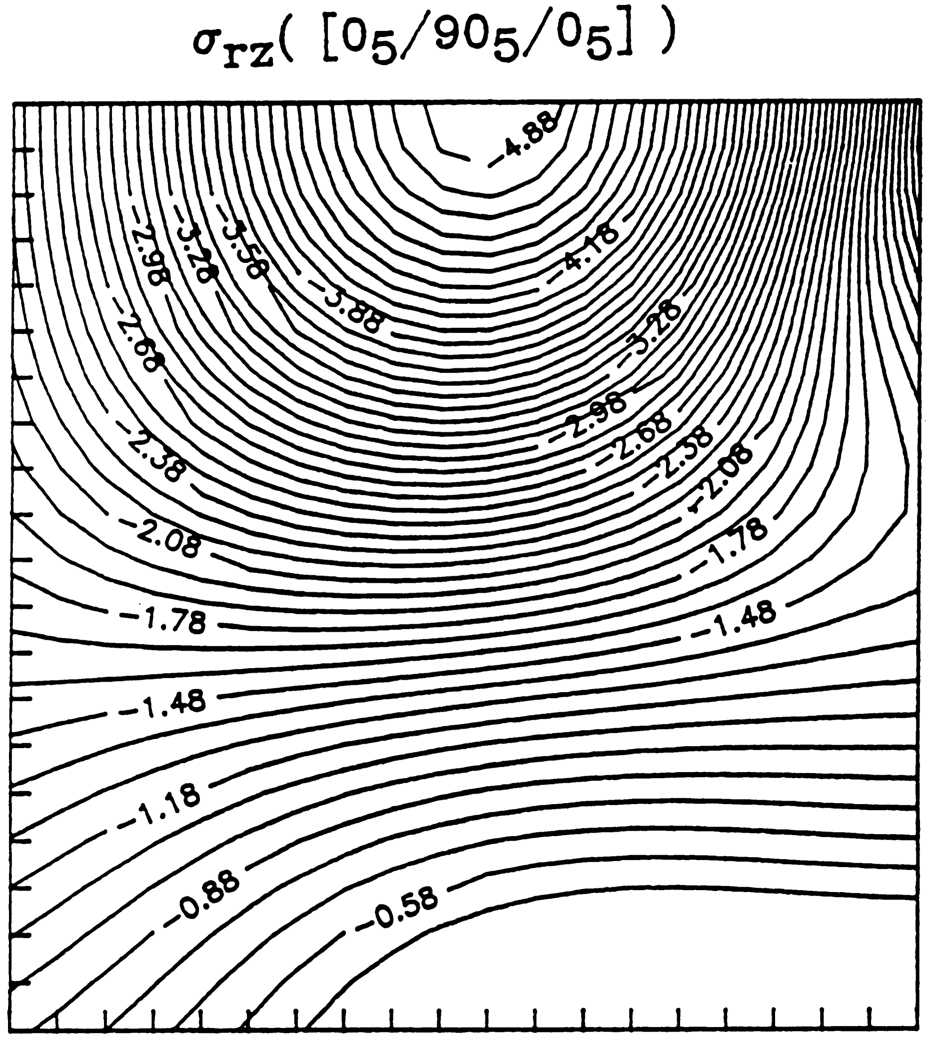

Fig 30 σ_{rz} in the interface of a $[0_5/90_5/0_5]$ laminate under central loading

4.5 Discussions

A. The Important Role of Interlaminar Stresses

Delamination is damage on the composite interface. Both interlaminar normal stress and interlaminar shear stress are responsible for delamination. However, in central loading, the former has a relatively uniform distribution in any direction in the neighborhood of the loading area, while the latter changes significantly with direction. Since there is no satisfactory failure criterion for delamination analysis, for simplicity, the analysis in this study is based on the maximum interlaminar shear stress. It is then concluded that delamination in a cross-ply laminate will be initiated at two points along the centerline of the composite laminate. See Figure 22. In other words, the delamination initiation is direction-dependent. Although the exact initiation points were not identified in the quasi-static testing, the results from both analytical and experimental approaches seem to be consistent. In addition, due to the similarity between the delamination shape and interlaminar shear stress distribution, it is believed that the nonuniform interlaminar shear stress distribution will eventually result in the peanut-shaped delamination. Consequently, it indicates the important role of the interlaminar shear stresses in delamination initiation. On the contrary, because of its compression in nature, the interlaminar normal stress cannot cause delamination in central loading. Due to the higher compressive stress on the first interface (which is the one close to the loading surface) than on the second interface (the one close to the unloaded surface), the delamination on the second interface is likely to take place before the first interface. In addition, the difference of the interlaminar normal stresses between the interfaces is believed to result in different sizes of delamination on the different interfaces. Accordingly, the delamination initiation at the second interface will be emphasized in the following study.

B. Effect of Fiber Orientation

As indicated in the previous section, there is a nonuniform shear stress distribution in a $[0_5/90_5/0_5]$ laminate. From stress analysis, it can be concluded that this is due to the anisotropy of the composite laminae above and below the interface. In order to further verify the effect of material anisotropy on the shear stress distribution, an isotropic laminate $[I_5/I_5/I_5]$, where I indicates an isotropic layer, and a unidirectional graphite/epoxy laminate $[0_5/0_5/0_5]$ were studied. The normalized interlaminar shear stresses, σ_{rz}, of the same area used in Figure 30, on the second interfaces of isotropic and unidirectional laminates are shown in Figures 31 and 32, respectively. Apparently, the interlaminar shear stress in the neighborhood of the loading area for the isotropic plate is less orientation-dependent than those in cross-ply and unidirectional laminates.

In addition to fiber orientation, stacking sequence is also important to shear stress distribution. Two hybrid laminates $[I_5/0_5/I_5]$ and $[0_5/I_5/0_5]$ were studied. The distributions of σ_{rz} are depicted in Figures 33 and 34, respectively. It is interesting to find that the shear stress distribution is likely to be affected by the lamina below the interface. That is, σ_{rz} in $[I_5/0_5/I_5]$ is not as highly orientation-dependent as that in $[0_5/I_5/0_5]$, since the bottom lamina of the former is an isotropic-ply and the latter 0°-ply. This result is consistent with the experimental observation that the major axis of delamination is

σ_{rz}($[I_5/I_5/I_5]$)

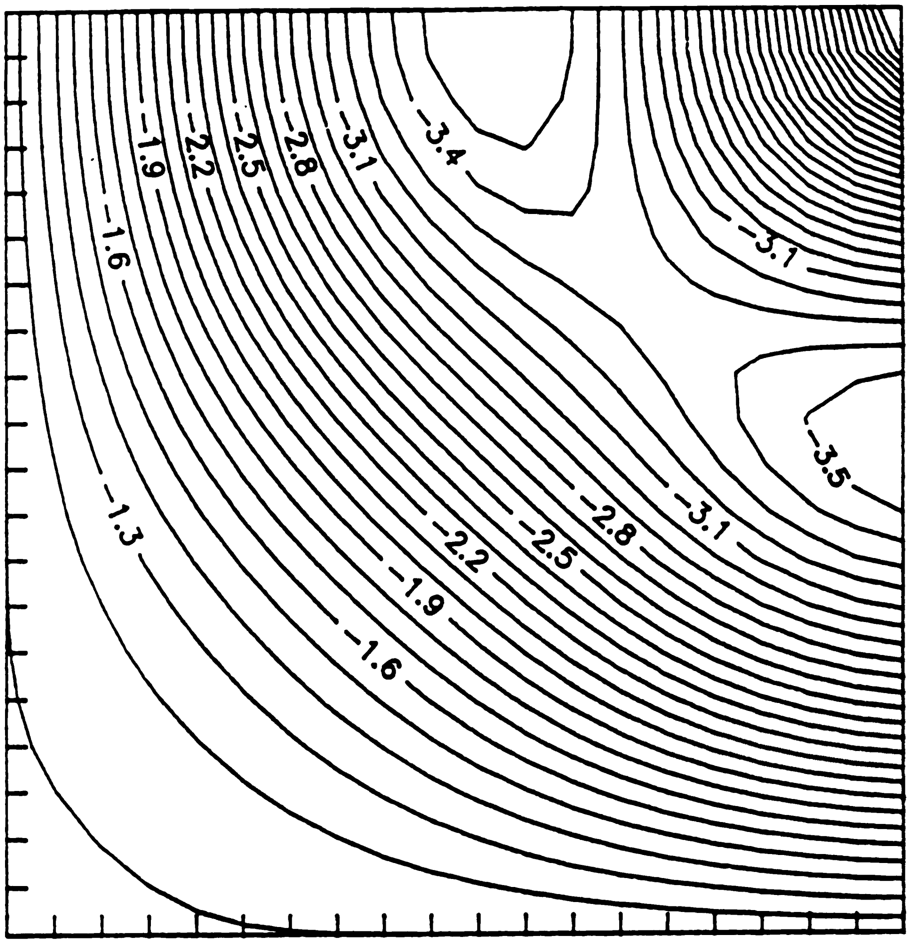

Fig 31 σ_{rz} in the interface of an $[I_5/I_5/I_5]$ laminate under central loading

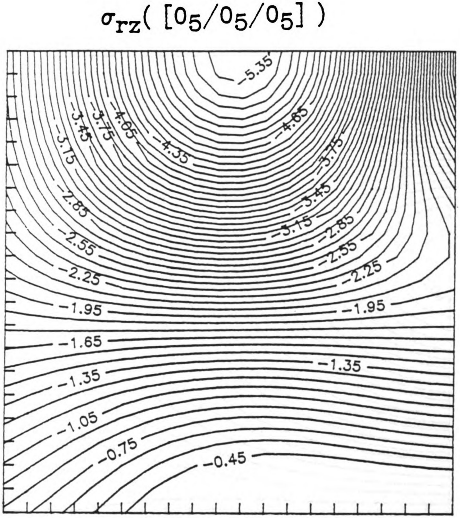

Fig 32 σ_{rz} in the interface of a $[0_5/0_5/0_5]$ laminate under central loading

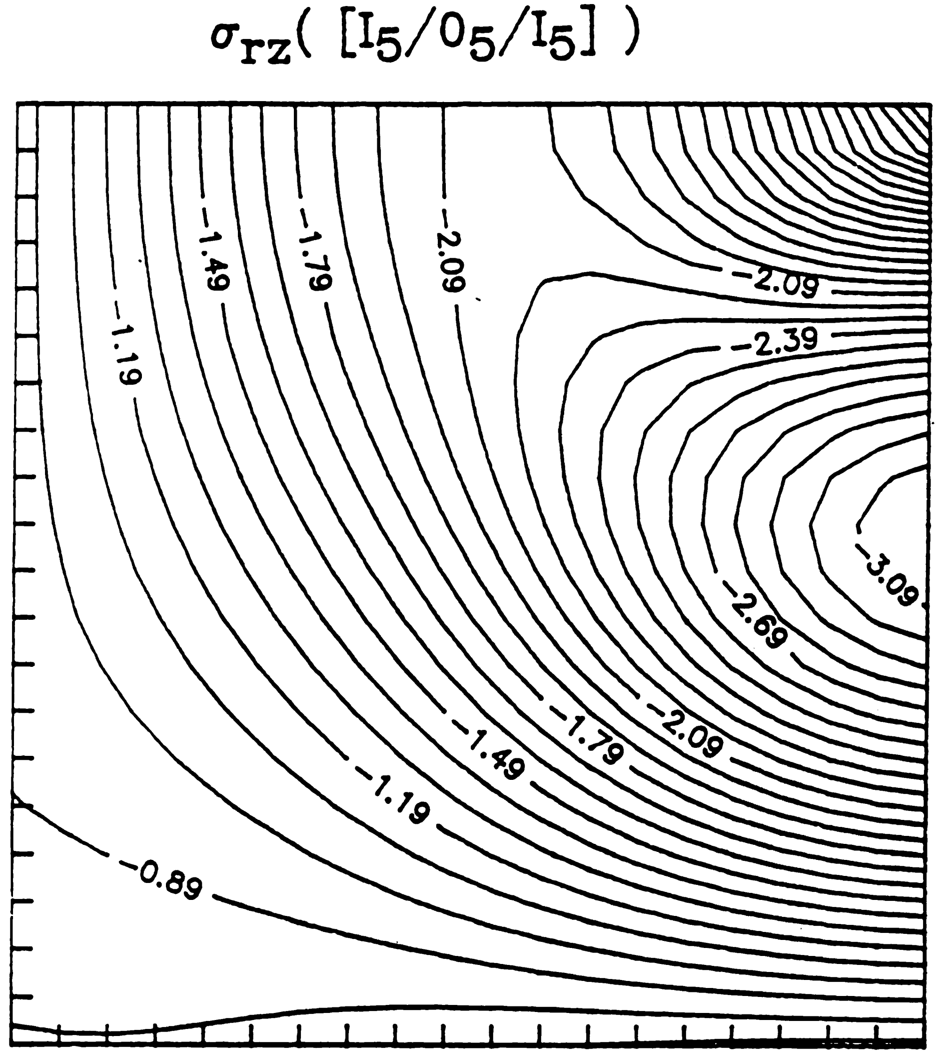

Fig 33 σ_{rz} in the interface of a [$I_5/0_5/I_5$] laminate under central loading

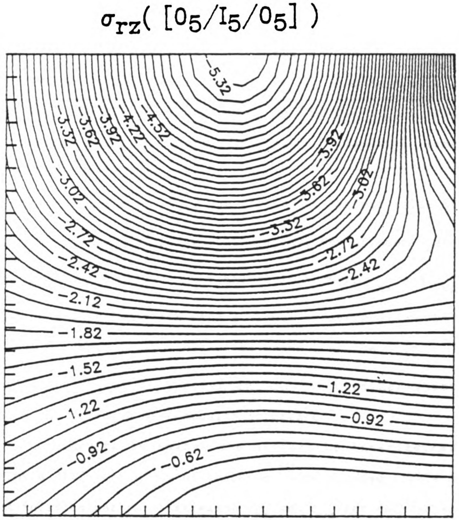

Fig 34 σ_{rz} in the interface of a [$0_5/I_5/0_5$] laminate under central loading strongly influenced by the fiber orientation of the composite lamina beneath the interface.

C. Effects due to Material Properties, Laminate Thickness, and Stacking Sequence

In addition to fiber orientation, the interlaminar shear stress is also affected by material properties, laminate thickness, and stacking sequence. Although types of material and thickness may be different, the overall interlaminar stress distributions for any symmetric cross-ply laminates are very similar to those shown in Figures 26-29. The maximum shear stresses for some cases are listed in Table 3. Some conclusions can be drawn as follows:

a. The anisotropy ratio, E_{11}/E_{22}, can affect the maximum value of $\sigma_{xz}:\sigma_{yz}$. Table 3 shows the results for graphite/epoxy, Kevlar/epoxy, and glass/epoxy. The results indicate that the ratio between σ_{xz} and σ_{yz} becomes higher for composite laminates with a higher anisotropic ratio, i.e. higher E_{11}/E_{22}. However, it should also be noted that the delamination initiation is not only dependent on interlaminar shear stress, but also on the strength of composite interface.

b. The thinner a composite laminate, the higher the interlaminar shear stresses. Three different kinds of thickness were studied. Table 3 shows the maximum interlaminar shear stresses σ_{xz} and σ_{yz} for each case.

c. Stacking sequence plays an important role in the delamination initiation. With the same material properties and thickness, the maximum interlaminar shear stresses change with stacking sequence. The results for both $[0_3/90_3/0_3/90_3/0_3]$ and $[0_5/90_5/0_5]$ are also listed in Table 3. In the $[0_3/90_3/0_3/90_3/0_3]$ laminate, it is interesting to recognize that σ_{xz} is larger than σ_{yz} on the fourth interface, where the fibers are

Table 3: Normalized Maximum Interlaminar Stresses due to Central Loading

graphite/epoxy		$[0_3/90_3/0_3]$	$[0_5/90_5/0_5]$	$[0_7/90_7/0_7]$
Thickness	σ_{xz}	-8.3925	-4.7946	-3.2320
	σ_{yz}	-1.9793	-1.2557	-0.9453
	σ_z (1st)	-2.0931	-2.0857	-2.0733
	σ_z (2nd)	-0.6638	-0.6712	-0.6836

$[0_5/90_5/0_5]$		graphite/epoxy	Kevlar/epoxy	glass/epoxy
Material	σ_{xz}	-4.7946	-4.7809	-4.0693
	σ_{yz}	-1.2557	-1.5035	-2.6365
	σ_z (1st)	-2.0857	-2.0678	-2.0173
	σ_z (2nd)	-0.6712	-0.6891	-0.7397

graphite/epoxy Stacking Sequence		$[0_5/90_5/0_5]$	$[0_3/90_3/0_3/90_3/0_3]$
	σ_{xz}(1st/4th)	-4.7946	-3.5413
	σ_{xz}(2nd/3rd)	-4.7946	-3.6549
	σ_{yz}(1st/4th)	-1.2557	-0.4501
	σ_{yz}(2nd/3rd)	-1.2557	-4.1000
	σ_z (1st)	-2.0857	-2.5238
	σ_z (2nd)	-0.6712	-1.8203
	σ_z (3rd)		-0.9211
	σ_z (4th)		-0.2494

graphite/epoxy	E_{11}= 171.8 GPa, E_{22}=E_{33}= 6.9 GPa, ν_{12}= ν_{13}=ν_{23}= 0.25
	G_{23}= 1.4 GPa , G_{12}= G_{31}= 3.4 GPa
Kevlar/epoxy	E_{11}= 81.5 GPa, E_{22}=E_{33}= 5.1 GPa, ν_{12}=ν_{13}=ν_{23}= 0.3
	G_{23}=G_{12}=G_{31}= 1.8 GPa
glass/epoxy	E_{11}= 36 GPa, E_{22}=E_{33}= 10.4 GPa, ν_{12}= ν_{13}= 0.26, ν_{23}= 0.3
	G_{23}= 2.5 GPa , G_{12}= G_{31}= 3.2 GPa

aligned in the x-direction beneath the interface. However, σ_{yz} is larger than σ_{xz} on the third interface, where the fiber alignment is in the y-direction beneath the interface. Likewise, in the $[0_5/90_5/0_5]$ laminate, σ_{xz} is larger than σ_{yz} on the second interface, where the fibers are aligned in the x-direction beneath the interface while σ_{yz} is larger than σ_{xz} on the first interface, where the fiber alignment is in the y-direction beneath the interface. These results are consistent with those in previous discussions.

4.6 Results for Glass/epoxy Laminates

A similar study was performed for glass/epoxy laminates. The results are listed in Table 4. Similar conclusions as those obtained from the graphite/epoxy analysis can be drawn.

4.7 Summary

Based on the numerical results and comparisons with previous experimental observations, the following conclusions can be drawn:

A. Interlaminar shear stresses are responsible for the initiation of central delamination. However, since the interlaminar normal stress is compressive in central loading, it can suppress the delamination.

B. The anisotropy of composite lamina on each side of an interface can cause nonuniform distribution of delamination, namely peanut-shaped delamination. The degree of anisotropy can affect the distribution of interlaminar shear stress.

C. Delamination is likely to be affected by the lamina beneath the composite interface.

Table 4: Normalized Maximum Interlaminar Stresses for glass/epoxy due to Central Loading

Thickness	$[0_3/90_3/0_3]$	$[0_5/90_5/0_5]$	$[0_7/90_7/0_7]$
σ_{xz}	-6.8463	-4.0693	-2.8707
σ_{yz}	-4.3618	-2.6365	-1.8998
σ_z (1st)	-2.0204	-2.0173	-2.0128
σ_z (2nd)	-0.7366	-0.7397	-0.7442

Stacking Sequence	$[0_5/90_5/0_5]$	$[0_3/90_3/0_3/90_3/0_3]$
σ_{xz}(1st/4th)	-4.0693	-3.0634
σ_{xz}(2nd/3rd)	-4.0693	-3.6400
σ_{yz}(1st/4th)	-2.6365	-1.6380
σ_{yz}(2nd/3rd)	-2.6365	-3.7600
σ_z (1st)	-2.0173	-2.4737
σ_z (2nd)	-0.7397	-1.7673
σ_z (3rd)		-0.9152
σ_z (4th)		-0.2894

glass/epoxy E_{11}= 36 GPa, E_{22}=E_{33}= 10.4 GPa, ν_{12}= ν_{13}= 0.26, ν_{23}= 0.3
G_{23}= 2.5 GPa , G_{12}= G_{31}= 3.2 GPa

Chapter 5

Stitching Effects

The interlaminar properties of a composite laminate can significantly affect delamination resistance. It was found in Chapter 2 that the delamination area in a composite laminate subjected to low-velocity impact is dependent on parameters such as fiber orientation, laminate thickness, and stacking sequence. Furthermore, some material properties also play important roles in delamination resistance. Since delamination is the damage on the interface between laminae, the properties which dominate the delamination resistance are the matrix strength and the bonding strength between fiber and matrix. Accordingly, it is possible to improve the delamination resistance of a composite laminate by improving these strengths. However, it is difficult to examine the effect due to each property independently, since by changing the surface chemical between fiber and matrix to increase the bonding strength, the matrix strength can also be changed. In this study, instead of improving the chemical bonding, a technique of changing the mechanical bonding - stitching - was investigated.

Stitching has been used by Mignery, Tan, and Sun [83] to improve free-edge delamination resistance. Ogo [84] performed comprehensive testing to study the effects of stitching on the in-plane strengths and interlaminar fracture toughnesses. In a study by Liu [85], the significant effects of stitching density on central delamination have been determined. However, the stitching pattern was found to have little influence on the delamination resistance. It was the objective of this study to investigate the delamination morphology, to characterize the interlaminar properties, and to further investigate the influences of stitching on the interlaminar properties such as the interlaminar shear strength and the critical strain energy release rate.

5.1 Scanning Electron Microscopy

The parameters which strongly affect the interlaminar strength of a composite laminate are the interfacial bonding between fiber and matrix and the strength of the matrix. Scanning electron microscope was used to investigate the delamination surface for an impacted glass/epoxy laminate. For comparison, graphite/epoxy and Kevlar/epoxy laminates were also examined. The results are shown in Figure 35. Apparently, Kevlar/epoxy and graphite/epoxy have poor bonding between fiber and matrix because of the clean fiber surfaces. However, there is some residual matrix left on the glass fiber surfaces. This indicates that delamination, in glass/epoxy laminates, actually occurs in the matrix.

5.2 Short Beam Shear Test

One of the important parameters which dominates delamination resistance is the interlaminar shear strength. The standard test for interlaminar shear strength is ASTM D2344 - short beam shear test [86-87]. Details of the testing configuration can be found in Figure 36. A series of stitching patterns, with density from 2 to 12 stitches per 156 mm^2, were performed manually. The stitching threads were cut directly from the prepreg tape and had a width of 1.5 mm. The mechanical properties of the stitching thread can be found in Table 5. A needle, with a diameter of 0.8 mm, was used for stitching. Simple up-and-down stitching was performed. The stitching patterns are shown in Figure 37 and the experimental results are shown in Figure 38. Also shown in Figure 38 is a least-squares line for the data points. There is a monotonic increase in interlaminar shear strength with an increase in stitching density.

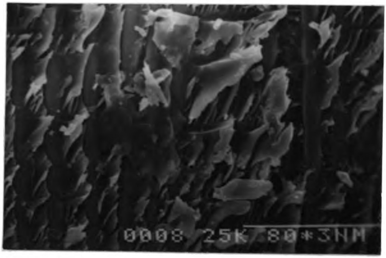

Glass/Epoxy

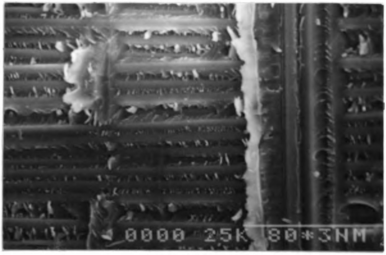

Graphite/Epoxy

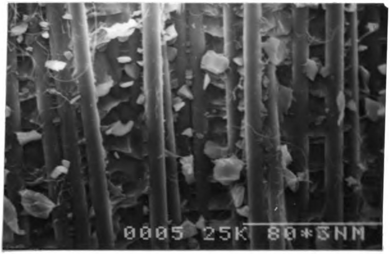

Kevlar/Epoxy

Fig 35 Comparison of interfacial bonding among glass/epoxy, graphite/epoxy, and kevlar/epoxy by scanning electron microscope

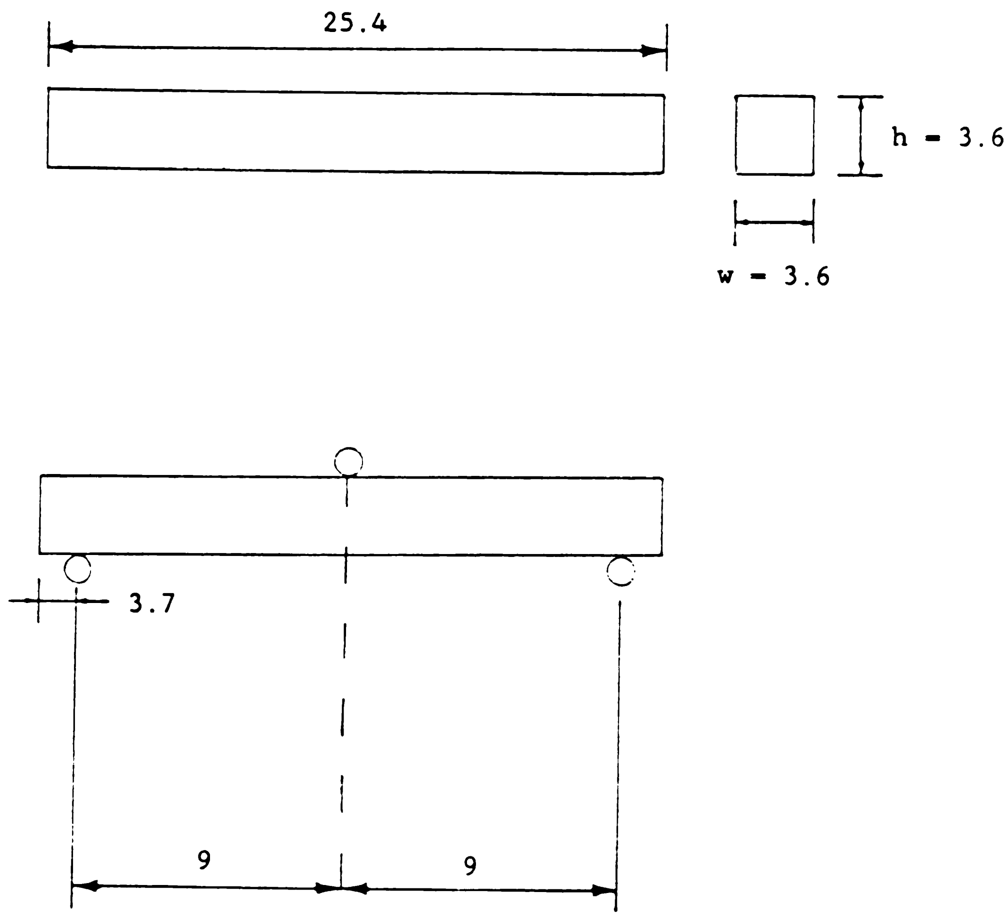

Fig 36   Short beam shear specimen geometry
All dimensions are in mm

Table 5: Mechanical Properties of 3M's 1003 Glass/Epoxy

Mechanical Property	Unidirectional Composites	Matrix	Stitching Thread
E_{11}(GPa)	36.0	4.77 (E)	79.95 (E)
E_{22}(GPa)	10.4		
E_{33}(GPa)	10.4		
G_{12}(GPa)	3.20	1.77 (G)	31.73 (G)
G_{13}(GPa)	3.20		
ν_{12}	0.26	0.35 (ν)	0.20 (ν)
ν_{13}	0.26		
ν_{23}	0.3		

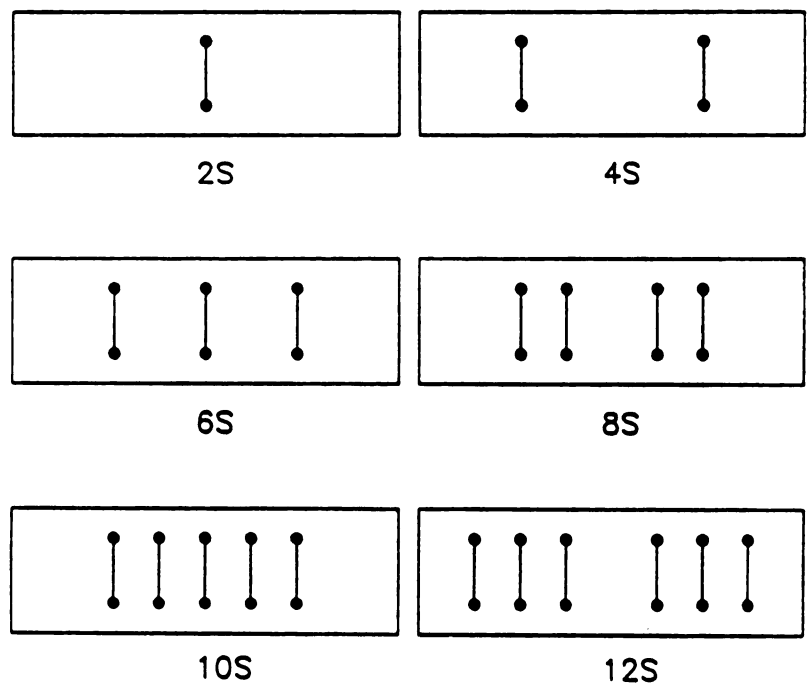

Fig 37 Stitching patterns for short beam shear test

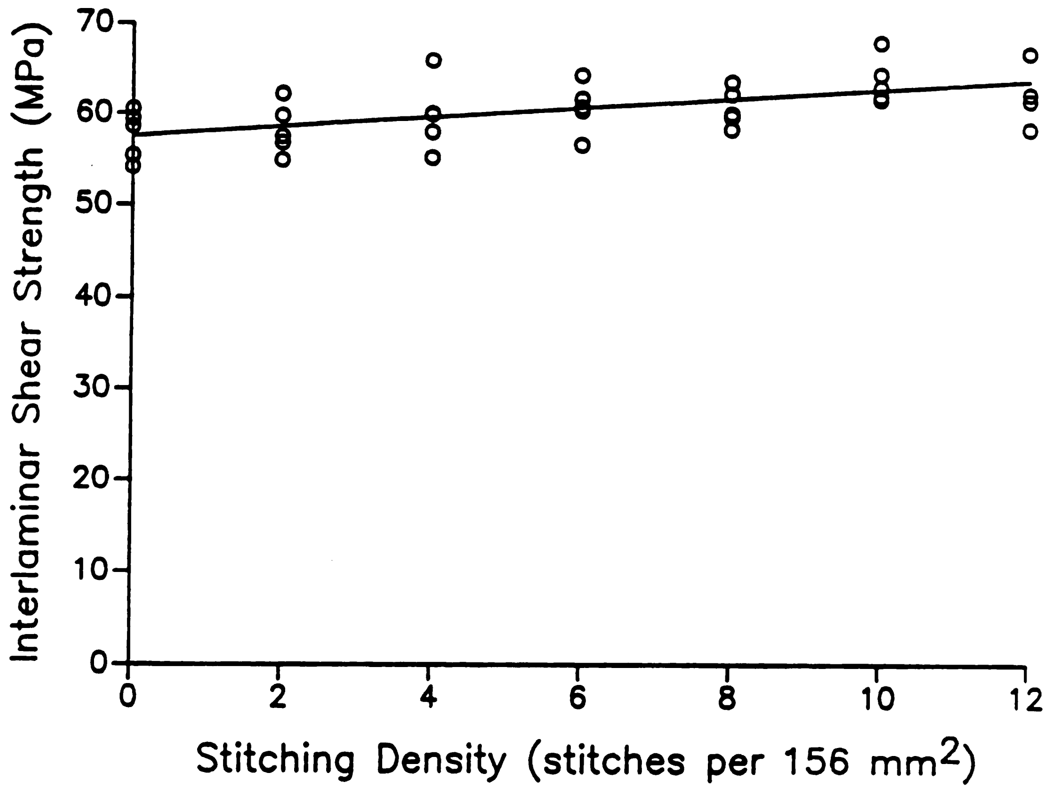

Fig 38 The relation between interlaminar shear strength and stitching density

5.3 End Notch Flexure Test

Another important indicator for delamination resistance is the interlaminar fracture toughness. Because mode I fracture did not occur in the central loading [49], only shear modes were necessary to be examined. In addition, because mode II was more significant than mode III, for simplicity, only mode II was considered. In this study, End Notch Flexure (ENF) test [88] was used to characterize the critical strain energy release rate of mode II, G_{IIc}. The stitching patterns for this test are shown in Figure 39 while the testing configuration is shown in Figure 40. The experimental results of G_{IIc}, for the stitched and unstitched composite laminates, can be seen in Figure 41; as well as the least-squares line. The experimental results indicates that G_{IIc} increases with the increase of stitching density. However, the G_{IIc} of 1S stitching is smaller than the unstitched laminate. This is believed to result from the local damage caused by the stitching point. As the stitching density becomes sufficiently high, the increase in G_{IIc} can surpass this negative effect.

5.4 Summary

A. Stitching can be used as a mechanical technique to improve the interlaminar properties of composite laminates.

B. The stitching can also cause local and global strength changes. Owing to stitching, the integrity of a composite laminate can be damaged locally. However, the stitching thread has much higher strength and toughness than the matrix. If the stitching density is high enough, the overall interlaminar properties can be improved.

C. In the cases of central impact and central loading, mode II fracture is found to be the dominant fracture mode.

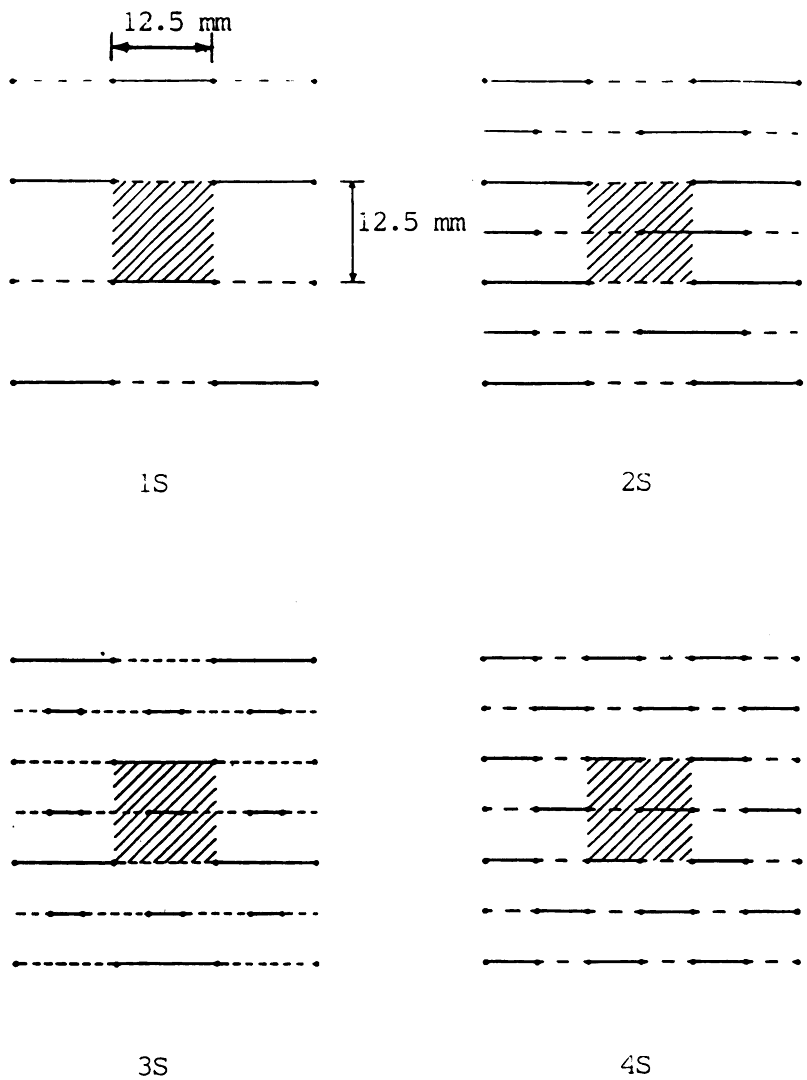

Fig 39 Stitching patterns for different stitching densities in experiments (shaded area emphasized a unit area)

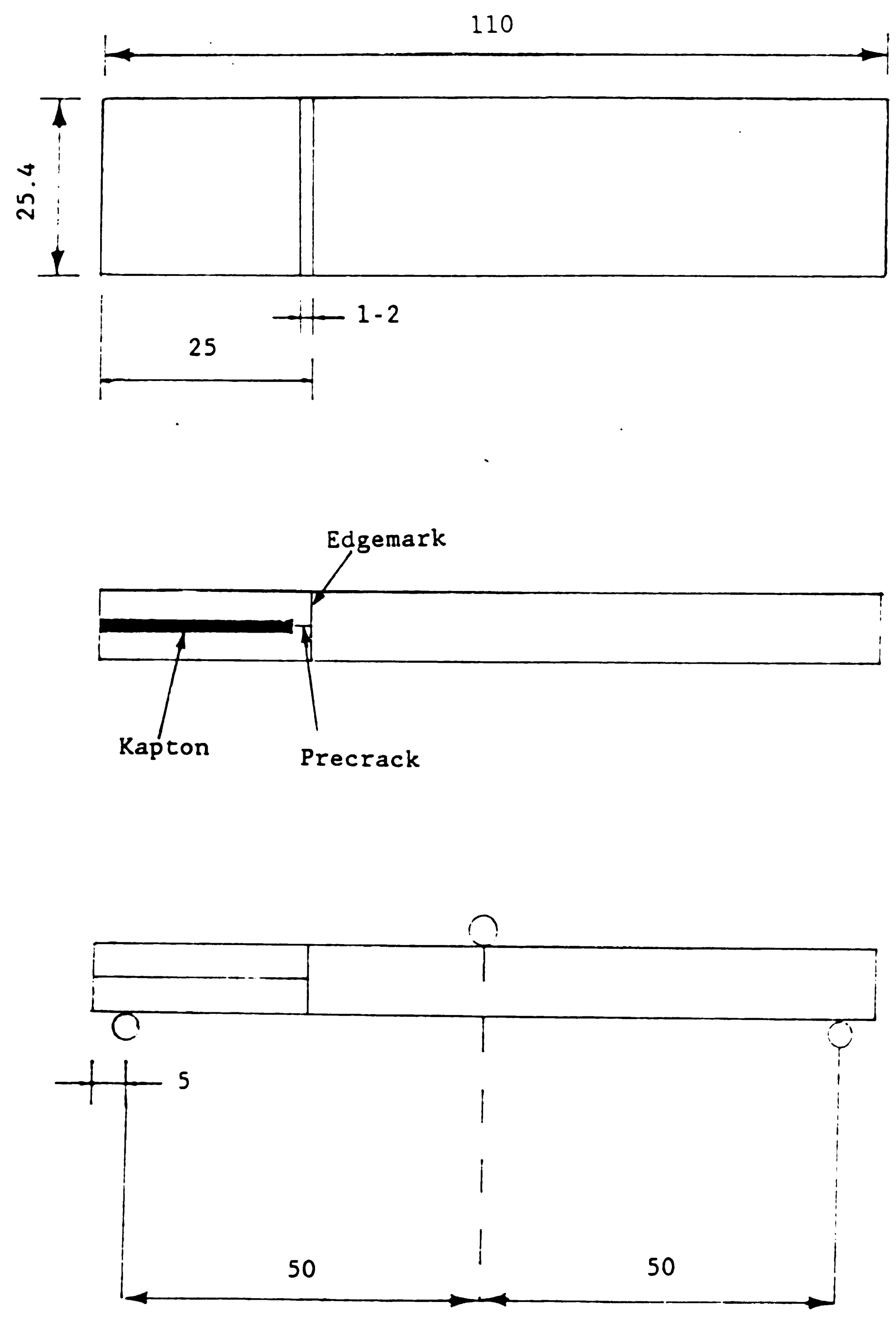

Fig 40 ENF specimen geometry and loading.
All dimensions are in mm

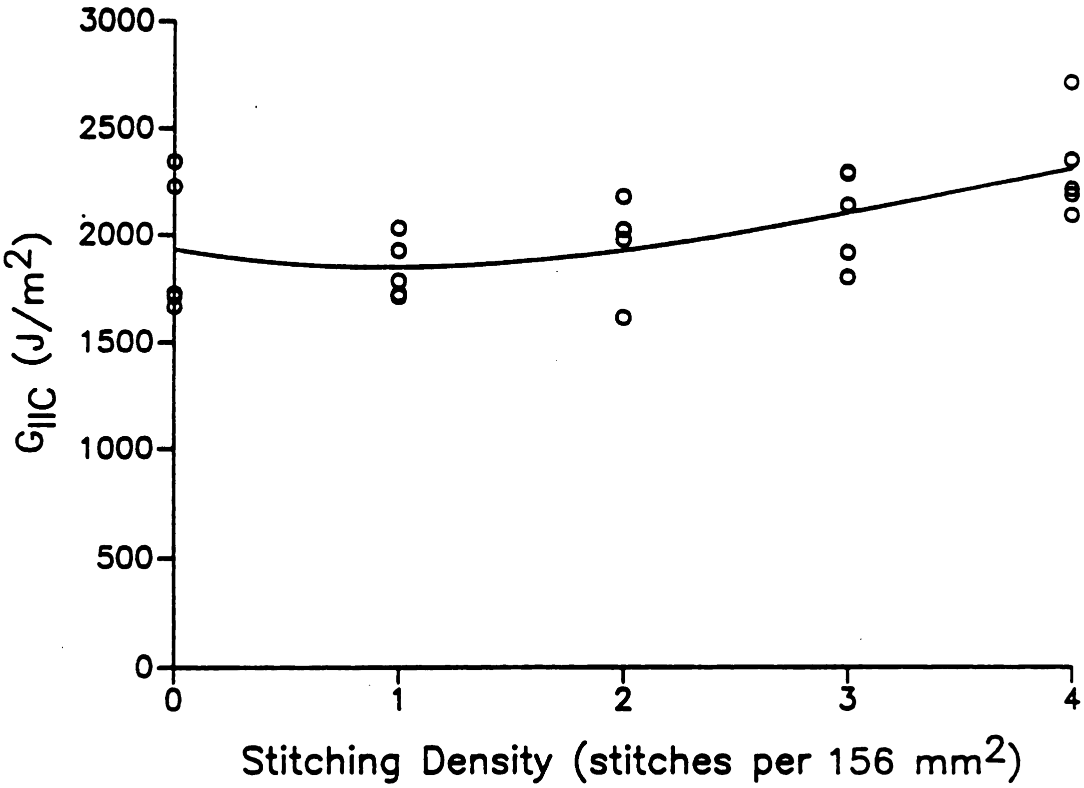

Fig 41 The relation between G_{IIc} and stitching density

Chapter 6

Conclusions

Both in-plane strength and interlaminar strength are key factors of the strength of a composite material. The former is strongly dependent on the fiber strength while the latter can be characterized by the delamination resistance. Delamination is invisible in most of composite materials. It takes place frequently in composite laminates. This study used low-velocity impact and quasi-static central loading to study central delamination. In addition, a static analysis based on a high-order shear deformation theory was used to examine the interlaminar stresses. The efficiency of a stitching technique to imporve the delamination resistance was also investigated. Some important research findings can be concluded as follows:

A. A linear relation seems to hold between delamination area and input energy for both low-velocity impact and quasi-static central loading. The experimental results based on delamination area and input energy from both cases agree each other. The results indicate that it is feasible to use energy and delamination area in the study of central delamination.

B. Peanut-shaped delamination has been found to be the fundamental unit of central delamination, which has been concluded to be the major damage mode in thin composite laminates subjected to both low-velocity impact and quasi-static central loading. A great deal of similarity between these two types of loading was also concluded. It then is feasible to use quasi-static central loading to study central delamination.

C. Since delamination is damage on the composite interface, the interlaminar stresses play the major role in delamination resistance. However, because the interlaminar normal stress is negative, only the interlaminar shear stress is responsible for delamination initiation. Analytical results show that it is feasible to use the maximum interlaminar shear stress to interpret the delamination initiation.

D. From interlaminar stress analysis, it has been concluded that peanut-shaped delamination is due to the mismatch of fiber orientation of orthotropic materials. It has also been concluded that the anisotropy of the lamina beneath a composite interface seems to have more significant effect on the delamination than the one above.

E. Through-the-thickness stitching can improve the interlaminar shear strength and the strain energy release rate of mode II moderately. However, it can also cause local damage. In order to improve the delamination resistance of a composite laminate, a minimum stitching density is required.

APPENDIX

APPENDIX A

INTERLAMINAR STRESSES FROM THE EQUILIBRIUM EQUATION

$$\sigma_{xz}^{(k)} = -\int_{-h/2}^{h/2} \left(\frac{\partial\sigma_x^{(k)}}{\partial x} + \frac{\partial\sigma_{xy}^{(k)}}{\partial y}\right)dz$$

$$= \sum_{m,n=1}^{\infty} \sum_{m,n=1}^{\infty} \Big[\frac{z^2}{2} \{X_{mn}(\alpha^2\bar{C}_{11}^{(k)} + \beta^2\bar{C}_{66}^{(k)}) + \alpha\beta Y_{mn}(\bar{C}_{12}^{(k)} + \bar{C}_{66}^{(k)})$$

$$- 2\alpha Z_{mn}\bar{C}_{13}^{(k)} - \frac{z^4}{3h^2}\{W_{mn}(\alpha^3\bar{C}_{11}^{(k)} + \alpha\beta^2\bar{C}_{12}^{(k)} + 2\alpha\beta^2\bar{C}_{66}^{(k)})$$

$$+ X_{mn}(\alpha^2\bar{C}_{11}^{(k)} + \beta^2\bar{C}_{66}^{(k)}) + \alpha\beta Y_{mn}(\bar{C}_{12}^{(k)} + \bar{C}_{66}^{(k)}) + \frac{Z_{mn}h^2}{4}(\alpha^3\bar{C}_{11}^{(k)} + \alpha\beta^2\bar{C}_{12}^{(k)}$$

$$+ 2\alpha\beta^2\bar{C}_{66}^{(k)})\}\Big]\cos\alpha x\ \sin\beta y + f^{(k)}(x,y)$$

$$\sigma_{yz}^{(k)} = -\int_{-h/2}^{h/2} \left(\frac{\partial\sigma_y^{(k)}}{\partial y} + \frac{\partial\sigma_{xy}^{(k)}}{\partial x}\right)dz$$

$$= \sum_{m,n=1}^{\infty} \sum_{m,n=1}^{\infty} \Big[\frac{z^2}{2} \{Y_{mn}(\alpha^2\bar{C}_{66}^{(k)} + \beta^2\bar{C}_{22}^{(k)}) + \alpha\beta X_{mn}(\bar{C}_{12}^{(k)} + \bar{C}_{66}^{(k)})$$

$$- 2\beta Z_{mn}\bar{C}_{23}^{(k)}\} - \frac{z^4}{3h^2}\{W_{mn}(\beta^3\bar{C}_{22}^{(k)} + \alpha^2\beta\bar{C}_{12}^{(k)} + 2\alpha^2\beta\bar{C}_{66}^{(k)})$$

$$+ Y_{mn}(\alpha^2\bar{C}_{66}^{(k)} + \alpha\beta\bar{C}_{22}^{(k)}) + \alpha\beta X_{mn}(\bar{C}_{12}^{(k)} + \bar{C}_{66}^{(k)}) + \frac{h^2 Z_{mn}}{4}(\beta^3\bar{C}_{22}^{(k)} + \alpha^2\beta\bar{C}_{12}^{(k)}$$

$$+ 2\alpha^2\beta\bar{C}_{66}^{(k)})\}\Big]\sin\alpha x\ \cos\beta y + g^{(k)}(x,y)$$

$$\sigma_z^{(k)} = -\int_{-h/2}^{h/2} \left(\frac{\partial\sigma_{xz}^{(k)}}{\partial x} + \frac{\partial\sigma_{yz}^{(k)}}{\partial y}\right)dz$$

$$-\sum_{m,n=1}^{\infty}\sum_{m,n=1}^{\infty}\Big[\frac{z^3}{6}\{X_{mn}(\alpha^3\bar{C}_{11}^{(k)} + \alpha\beta^2\bar{C}_{12}^{(k)} + 2\alpha\beta^2\bar{C}_{66}^{(k)})$$

$$+ Y_{mn}(\beta^3\bar{C}_{22}^{(k)} + \alpha^2\beta\bar{C}_{12}^{(k)} + 2\alpha^2\beta\bar{C}_{66}^{(k)}) - 2Z_{mn}(\alpha^2\bar{C}_{13}^{(k)} + \alpha^2\bar{C}_{23}^{(k)})\}$$

$$-\frac{z^5}{15h^2}\{W_{mn}(\alpha^4\bar{C}_{11}^{(k)} + 2\alpha^2\beta^2\bar{C}_{12}^{(k)} + 4\alpha^2\beta^2\bar{C}_{66}^{(k)} + \beta^4\bar{C}_{22}^{(k)})$$

$$+ X_{mn}(\alpha^3\bar{C}_{11}^{(k)} + \alpha\beta^2\bar{C}_{12}^{(k)} + 2\alpha\beta^2\bar{C}_{66}^{(k)}) + Y_{mn}(\alpha^2\beta\bar{C}_{12}^{(k)} + \alpha\beta^2\bar{C}_{22}^{(k)} + 2\alpha^2\beta\bar{C}_{66}^{(k)})$$

$$+ \frac{h^2 Z_{mn}}{4}(\alpha^4\bar{C}_{11}^{(k)} + 2\alpha^2\beta^2\bar{C}_{12}^{(k)} + 4\alpha^2\beta^2\bar{C}_{66}^{(k)} + \beta^4\bar{C}_{22}^{(k)})\}\Big]\sin\alpha x\ \sin\beta y$$

$$-z\frac{\partial f^{(k)}}{\partial x} - z\frac{\partial g^{(k)}}{\partial y} + h^{(k)}(x,y)$$

$$f^{(1)}(x,y) = -\sum_{m,n=1}^{\infty}\sum_{m,n=1}^{\infty}\Big[\frac{h^2}{8}\{X_{mn}(\alpha^2\bar{C}_{11}^{(1)} + \beta^2\bar{C}_{66}^{(1)}) + \alpha\beta Y_{mn}(\bar{C}_{12}^{(1)} + \bar{C}_{66}^{(1)})$$

$$- 2\alpha Z_{mn}\bar{C}_{13}^{(1)}\} - \frac{h^2}{48}\{W_{mn}(\alpha^3\bar{C}_{11}^{(1)} + \alpha\beta^2\bar{C}_{12}^{(1)} + 2\alpha\beta^2\bar{C}_{66}^{(1)})$$

$$+ X_{mn}(\alpha^2\bar{C}_{11}^{(1)} + \beta^2\bar{C}_{66}^{(1)}) + \alpha\beta Y_{mn}(\bar{C}_{12}^{(1)} + \bar{C}_{66}^{(1)})$$

$$+ \frac{h^2 Z_{mn}}{4}(\alpha^3\bar{C}_{11}^{(1)} + \alpha\beta^2\bar{C}_{12}^{(1)} + 2\alpha\beta^2\bar{C}_{66}^{(1)})\}\Big]\cos\alpha x\ \sin\beta y$$

$$f^{(2)}(x,y) = \sum_{m,n=1}^{\infty}\sum_{m,n=1}^{\infty}\Big[\frac{h^2}{72}\{X_{mn}(\alpha^2(\bar{C}_{11}^{(1)} - \bar{C}_{11}^{(2)}) + \beta^2(\bar{C}_{66}^{(1)} - \bar{C}_{66}^{(2)}))$$

$$+ \alpha\beta Y_{mn}(\bar{C}_{12}^{(1)} + \bar{C}_{66}^{(1)} - \bar{C}_{12}^{(2)} - \bar{C}_{66}^{(2)}) - 2\alpha Z_{mn}(\bar{C}_{13}^{(1)} - \bar{C}_{13}^{(2)})\}$$

$$+\frac{h^2}{3888}\{W_{mn}(\alpha^3(\bar{C}_{11}^{(2)} - \bar{C}_{11}^{(1)}) + \alpha\beta^2(\bar{C}_{12}^{(2)} - \bar{C}_{12}^{(1)}) + 2\alpha\beta^2(\bar{C}_{66}^{(2)} - \bar{C}_{66}^{(1)}))$$

$$+ X_{mn}(\alpha^2(\bar{C}_{11}^{(2)} - \bar{C}_{11}^{(1)}) + \beta^2(\bar{C}_{66}^{(2)} - \bar{C}_{66}^{(1)})) + \alpha\beta Y_{mn}(\bar{C}_{12}^{(2)} + \bar{C}_{66}^{(2)} - \bar{C}_{12}^{(1)}$$

$$- \bar{C}_{66}^{(1)}) + \frac{h^2 Z_{mn}}{4}(\alpha^3(\bar{C}_{11}^{(2)} - \bar{C}_{11}^{(1)}) + \alpha\beta^2(\bar{C}_{12}^{(2)} - \bar{C}_{12}^{(1)})$$

$$+ 2\alpha\beta^2(\bar{C}_{66}^{(2)} - \bar{C}_{66}^{(1)}))\}\Big]\cos\alpha x\ \sin\beta y + f^{(1)}(x,y)$$

$$f^{(3)}(x,y) = f^{(1)}(x,y)$$

$$g^{(1)}(x,y) = -\sum_{m,n=1}^{\infty}\sum_{m,n=1}^{\infty}\Big[\frac{h^2}{8}\{Y_{mn}(\alpha^2\bar{C}_{66}^{(1)} + \beta^2\bar{C}_{22}^{(1)}) + \alpha\beta X_{mn}(\bar{C}_{12}^{(1)} + \bar{C}_{66}^{(1)})$$

$$- 2\beta Z_{mn}\bar{C}_{23}^{(1)}\} - \frac{h^2}{48}\{W_{mn}(\beta^3\bar{C}_{22}^{(1)} + \beta\alpha^2\bar{C}_{12}^{(1)} + 2\beta\alpha^2\bar{C}_{66}^{(1)})$$

$$+ Y_{mn}(\alpha^2\bar{C}_{66}^{(1)} + \alpha\beta\,\bar{C}_{22}^{(1)}) + \alpha\beta X_{mn}(\bar{C}_{12}^{(1)} + \bar{C}_{66}^{(1)})$$

$$+ \frac{h^2 Z_{mn}}{4}(\beta^3\bar{C}_{22}^{(1)} + \beta\alpha^2\bar{C}_{12}^{(1)} + 2\beta\alpha^2\bar{C}_{66}^{(1)})\}\Big]\sin\alpha x\,\cos\beta y$$

$$g^{(2)}(x,y) = \sum_{m,n=1}^{\infty}\sum_{m,n=1}^{\infty}\Big[\frac{h^2}{72}\{Y_{mn}(\alpha^2(\bar{C}_{66}^{(1)} - \bar{C}_{66}^{(2)}) + \beta^2(\bar{C}_{22}^{(1)} - \bar{C}_{22}^{(2)}))$$

$$+ \alpha\beta X_{mn}(\bar{C}_{12}^{(1)} + \bar{C}_{66}^{(1)} - \bar{C}_{12}^{(2)} - \bar{C}_{66}^{(2)}) - 2\beta Z_{mn}(\bar{C}_{23}^{(1)} - \bar{C}_{23}^{(2)})\}$$

$$+ \frac{h^2}{3888}\{W_{mn}(\beta^3(\bar{C}_{22}^{(2)} - \bar{C}_{22}^{(1)}) + \beta\alpha^2(\bar{C}_{12}^{(2)} - \bar{C}_{12}^{(1)}) + 2\beta\alpha^2(\bar{C}_{66}^{(2)} - \bar{C}_{66}^{(1)}))$$

$$+ Y_{mn}(\alpha^2(\bar{C}_{66}^{(2)} - \bar{C}_{66}^{(1)}) + \alpha\beta(\bar{C}_{22}^{(2)} - \bar{C}_{22}^{(1)})) + \alpha\beta X_{mn}(\bar{C}_{12}^{(2)} + \bar{C}_{66}^{(2)} - \bar{C}_{12}^{(1)}$$

$$- \bar{C}_{66}^{(1)}) + \frac{h^2 Z_{mn}}{4}(\beta^3(\bar{C}_{22}^{(2)} - \bar{C}_{22}^{(1)}) + \beta\alpha^2(\bar{C}_{12}^{(2)} - \bar{C}_{12}^{(1)})$$

$$+ 2\beta\alpha^2(\bar{C}_{66}^{(2)} - \bar{C}_{66}^{(1)}))\}\Big]\sin\alpha x\,\cos\beta y + g^{(1)}(x,y)$$

$$g^{(3)}(x,y) = g^{(1)}(x,y), \quad \frac{\partial f^{(k)}}{\partial x} = -\alpha f^{(k)}, \quad \frac{\partial g^{(k)}}{\partial y} = -\alpha g^{(k)}$$

$$h^{(1)}(x,y) = \sum_{m,n=1}^{\infty}\sum_{m,n=1}^{\infty}\Big[\frac{-h^2}{48}\{X_{mn}(\alpha^3\bar{C}_{11}^{(1)} + 2\alpha\beta^2\bar{C}_{66}^{(1)} + \alpha\beta^2\bar{C}_{12}^{(1)})$$

$$+ Y_{mn}(\alpha^2\beta\bar{C}_{12}^{(1)} + 2\alpha^2\beta\bar{C}_{66}^{(1)} + \beta^3\bar{C}_{22}^{(1)}) - 2Z_{mn}(\alpha^2\bar{C}_{13}^{(1)} + \beta^2\bar{C}_{23}^{(1)})\}$$

$$+ \frac{h^3}{480}\{W_{mn}(\alpha^4\bar{C}_{11}^{(1)} + 2\alpha^2\beta^2\bar{C}_{12}^{(1)} + 4\alpha^2\beta^2\bar{C}_{66}^{(1)} + \beta^4\bar{C}_{22}^{(1)})$$

$$+ X_{mn}(\alpha^3\bar{C}_{11}^{(1)} + \alpha\beta^2\bar{C}_{12}^{(1)} + 2\alpha\beta^2\bar{C}_{66}^{(1)}) + Y_{mn}(\beta\alpha^2\bar{C}_{12}^{(1)} + 2\beta\alpha^2\bar{C}_{66}^{(1)} + \alpha\beta^2\bar{C}_{22}^{(1)})$$

$$+ \frac{h^2 Z_{mn}}{4}(\alpha^4\bar{C}_{11}^{(1)} + 2\alpha^2\beta^2\bar{C}_{12}^{(1)} + 4\alpha^2\beta^2\bar{C}_{66}^{(1)} + \beta^4\bar{C}_{22}^{(1)})\}\Big]\sin\alpha x\,\sin\beta y$$

$$+ \frac{h}{2} \left(\frac{\partial f^{(1)}}{\partial x} + \frac{\partial g^{(1)}}{\partial y}\right) + q$$

$$h^{(2)}(x,y) = \sum_{m,n=1}^{\infty} \sum_{m,n=1}^{\infty} \left[\frac{h^3}{1296}\{X_{mn}(\alpha^3(\bar{C}_{11}^{(1)} - \bar{C}_{11}^{(2)}) + 2\alpha\beta^2(\bar{C}_{66}^{(1)} - \bar{C}_{66}^{(2)})\right.$$

$$+ \alpha\beta^2(\bar{C}_{12}^{(1)} - \bar{C}_{12}^{(2)})) + Y_{mn}(\alpha^2\beta(\bar{C}_{12}^{(1)} - \bar{C}_{12}^{(2)}) + 2\alpha^2\beta(\bar{C}_{66}^{(1)} - \bar{C}_{66}^{(2)})$$

$$+ \beta^3(\bar{C}_{22}^{(1)} - \bar{C}_{22}^{(2)})) - 2Z_{mn}(\alpha^2(\bar{C}_{13}^{(1)} - \bar{C}_{13}^{(2)}) + \beta^2(\bar{C}_{23}^{(1)} - \bar{C}_{23}^{(2)}))\}$$

$$\frac{-h^3}{116640}\{W_{mn}(\alpha^4(\bar{C}_{11}^{(1)} - \bar{C}_{11}^{(2)}) + 2\alpha^2\beta^2(\bar{C}_{12}^{(1)} - \bar{C}_{12}^{(2)})$$

$$+ 4\alpha^2\beta^2(\bar{C}_{66}^{(1)} - \bar{C}_{66}^{(2)}) + \beta^4(\bar{C}_{22}^{(1)} - \bar{C}_{22}^{(2)}))$$

$$+X_{mn}(\alpha^3(\bar{C}_{11}^{(1)} - \bar{C}_{11}^{(2)}) + \alpha\beta^2(\bar{C}_{12}^{(1)} - \bar{C}_{12}^{(2)}) + 2\alpha\beta^2(\bar{C}_{66}^{(1)} - \bar{C}_{66}^{(2)}))$$

$$+Y_{mn}(\beta\alpha^2(\bar{C}_{12}^{(1)} - \bar{C}_{12}^{(2)}) + 2\beta\alpha^2(\bar{C}_{66}^{(1)} - \bar{C}_{66}^{(2)}) + \alpha\beta^2(\bar{C}_{22}^{(1)} - \bar{C}_{22}^{(2)}))$$

$$+ \frac{h^2 Z_{mn}}{4}(\alpha^4(\bar{C}_{11}^{(1)} - \bar{C}_{11}^{(2)}) + 2\alpha^2\beta^2(\bar{C}_{12}^{(1)} - \bar{C}_{12}^{(2)})$$

$$\left. + 4\alpha^2\beta^2(\bar{C}_{66}^{(1)} - \bar{C}_{66}^{(2)}) + \beta^4(\bar{C}_{22}^{(1)} - \bar{C}_{22}^{(2)}))\}\right] \sin\alpha x \sin\beta y$$

$$+\frac{h}{6}\left(\frac{\partial f^{(2)}}{\partial x} + \frac{\partial g^{(2)}}{\partial y} - \frac{\partial f^{(1)}}{\partial x} + \frac{\partial g^{(1)}}{\partial y}\right) + h^{(1)}(x,y)$$

$$h^{(3)}(x,y) = \sum_{m,n=1}^{\infty} \sum_{m,n=1}^{\infty} \left[\frac{h^2}{48}\{X_{mn}(\alpha^3\bar{C}_{11}^{(3)} + 2\alpha\beta^2\bar{C}_{66}^{(3)} + \alpha\beta^2\bar{C}_{12}^{(3)})\right.$$

$$+ Y_{mn}(\alpha^2\beta\bar{C}_{12}^{(3)} + 2\alpha^2\beta\bar{C}_{66}^{(3)} + \beta^3\bar{C}_{22}^{(3)}) - 2Z_{mn}(\alpha^2\bar{C}_{13}^{(3)} + \beta^2\bar{C}_{23}^{(3)})\}$$

$$\frac{-h^3}{480}\{W_{mn}(\alpha^4\bar{C}_{11}^{(3)} + 2\alpha^2\beta^2\bar{C}_{12}^{(3)} + 4\alpha^2\beta^2\bar{C}_{66}^{(3)} + \beta^4\bar{C}_{22}^{(3)})$$

$$+X_{mn}(\alpha^3\bar{C}_{11}^{(3)} + \alpha\beta^2\bar{C}_{12}^{(3)} + 2\alpha\beta^2\bar{C}_{66}^{(3)}) + Y_{mn}(\beta\alpha^2\bar{C}_{12}^{(3)} + 2\beta\alpha^2\bar{C}_{66}^{(3)} + \alpha\beta^2\bar{C}_{22}^{(3)})$$

$$\left. + \frac{h^2 Z_{mn}}{4}(\alpha^4\bar{C}_{11}^{(3)} + 2\alpha^2\beta^2\bar{C}_{12}^{(3)} + 4\alpha^2\beta^2\bar{C}_{66}^{(3)} + \beta^4\bar{C}_{22}^{(3)}))\}\right] \sin\alpha x \sin\beta y$$

$$- \frac{h}{2} \left(\frac{\partial f^{(3)}}{\partial x} + \frac{\partial g^{(3)}}{\partial y}\right)$$

LIST OF REFERENCES

LIST OF REFERENCES

1. R.M. Jones, Mechanics of composite materials, McGraw-Hill Co., 1976.

2. H. Chai, W.G. Knauss, and C.D. Babcock, "Observation of damage growth in compressively loaded laminates," Experimental Mechanics, pp.329-337, 1983.

3. D. Liu, C.T. Sun, and L.E. Malvern, "Structual degradation of impacted graphite/epoxy laminates," 56th Shock & Vibration Bulletin, pp.51-60, 1985.

4. E.G. Guynn and T.K. O'brien, "The influence of lay-up and thickness on composite impact damage and compression strength," AIAA/ASME/SAE 26th Structures, Structural Dynamics. and Materials Conference, Orlando, FL, pp187-196, 1985.

5. D. Liu, L.E.Malvern, and C.T. Sun, "Delamination in central impact in graphite/epoxy laminates," Proceeding of Society of Engineering Mechanics, pp.8-13, 1986.

6. Foreign object impact damage to composite, ASTM 568, 1973.

7. B.O. Agrawal and L.J. Broutman, Analysis and performance of fiber composites, John Wiley & Sons. NY, 1980.

8. P.K. Raghunath and D.C. Chang, "Surface damage of sheet molding compound panels subject to a point impact loading," J. Composite Materials, pp.182-194, 1983.

9. T.M. Cordell and O.S. Peter, "Low velocity impact testing of composites," Proceeding of the American Society for Composites, pp.297-312, 1986.

10. H.T. Wu and G.S. Springer, "Impact damage of composites," Proceeding of the American Society for Composites, pp.346-351, 1986.

11. Mechanics of nondestructive testing, edited by W.W. Stinchcomb, Plenum Press, 1980.

12. B. Ho, A. Jayasumana, and C.G. Fang, "A dual B-scan for attenuation," Acoustic Imaging, pp.495-499, 1983.

13. D. Liu, L.S. Lillycrop, L.E. Malvern, and C.T. Sun, "The evaluation of delamination-An edge replication study," Experimental Techniques, pp.20-25, 1987.

14. S.H. Hong and D. Liu, "On the relationship between impact energy and Delamination Area," Experimental Mechanics, pp. 115-120, 1989.

15. K.M. Lal, "Residual strength assessment of low velocity impact damage of graphite/epoxy laminates," J. Reinforced Plastics and Composites, pp.226-238, 1983.

16. R. Jones, J. Paul, T.E. Tay, and J.F. Williams, "Assessment of the effect of impact damage in composites: some problems and answers," Composite structures, pp.51-73, 1983.

17. R. Jones, A.A. Baker, and R.J. Callinan, "Residual strength of impact damaged composites," Composite structures, pp.371-372, 1984.

18. T.A. Bogetti, J.W. Gillespie, and B.R. Pipes, "Evaluation of the IITRI compression test method for stiffness and strength determination," Center for composite materials, College of Engineering, University of Delaware, 1987.

19. C.C. Chamis and J.H. Sinclair, "Longitudinal compressive failure modes in fiber composites: End attachment effects on IITRI type test specimens, J. Composites technology and research, pp.129-135, 1985.

20. A.K. Ditcher and J.P.H. Webber, "Edge effects in uniaxial compression testing of cross-ply carbon fiber laminates," J. Composite Materials, pp.228-243, 1982.

21. G.A. Kardomateas and D.W. Schmueser, "Buckling and postbuckling of delaminated composites under compressive loads including transverse shear effects," AIAA Journal, pp.877-813, 1988.

22. H. Chai, C.D. Babcock, and W.G. Knauss, "One dimensional modelling of failure in laminated plates by delamination buckling," International Journal of Solids and Structures, pp.1069-1083, 1981.

23. T. Mohlin, A.F. Blom, L.F. Carlsson, and A.I. Gustavsson, "Delamination growth in a notched graphite/epoxy laminate under compression fatigue loading," ASTM 876, pp.168-188, 1985.

24. R.L. Ramkumar and J.D. Whitcomb, "Characterization of mode I and mixed mode delamination growth in T300/5208 graphite/epoxy," ASTM 876, pp.315-335, 1985.

25. H. Chai, "The characterization of mode I delamination failure in non-woven multidirectional laminates." Composites, pp.277-290, 1984.

26. T.K. O'Brien, "Characterization of delamination onset and growth in composite laminate," ASTM 775, pp.140-167, 1985.

27. K.S. Kim and C.S. Hong, "Delamination growth in angle-ply laminated composites," J. Composite Materials, pp.423-438, 1986.

28. J.D. Whitcomb and I.S. Raju, "Analysis of interlaminar stresses in thick composite laminates with and without edge delamination," ASTM 876, pp.69-94, 1985.

29. S.S. Wang, "Fracture mechanics for delamination problems in composite materials," J. Composte Materials, pp.210-223, 1983.

30. R.Y. Kim and S.R. Soni, "Experimental and analytical studies on the onset of delamination in laminated composites," J. Composite Materials, pp.70-80, 1984.

31. T.K. O'Brien, "Analysis of local delaminations and their influence on composite laminate behavior," ASTM 876, pp.282-297, 1985.

32. N. Cristescu, L.E. Malvern, and R.L. Sierakowski, "Failure mechanisms in composite plates impacted by blunt-ended penetrators," ASTM 568, pp.159-172, 1975.

33. R.L. Sierakowski, L.E.Malvern, and C.A. Ross, "Dynamic failure modes in impacted composite plates," Failure modes in composite III, Amer. Inst. of Mining, Metallurgial, and Petroleurm Eng., Inc., pp.1-16, 1976.

34. L.E. Malvern, R.L. Sierakowski, and C.A. Ross, "Impact failure mechanisms in fiber-reinforced composite plates," Proceeding IUTAM Symp. High velocity deformation of solids, Kawata, K. and Shioiri, J., ed., Tokyo, pp.120-131, 1977.

35. N. Takeda and R.L. Sierakowski, "Localized impact problems of composite laminates," Shock Vibration Digest, pp.3-10, 1980.

36. D. Liu, "Impact-induced delamination- A view of material properties mismatching," J. Composite Material, pp.674-691, 1988.

37. N.J. Pagano and R.B. Pipes," Some observations on the interlaminar strength of composite laminates," International Journal of Applied Mechanical Sciences, pp.678-688, 1973.

38. J.M. Whitney and R.Y. Kim," Effect of stacking sequence on the notched strength of laminated composites," Composite materials: Testing and design ASTM 617, pp.229-242, 1977.

39. J.H. Schmitt, "Transverse cracks in glass/epoxy cross-ply laminates impacted by projectiles,",J. Materials Science, pp.2008-2011, 1981.

40. N. Takeda, R.L. Sierakowski, and L.E. Malvern, "Wave propagation experiments on ballistically impacted composite laminates," J. Composite Materials, pp.157-174, 1981.

41. N. Takeda, R.L. Sierakowski, and L.E. Malvern, "Studies of impacted glass fiber-reinforced composite laminates," Sampe Quarterly, pp.9-17, 1981.

42. R.L. Ramkumar and P.C. Chen, "Low-velocity impact response of laminated plates," AIAA J., pp.1448-1452, 1982.

43. S.K. Chaturvedi and R.L. Sierakowski,"Effects of impactor size on impact damage-growth and residual properties in an smc-r50 composite," J. Composite Materials, pp.100-113, 1985.

44. N. Takeda, R.L. Sierakowski, C.A. Ross, and L.E. Malvern, "Delamination crack propagation in ballistically impacted glass/epoxy composite laminates," Experimental Mechanics, pp.19-25, 1982.

45. C.T. Sun and J.K. Chen, "On the impact of initially stressed composite laminates," J. Composite Materials, pp.490-504, 1985.

46. C.T. Sun and K.C. Jen, "On the effect of matrix cracks on laminate strength,"Proceeding of the American Society for Composites, pp.352-367, 1986.

47. D. Liu, "Matrix cracking in impacted glass/epoxy plates," J. Composite Materials, pp.594-609, 1987.

48. H.T. Wu and G.S. Springer, "Measurements of matrix cracking and delamination caused by impact on composite plates," J. Composite Materials, pp.518-532, 1988.

49. H.T. Wu and G.S. Springer, "Impact induced stresses, strains, and delaminations in composite plates," J. Composite Materials, pp.533-559, 1988.

50. Klas Levin, "Effect of low-velocity impact on compression strength of quasi-isotropic laminate," Proceeding of the American Society for Composites, pp.313-325, 1986.

51. K.M. Lal,"Low velocity transverse impact behavior of 8-ply, graphite/epoxy laminates," J. Reinforced Plastics and Composites, pp.216-225, 1983.

52. Wolf Elber,"Failure mechanics in low-velocity impacts on thin composite plates," NASA technical paper 2152, pp.1-23, 1983.

53. C.G. Jonathan, "Impact response of composite laminates," Proceeding of the American Society for Composites, pp.326-345, 1986.

54. S.B. Driscoll, "Variable-rate impact testing of polymeric materials," ASTM 936, pp.163-186, 1987.

55. O.S. Peter, J.T. Hartness, and T.M. Cordell, "On low-velocity impact testing of composite materials,",J. Composite Materials, pp.30-52, 1988.

56. T.M. Tan and C.T. Sun, "Use of statical indentation laws in the impact analysis of laminated composite plates," J. Applied Mechanics, pp.6-12, 1985.

57. C.A. Ross, L.E. Malvern, R.L. Sierakowski, and N. Takeda,"Finite element analysis of interlaminar shear stress due to local impact," ASTM 864, pp.355-367, 1985.

58. S.P. Joshi and C.T. Sun,"Impact induced fracture in a laminated composite," J. Composite Materials, pp.51-66, 1985.

59. J.A. Zukas, T. Nicholas, H.F. Swift, L.B. Greszczuk, and D.R. Curran, Impact dynamics, John wiley and sons, Chapt.5, 1982.

60. J.A. Zukas, T. Nicholas, H.F. Swift, L.B. Greszczuk, and D.R. Curran, Impact dynamics, John wiley and sons, Chapt.3, 1982.

61. L.T. Drzal, "Interfacial behavior of aramid and graphite fibers in epoxy matrix," 15th national AAMPE Tech. Conf., Cincinnati, OH Oct. 1983.

62. P.K. Mallick, Fiber-reinforced composites materials, manufacturing, and design, MARCEL DEKKER INC., 1988.

63. John Morton, "Scaling of impact-loaded carbon-fiber composites," AIAA Journal, pp.989-994, 1988.

64. A.C. Ugural, Stresses in plates and shells, McGraw-Hill Co.,1981.

65. Rudolph Szilard, Theory and analysis of plates classical and numerical methods, Rainbow-Bridge Co., 1974.

66. N.J. Pagano, "Exact solutions for rectangular bidirectional composites and sandwich plates," J. Composite Materials , pp.20-34, 1970.

67. K.H. Lo, R.M. Christensen, and E.M. Wu,"A high-order theory of plate deformation Part 2: Laminated plates," J. Applied Mechanics, pp.669-676, 1977.

68. R.M. Christensen, Mechanics of composite materials, John Wiely & Sons Co., 1979.

69. J.N. Reddy, "A simple higher-order theory for laminated composite plates," J. Applied Mechanics, pp.745-752, 1984.

70. E. Reissner, "The effect of transverse shear deformation on the bending of elastic plates," J. Applied Mechanics, pp.69-77, 1945.

71. A.V.K. Murty, "Higher-order theory of homogeneous plate flexure," AIAA Journal, pp.719-725, 1988.

72. C.P. Fung and J.L. Doong, "Bending of a bimodulus laminated plate based on a higher-order shear deformation theory," Composite structures, pp.121-144, 1988.

73. R.K. Kapania and Stefano Raciti, "Recent advances in analysis of laminated beams and plates, Part I:shear effects and buckling," AIAA Journal, pp.923-934, 1989.

74. J.M. Whitney and C.T. Sun, "A higher order theory for extensional motion of laminated composites," J. Sound and Vibration, pp.85-97, 1973.

75. L. Librescu and J.N. Reddy, "A critical evaluation and generalization of the theory of anisotropic laminated composite panels," Proceeding of the American Society for composites, pp.472-489, 1986.

76. K.N. Cho, C.W. Bert, and A.G. Striz, "Higher-order individual-layer theory for cylindrical bending and plate bending of rectangular laminates," 26th Annual Technical meeting Society of Engineering Science, pp.1-10, 1989.

77. K.N. Cho, C.W. Bert, and A.G. Striz, "Natural Frequencies of rectangular laminates by improved higher-order individual-layer theory," 26th Annual Technical meeting Society of Engineering Science, pp.1-10, 1989.

78. K.H. Lo, R.M. Christensen, and E.M. Wu, "Stress solution determination for high-order plate theory" J. Solids Structures, pp.655-662, 1978.

79. K.H. Lo, R.M. Christensen, and E.M. Wu, "A high-order theory of plate deformation Part 1: Homogeneous plates," J. Applied Mechanics, pp.663-668, 1977.

80. B.N. Pandya and T. Kant, "Finite element analysis of laminated composite plates using a higher-order displacement model," Composites Science and Technology, pp.137-155, 1988.

81. M.V.V. Murthy, "An improved transverse shear deformation theory for laminated anisotropic plates," NASA technical paper 1903, pp.1-37, 1981.

82. J.N. Reddy, Energy and variational methods in applied mechanics, Johns Wiely & Sons Co., 1984.

83. L.A. Mignery, T.M. Tan, and C.T. Sun, "The use of stitching to suppress delamination in laminated composites," Delamination and Debonding, ASTM 876, pp.371-385, 1985.

84. Y. Ogo, "The effect of stitching on in-plane and interlaminar properties of carbon-epoxy fabric laminates," M.S. Thesis, University of Delaware, 1987.

85. D. Liu, "Delamination resistance in stitched and unstitched composite plates subjected to impact loading," J. Reinforced Plastics and Composites, pp.59-69, 1990.

86. R. Feldman, D. Enkaoua, and H. Rosenthal, "Improved quality acceptance procedure for interlaminar shear strength," Composites, pp.253-254, 1987.

87. W.W. Stinchcomb, E.G. Henneke, and H.L. Price, "Use of the short-beam shear test for quality control of graphite-polyimide laminates," ASTM 626, pp.96-109, 1977.

88. L.A. Carlsson and R.B. Pipes, Experimental characterization of advanced composite materials, Prentice-Hall Inc., 1987.